Taxonomic Variation in the Supraorbital Region of Catarrhine Primates

Running title: Taxonomic variation in the primate supraorbital torus

Suzanna White*[a], Christophe Soligo[a], Matt Pope[b], Simon Hillson[b]

a - Department of Anthropology, University College London, 14 Taviton Street, London, WC1H 0BW

b - Institute of Archaeology, University College London, 31-34 Gordon Square, London, WC1H 0PY

*Corresponding author. E-mail address: suzanna.white@ucl.ac.uk

Abstract

Objectives

This study aimed to test the taxonomic utility of the catarrhine supraorbital region using 3D geometric morphometrics, with the aim of establishing its potential use in elucidating the position of more debated hominin groups.

Materials and Methods

230 3D coordinates were used to record the supraorbital morphology of two datasets: one containing 460 non-hominin catarrhine primates from species and subspecies of *Gorilla*, *Pan*, *Papio*, and *Macaca*; and the other containing 55 Pleistocene hominins from *Homo*, *Australopithecus*, and *Paranthropus*. Principal Component Analyses in tangent, form, and allometry-free shape space were used to assess differentiation of taxa, with biological distinctiveness of taxa being established using step-wise discriminant analysis with subsampling.

Results

Results indicated that the recorded supraorbital morphology could be used to separate non-hominin catarrhine primate genera, species, and subspecies, although accuracy was found to decrease with decreasing Linnaean rank. In addition, analyses in tangent space were found to produce the highest accuracy when classifying primates of known taxonomy. Biological distinctiveness of the middle and later *Homo* species was comparable to or higher than that of the non-hominin primates, and relatively lower for the earlier groups of *Homo*.

Discussion

This study indicates that the supraorbital region preserves taxonomic information that can be used to delineate between closely-related groups, both within hominins and wider catarrhine primates. Therefore, this region may be used to provide insight when assessing the taxonomic affiliation of disputed hominin specimens.

Key terms

Supraorbital morphology
Biological distinctiveness
Taxonomy
Primates
Hominins

Citation for published version: White, S., Soligo, C., Pope, M., Hillson, S. (2020). Taxonomic variation in the supraorbital region of catarrhine primates. *American Journal of Physical Anthropology*, 171(2), pp. 198-218. DOI: 10.1002/ajpa.23975

Introduction

Assessment of craniofacial morphology is a primary method in establishing the taxonomy of hominin fossils (Athreya, 2006, 2009; Cramon-Taubadel, 2013; Lieberman, 2000; Lieberman, 1995, 2011). Fossil species play a dual role in palaeontology: they are a basis for the study of evolutionary processes giving rise to current groups (along with extant species); and they allow us to record past levels of biodiversity, and link this to changing factors such as geographic expansion and climate change (Tattersall, 1986). As such, the ability to identify and delineate different taxonomic groups is an important aspect of palaeontology (Tattersall, 1986). Classification of fossil specimens is intrinsically linked to the available evidence (Stringer, Howell, & Melentis, 1979), however the fossil record only preserves small, incomplete samples of hominins from which to build our understanding (Simpson, 1961). In addition, the fossil record typically only preserves hard-tissue evidence, yet many taxonomic differences in extant animals are only apparent in behavioural or soft-tissue evidence (Simpson, 1961; Smith, 1994; Tattersall, 1986, 1992), making application of popular taxonomic criteria to the fossil record extremely difficult.

Palaeoanthropologists use morphology to differentiate between hominin groups (Kimbel, 1991; Smith, 1994; Tattersall, 2005; Wood, 2010), for instance through the application of a morphological species concept. Such a concept can be applied by comparing levels of within- and between-group variation in skeletal morphology of fossil specimens to that of individuals of known taxonomic classification. In palaeoanthropology, non-hominin primates, and especially the Catarrhini, are generally used as reference taxa. Researchers have proposed the use of multiple model taxa when attempting to address taxonomic questions (Harvati, Frost, & McNulty, 2004), partly due to the great ecological and biological diversity found in animals, and primates in particular (Ackermann, 2002; Baab, 2008; Jiménez-Arenas, Palmqvist, & Pérez-Claros, 2011; O'Higgins & Dryden, 1993; Schaefer, Mitteroecker, Gunz, Bernhard, & Bookstein, 2004; Wood, Li, & Willoughby, 1991).

The inclusion of non-human apes provides an opportunity to model taxonomic variation in groups with different levels of sexual dimorphism, which is relevant to palaeoanthropology as studies have indicated that some extinct hominins may have been more sexually dimorphic than recent *Homo sapiens* (Garvin et al., 2017; Lockwood, 1996, 1999; Plavcan, 2012; Richmond & Jungers, 1995; Royer, Lockwood, Scott, & Grine, 2009). Non-human apes share a close relationship to *Homo*, with the *Pan* and *Homo* clades diverging approximately 6-9 Mya (Dos Reis et al., 2018; Langergraber et al., 2012; Perelman et al., 2011; Schrago & Voloch, 2013; Wilkinson et al., 2011), and the divergence between *Gorilla* and the *Pan/Homo* clade being dated to between 6-19 Mya (Glazko & Nei, 2003; Langergraber et al., 2012).

Papionins, as members of Cercopithecoidea, are more distantly related to hominins. Nevertheless, numerous researchers have suggested that they are appropriate models for the study of our evolutionary past (Baab, 2008; Delson, 1978; DeVore, 1963; Frost, Marcus, Bookstein, Reddy, & Delson, 2003; Harvati et al., 2004; Jolly, 1970; Jolly, 2001; Zinner, Groeneveld, Keller, & Roos, 2009). Their suitability arises from many characteristics, including: the numerous homologous traits they share with hominins; their phylogenetic distance to our own group, which may highlight possible parallelisms in primate evolution; their increased range in comparison to non-human apes, both geographically and ecologically; the existence of multiple species which diverged at similar time-depths and in broadly analogous habitats to hominins; the occurrence of hybridisation across different taxonomic boundaries; and the occurrence of relatively great biodiversity and craniofacial variation in some groups (Ackermann & Bishop, 2010; Alberts & Altmann, 2001; Baab, 2008; Frost et al., 2003; Harvati et al., 2004; Jolly, 2001; Pan, Oxnard, & Milne, 2002; Pan & Oxnard, 2002, 2004; Zinner et al., 2009; Zinner, Wertheimer, Liedigk, Groeneveld, & Roos, 2013).

This paper aimed to test whether the morphology of the supraorbital region can be used to detect taxonomic boundaries in primates, particularly at the species and subspecies level. The supraorbital region is one of the best-preserved in key periods of the hominin fossil record, potentially due to the robusticity of this area. It has also been suggested to document a moderate phylogenetic signal (McNulty, 2005; Smith, 2009; Weidenreich, 1947), and displays established phenetic differences between primate taxa (Aiello & Dean, 1990; Hublin et al., 2017; Lahr & Wright, 1996; Lieberman, 2000; Lieberman, 2011; Russell, 1985; Schwartz & Tattersall, 2010; Smith & Ranyard, 1980), indicating its potential usefulness for assessing the taxonomy of extinct hominins. Reference non-hominin primates included members of *Gorilla*, *Pan*, *Papio*, and *Macaca*. Following a test of the taxonomic information content of the supraorbital region in extant non-hominin primates, the same methods were applied to a dataset of Pleistocene hominin fossils, to test whether supraorbital morphology could provide valid insights into the hominin fossil record and, ultimately, the taxonomy of more debated hominin groups.

Materials and Methods

Sample

Only adult specimens were included in this study. Adult status was assessed dentally, by the full eruption of the third molars (both maxillary and mandibular, if present), and cranially, by full fusion of the basioccipital-basisphenoidal synchondrosis (Wood et al., 1991). When assessment of the fusion of the basioccipital-basisphenoidal synchondrosis could not be conducted, dental maturity was used as

the sole criterion. Specimens showing evidence of pathology or trauma in the cranium were excluded. Specimens with detailed geographical locations were favoured, although some with unknown origin were included when available specimen numbers were low.

Non-Hominin Primate Dataset

This study used a dataset of non-hominin primates consisting of 460 adult specimens from 10 species within *Gorilla*, *Pan*, *Papio*, and *Macaca* (see table 1 and SI-1). Previous researchers and collectors did not always recognise current subspecific distinctions within the non-hominin apes, therefore geographical information was used to establish subspecies categories of *Pan* and *Gorilla* specimens, using data on current taxonomic distribution from the IUCN (2017). Due to the relatively recent taxonomic separation of *Papio cynocephalus* and *Papio kindae*, geographic data from the IUCN was used to inform classification, although this was not possible for all specimens. Sex information was taken from collection material, and the ratio of males to females across the sample was approximately equal (225 females, 226 males, 9 unknown). Sample sizes varied between groups due to unequal representation of the included taxa in the various collections used. A maximum of 50 individuals were selected from each taxon. All non-hominin primate data was taken from original specimens, either in the form of 3D laser scans collected with a NextEngine Desktop Laser Scanner, or surface models generated from available CT data using 3D Slicer (Fedorov et al., 2012; see SI-1 and SI-2 in Supplementary Information).

Table 1 - Summary of non-hominin primate dataset (n=460) by taxon and sex. Abbr. indicates group abbreviations. Data for sex was taken from museum records. *Some *Macaca fuscata* and *Papio cynocephalus sensu lato* specimens could not be assigned a subspecies classification

Taxon	Abbr.	Count			%			Total
		Female	Male	Unknown	Female	Male	Unknown	
Gorilla beringei beringei	*GBB*	6	8		42.9%	57.1%		14
Gorilla beringei graueri	*GBG*	23	18		56.1%	43.9%		41
Gorilla gorilla gorilla	*GGG*	25	25		50.0%	50.0%		50
Gorilla gorilla diehli	*GGD*	9	9		50.0%	50.0%		18
Pan paniscus	*PP*	21	18	4	48.8%	41.9%	9.3%	43
Pan troglodytes troglodytes	*PTT*	25	25		50.0%	50.0%		50
Pan troglodytes schweinfurthii	*PTS*	16	11	3	53.3%	36.7%	8.8%	30
Pan troglodytes verus	*PTV*	6	10		37.5%	62.5%		16
Pan troglodytes ellioti	*PTE*	2	3		40.0%	60.0%		5
Papio anubis	*PA*	17	25		40.5%	59.5%		42
*Papio cynocephalus sensu lato**	*PC?*	3	2		60.0%	40.0%		5
Papio cynocephalus	*PC*	2	6		25.0%	75.0%		8
Papio kindae	*PK*	10	13		43.5%	56.5%		23
Macaca fascicularis	*MFa*	24	25		49.0%	51.0%		49
*Macaca fuscata**	*MFu?*	3	6		33.3%	66.7%		9
Macaca fuscata fuscata	*MFuF*	3	1	2	50.0%	16.7%	33.3%	6
Macaca fuscata yakui	*MFuY*	5	2		71.4%	28.6%		7

Hominin Dataset

A Pleistocene hominin dataset was also used in this study, and consisted of 55 specimens from *Paranthropus*, *Australopithecus*, and *Homo* (see table 2 and SI-1). Earlier *Homo* and Late *Australopithecus* specimens, from purported species such as *Homo rudolfensis* and *Homo habilis*, were included, along with a reconstruction of Dinaledi Hominin 1 (DH1; *Homo naledi*). This specimen has been dated to the Middle Pleistocene (Dirks et al., 2017; Hawks & Berger, 2016), although its morphology indicates a closer relationship to Early Pleistocene hominins (Berger et al., 2015; Laird et al., 2017; Schroeder et al., 2017). *Homo erectus (sensu lato)* specimens from three subgroups (*Homo georgicus*, *Homo ergaster*, and *Homo erectus sensu stricto*) were also included, allowing modelling of craniofacial variation in a widespread and generally well-accepted hominin species with a considerable life span (over 1.5 million years (Antón, 2003)). Middle Pleistocene hominins (MPH) were included, although, while these hominins have previously been classified as *Homo heidelbergensis sensu lato*, they have an unresolved taxonomy, possibly constituting multiple species (Buck & Stringer, 2014; Harvati, 2007; Hublin, 2013; Stringer, 2012). As such, they were included to avoid inflating the morphological distance between earlier and later *Homo* species, but were not considered as a taxon for the purposes of this study. Late Pleistocene fossils included both *Homo neanderthalensis* and *Homo sapiens*, providing a model of variation between two sister-species. Hominin data were taken from research-quality casts of specimens, although original data were available in a number of cases (see table 2), either from 3D laser scans of the original fossil, or from surface models generated from available CT data (see SI-1 and SI-2).

Table 2 - Summary of Pleistocene hominin dataset (n=55), showing species classifications and subgroup where applicable. Abbr. indicates group abbreviations. *indicates specimens where surface models were collected from the original fossil. #indicates specimens where surface models were generated from available CT data. *Homo sapiens* were separated into two subgroups based on their morphology. Older specimens not showing the full suite of *Homo sapiens* craniofacial traits were classified within Early Modern Humans (EMH), while later specimens showing modern craniofacial traits were classified as Anatomically Modern Humans (AMH)

Specimen	Species	Abbr.	Subgroup	Abbr.
Chancelade	*Homo sapiens*	*HS*	Anatomically Modern Human	AMH
Furfooz I	*Homo sapiens*	*HS*	Anatomically Modern Human	AMH
Keilor	*Homo sapiens*	*HS*	Anatomically Modern Human	AMH
Oberkassel I	*Homo sapiens*	*HS*	Anatomically Modern Human	AMH
Oberkassel II	*Homo sapiens*	*HS*	Anatomically Modern Human	AMH
Abri Pataud	*Homo sapiens*	*HS*	Anatomically Modern Human	AMH
Brno II	*Homo sapiens*	*HS*	Anatomically Modern Human	AMH
Cro-Magnon I	*Homo sapiens*	*HS*	Anatomically Modern Human	AMH
Cro-Magnon II	*Homo sapiens*	*HS*	Anatomically Modern Human	AMH
Dolní Věstonice III	*Homo sapiens*	*HS*	Anatomically Modern Human	AMH
Mladeč 1#	*Homo sapiens*	*HS*	Anatomically Modern Human	AMH
Mladeč 2	*Homo sapiens*	*HS*	Anatomically Modern Human	AMH
Předmostí III	*Homo sapiens*	*HS*	Anatomically Modern Human	AMH
Předmostí IV	*Homo sapiens*	*HS*	Anatomically Modern Human	AMH
Zhoukoudian UC.101	*Homo sapiens*	*HS*	Anatomically Modern Human	AMH

Zhoukoudian UC.102	*Homo sapiens*	*HS*	Anatomically Modern Human	AMH
Border Cave 1	*Homo sapiens*	*HS*	Early Modern Human	EMH
Jebel Irhoud 1	*Homo sapiens*	*HS*	Early Modern Human	EMH
Herto	*Homo sapiens*	*HS*	Early Modern Human	EMH
Liujiang	*Homo sapiens*	*HS*	Early Modern Human	EMH
Omo 1	*Homo sapiens*	*HS*	Early Modern Human	EMH
Qafzeh 9	*Homo sapiens*	*HS*	Early Modern Human	EMH
Skhūl V[#]	*Homo sapiens*	*HS*	Early Modern Human	EMH
Tabun I	*Homo neanderthalensis*	*HN*		
La Quina H5	*Homo neanderthalensis*	*HN*		
Spy 1[#]	*Homo neanderthalensis*	*HN*		
La Chapelle	*Homo neanderthalensis*	*HN*		
Guattari	*Homo neanderthalensis*	*HN*		
Gibraltar 1*	*Homo neanderthalensis*	*HN*		
Le Moustier 1	*Homo neanderthalensis*	*HN*		
Amud 1	*Homo neanderthalensis*	*HN*		
Krapina C	*Homo neanderthalensis*	*HN*		
Krapina E	*Homo neanderthalensis*	*HN*		
Saint-Césaire I	*Homo neanderthalensis*	*HN*		
Shanidar I	*Homo neanderthalensis*	*HN*		
Shanidar V	*Homo neanderthalensis*	*HN*		
Bodo[#]	Middle Pleistocene hominin	MPH		
Kabwe (Broken Hill) 1*	Middle Pleistocene hominin	MPH		
Petralona	Middle Pleistocene hominin	MPH		
Sima de los Huesos 5 (SH5)	Middle Pleistocene hominin	MPH		
Solo VI	*Homo erectus sensu lato*	*HEsl*	*Homo erectus sensu stricto*	*HE*
Sangiran 17	*Homo erectus sensu lato*	*HEsl*	*Homo erectus sensu stricto*	*HE*
Zhoukoudian XII	*Homo erectus sensu lato*	*HEsl*	*Homo erectus sensu stricto*	*HE*
KNM-ER 3773	*Homo erectus sensu lato*	*HEsl*	*Homo ergaster*	*HEr*
KNM-ER 3883	*Homo erectus sensu lato*	*HEsl*	*Homo ergaster*	*HEr*
Dmanisi D4500	*Homo erectus sensu lato*	*HEsl*	*Homo georgicus*	*HG*
Dmanisi D2282	*Homo erectus sensu lato*	*HEsl*	*Homo georgicus*	*HG*
Dinaledi hominin 1 (DH1)	*Homo naledi*	*HNa*		
KNM-ER 1813	*Homo habilis*	*HHa*		
OH 24	*Homo habilis*	*HHa*		
KNM-ER 1470	*Homo rudolfensis*	*HRu*		
Sts 5[#]	*Australopithecus afarensis*	*AAfr*		
KNM-WT 17000	*Paranthropus aethiopicus*	*ParA*		
KNM-ER 406	*Paranthropus boisei*	*ParB*		
KNM-ER 732	*Paranthropus boisei*	*ParB*		
OH 5	*Paranthropus boisei*	*ParB*		

Reconstruction

Given the nature of the fossil record, it is unsurprising that most fossil hominin specimens included in this study were not intact across the region of interest, and some specimens had suffered post-depositional distortion. While efforts were made to select only the most well-preserved extant non-hominin primate specimens, this was not possible for members of the less numerous taxa, and a number of extant non-hominin primates in the final sample had missing data. While the simplest way to deal with missing data is to remove the affected landmarks from the dataset, this is unrealistic in larger samples. The alternative is to reconstruct the missing data so that the incomplete specimens may still be included in the analysis (Gunz, 2005). Each specimen was assessed individually in order to apply the most appropriate method given the above considerations. Details of the reconstruction methods and reference specimens can be found in SI-3. Effects of reconstruction methods and reference specimens were assessed (SI-4). These were found to have a non-significant impact on intragroup variation.

Landmarking

Landmarking was conducted in Stratovan Checkpoint. 230 3D landmarks and surface semilandmarks were used in this study. These included nine landmarks placed around the orbital area, and a mesh of 221 points across the supraorbital region, consisting of 11 control landmarks and 210 automatically generated semilandmarks. Two additional landmark points (Auriculare) were used to guide placement of the mesh but were not included in the final configuration (see figure 1 and table 3).

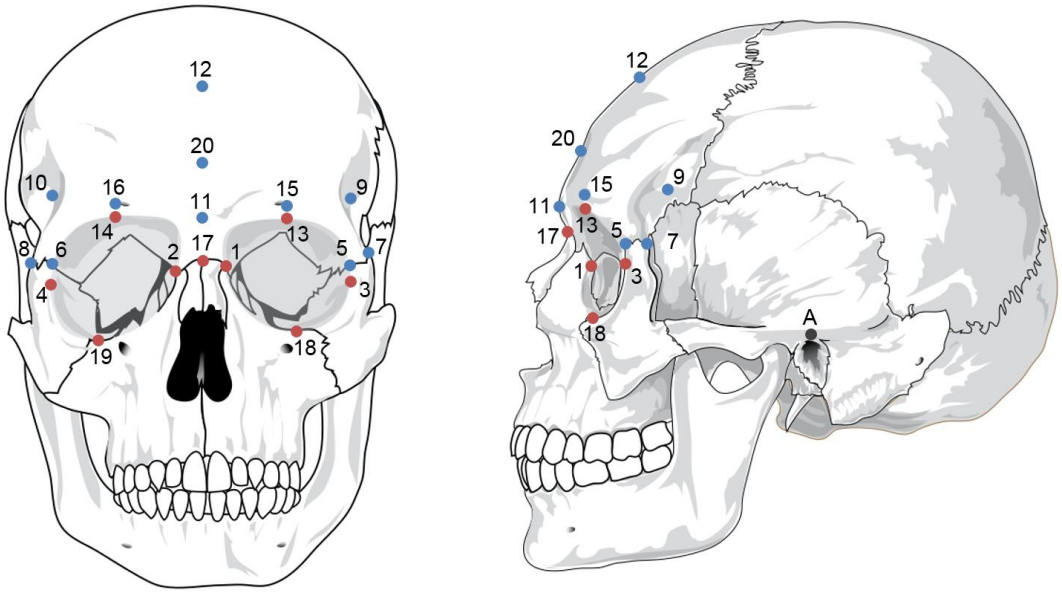

Figure 1 - Diagrams showing location of landmarks used in this study, from frontal and left lateral view. Landmarks are numbered as in table 3. Points shown in blue were control landmarks for the mesh of surface semilandmarks. Points shown in red were independent landmarks used to record the orbital morphology. Points shown in grey were not included in the final configuration

Table 3 - List of landmarks used in this study along with their definitions. Auriculare points are shown in italics as these were used, along with the Orbitale points, to define the Frankfurt horizontal, but were not included in the final landmark configuration dataset. Landmark definitions were amended from McNulty (2005), Baab (2008), and Howells (1973)

#	Landmark	Laterality	Definition
A, B	*Auriculare*	*Bilateral*	*The point vertically above the midpoint of the external auditory meatus on the zygomatic root*
1, 2	Dacryon	Bilateral	The point where a line from Ectoconchion dividing the orbit into two along the long axis intersects with the medial orbital margin
3, 4	Ectoconchion	Bilateral	The intersection of the most anterior surface of the lateral border of the orbit and a line bisecting the orbit along the long axis
5, 6	Frontomalare Anterior	Bilateral	The point where the frontomalare suture intersects with the lateral orbital margin
7, 8	Frontomalare Posterior	Bilateral	The most posterior point on the frontomalare suture of the zygomatic process
9, 10	Frontotemporale	Bilateral	The most medial point on the lateral curve of the frontal bone, when viewed from *norma verticalis*
11	Glabella	Unilateral	The most anterior point on the frontal bone, between the supraorbital tori, on the midsagittal plane
12	Mid-Frontotemporale	Unilateral	The point where a line between the frontotemporale points intersects with the midsagittal plane
13, 14	Mid-torus Anterior	Bilateral	The most anterior point on the frontal bone directly above the midpoints of the orbit
15, 16	Mid-torus Inferior	Bilateral	The point on the superior orbital margin, at the midpoint of the orbit
17	Nasion	Unilateral	The point where the nasofrontal suture intersects the midsagittal plane
18, 19	Orbitale	Bilateral	The most inferior point on the infraorbital margin
20	Post-toral Sulcus	Unilateral	The most inferior point on the region posterior to glabella, in the midsagittal plane

Analyses

The final configurations of 230 3D points were registered using Generalised Procrustes Analysis (GPA) with a partial Procrustes fit (Rohlf, 1999; Rohlf & Slice, 1990) using the gpagen function in Geomorph (Adams, Otárola-Castillo, & Paradis, 2013). Surface semilandmarks were slid to minimise bending energy during this process. This method is favourable over the minimisation of Procrustes distances when samples include multiple taxa with significantly different morphology, as in the present study, as it maintains geometric homology (Gunz & Mitteroecker, 2013). This process was repeated for both the non-hominin primate and hominin datasets, and was conducted in tangent space (a Euclidean approximation of Kendall's shape space), form space (where the effect of scaling was not removed, by scaling the Procrustes shape coordinates by Centroid size (Dryden & Mardia, 1998)), and allometry-free shape space (where the residuals from a regression of size (lnCS) on the Procrustes coordinates were used, using the procD.lm and shape.resid functions in Geomorph). Results from the three shape spaces can be usefully compared to bring to light dissociation between form and shape variation within a sample, and to assess the effect of both isometry and allometry (Mitteroecker & Gunz, 2009; Mitteroecker, Gunz, Windhager, & Schaefer, 2013).

Procrustes shape coordinates resulting from the above GPA were put through Principal Component Analysis (PCA), to reduce the datasets into a few dimensions which summarised the key aspects of variation (Mitteroecker & Gunz, 2009; O'Higgins, 2000). This study used the first two principal

components for preliminary assessment and visualisation, while including the loadings along the principal components accounting for over 95% of total sample variance combined in subsequent analyses, to avoid misinterpretation of morphological variation. Mean shapes were produced for each taxon, using the Procrustes coordinates and the mshape function in Geomorph, and were visualised as 3D scatterplots in SPSS 25. Mean pair-wise Procrustes distances were calculated within and between taxa.

Step-wise, cross-validated discriminant analyses with subsampling were performed for both datasets, using the principal components that accounted for over 95% of total variance, to assess biological distinctiveness following the methods of Cardini et al. (2009). Specimens which were the only representative of their species were excluded (i.e. *Homo naledi*, *Homo rudolfensis*, *Australopithecus africanus*, and *Paranthropus aethiopicus*), along with *Paranthropus boisei* due to the lack of closely-related specimens, resulting in a hominin dataset of 48 specimens. Discriminant analyses were repeated using three classification systems: the first and second classified specimens into genus and species, respectively, and were applied to both the non-hominin primate and hominin datasets; the third classified the non-hominin primate dataset into subspecies where applicable. 1000 random subsamples were taken from each taxonomic group. For the non-hominin primate dataset, subsample size was set to n=16 for genus-, n=8 for species-, and n=4 for subspecies-level analyses. These values were chosen due to low sample sizes for some of the subspecific groups, and to reflect the hierarchical composition of each increasing taxonomic rank. For the hominin dataset, sample size was set to n=7 due to the number of *Homo erectus sensu lato* included, except for the MPH where n=4, and *Homo habilis* where n=2 due to lower sample sizes, resulting in a total subsample of 27 individuals for each repeat. Classification accuracy was taken to reflect biological distinctiveness for each taxonomic rank (Cardini & Elton, 2011; Cardini et al., 2009). MPH and *Homo habilis* were excluded from the final calculation of cross-group hominin species-level classification accuracy, due to the uncertainties around the former group's taxonomic status, and the small sample size of the latter.

Intraobserver Error

All landmarking was conducted by SW. 26 specimens (18 non-hominin primates and eight Pleistocene hominins) were used in the assessment of intraobserver error (see table S13). Landmarks defined above in table 3 were placed on these 26 specimens on four occasions. As this study focused on morphological differences between genera, species, and subspecies, this study followed the method of Lockwood, Lynch, and Kimbel (2002). The repeats for the intraobserver specimens were added to the non-hominin primate and hominin datasets, after which both datasets were put through a GPA. Procrustes distances (which should approximate Euclidean distances from principal components) for

intraobserver repeats were then compared to intra- and inter-genus, species, and subspecies Procrustes distances using a one-way ANOVA with post-hoc Tukey HSD (Honestly Significant Difference) tests in SPSS 25. Results showed that intraobserver error was significantly lower than intra- and intertaxonomic distances for both datasets (see tables S14 and S15). It was therefore concluded that any intraobserver error should not significantly affect the outcome of later taxonomic analyses.

Results

Non-Hominin Primates

Group Morphology

Differences between the non-hominin primate genera are shown in figure 2 (figures are scaled to unit centroid size, and therefore show differences in shape, not overall form). In comparison to *Pan*, *Gorilla* were found to have more laterally flaring supraorbital tori that were more anteriorly projecting, and wider nasal columns, narrower frontal bones, and deeper supraorbital sulci relative to overall size. The differences between *Papio* and *Macaca* appear to be less marked, reflected in the lower pairwise Procrustes distances (0.117 compared to 0.155 for *Gorilla-Pan* comparisons; see table S16). Members of *Papio* were found to have shorter orbits, thicker supraorbital trigones, and less vertical frontal squamae in comparison to *Macaca*.

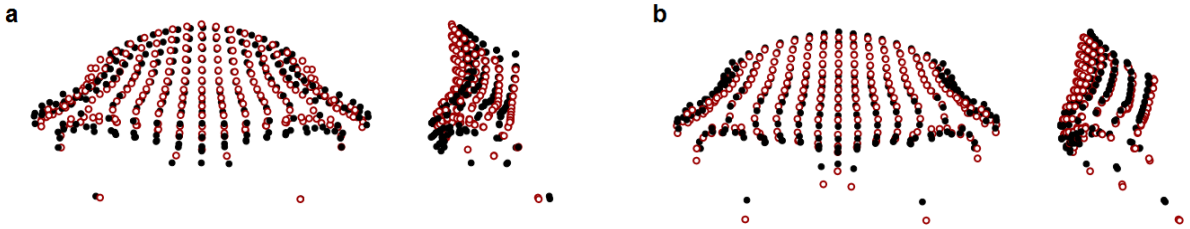

Figure 2 - Mean shapes of specimens of non-hominin primate genera. **a** - *Gorilla* (black) superimposed with *Pan* (red and white); **b** - *Papio* (black) superimposed with *Macaca* (red and white)

There were slight differences apparent between the *Gorilla gorilla* subspecies (mean pairwise PrD: 0.112), which were largely focused in the lateral and inferior aspects of the supraorbital tori (figure 3). Slightly larger differences (mean pairwise PrD: 0.119) were apparent between the *Gorilla beringei* subspecies, with *Gorilla beringei beringei* having more superiorly placed dacryon points, more anteriorly projecting frontal squamae and supraorbital tori, and slightly narrower frontal squamae than *Gorilla beringei graueri*. The differences between the *Gorilla* species were more marked (mean pairwise PrD: 0.123), with *Gorilla gorilla* having anteroposteriorly thicker lateral aspects of their

supraorbital tori, more anteriorly projecting supraorbital tori in the midsagittal region, and more superiorly placed orbital points than *Gorilla beringei*.

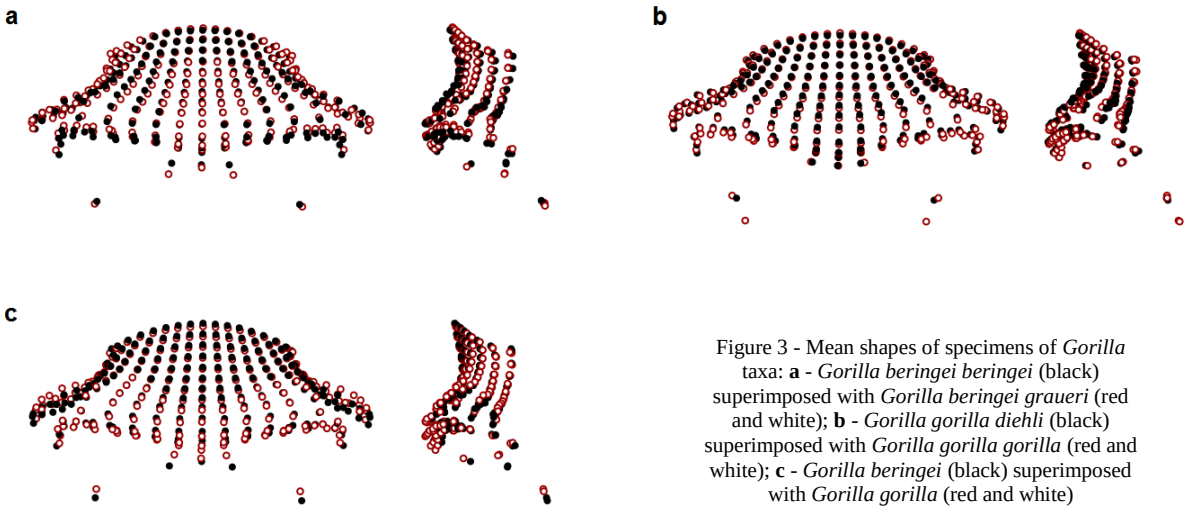

Figure 3 - Mean shapes of specimens of *Gorilla* taxa: **a** - *Gorilla beringei beringei* (black) superimposed with *Gorilla beringei graueri* (red and white); **b** - *Gorilla gorilla diehli* (black) superimposed with *Gorilla gorilla gorilla* (red and white); **c** - *Gorilla beringei* (black) superimposed with *Gorilla gorilla* (red and white)

Figure 4 shows minimal differences (mean pairwise PrD: 0.090) between the subspecies of *Pan troglodytes*. *Pan troglodytes troglodytes* was found to have more anteroinferiorly placed inferior aspects of the supraorbital tori, deeper post-toral sulci, and more vertical frontal squamae than the average *Pan troglodytes schweinfurthii* configuration. *Pan troglodytes ellioti* had slightly more laterally expanded supraorbital trigones, less anteriorly placed supraorbital tori and frontal squamae, and more posteriorly placed orbits than *Pan troglodytes troglodytes*. *Pan troglodytes verus* had slightly more anteriorly projecting supraorbital tori, which were taller in the midsagittal region, and less vertical frontal squamae than *Pan troglodytes ellioti*. In terms of species-level differences within *Pan* (mean pairwise PrD: 0.096), *Pan troglodytes* had more projecting supraorbital tori on average, with laterally expanded supraorbital trigones, and more posteriorly placed lower orbital margins, while the uppermost part of the frontal squama of the average *Pan paniscus* configuration was more anteroinferiorly placed.

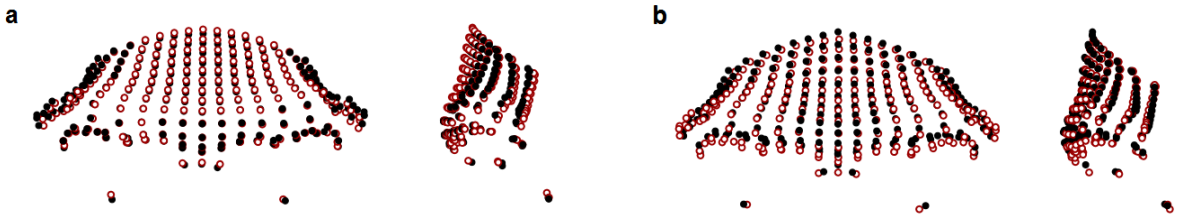

Figure 4 - Mean shapes of specimens of *Pan* taxa: **a** - *Pan troglodytes troglodytes* (black) superimposed with *Pan troglodytes schweinfurthii* (red and white); **b** - *Pan troglodytes troglodytes* (black) superimposed with *Pan troglodytes ellioti* (red and white); **c** - *Pan troglodytes verus* (black) superimposed with *Pan troglodytes ellioti* (red and white); **d** - *Pan paniscus* (black) superimposed with *Pan troglodytes* (red and white)

Comparisons between the average shapes of the *Papio* groups are shown in figure 5. The differences between *Papio anubis* and *Papio cynocephalus* were relatively small (mean pairwise PrD: 0.098), with the latter having slightly narrower supraorbital tori and more anteriorly placed frontal squamae in the medial region, while the lateral aspects were relatively more inferiorly placed. *Papio anubis* had more anteriorly protruding supraorbital tori in the glabella region in comparison to *Papio cynocephalus*. Differences between *Papio anubis* and *Papio kindae* were more apparent (mean pairwise PrD: 0.106), with the latter having taller, more anteriorly and laterally projecting frontal squamae, and the former having more inferiorly placed supraorbital margins and orbits. The differences between *Papio cynocephalus* and *Papio kindae* were less apparent (mean pairwise PrD: 0.094), although the latter again was found to have a more superiorly and laterally projecting frontal squamae on average.

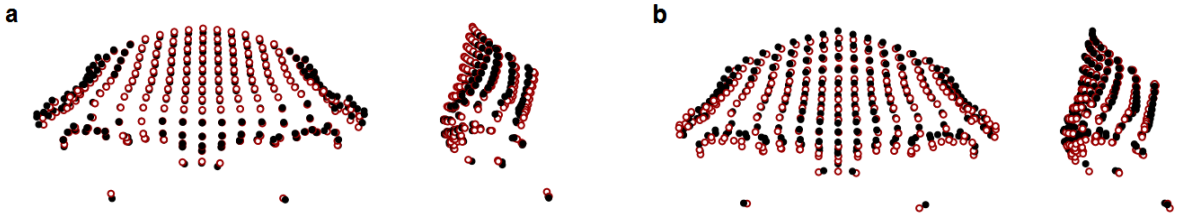

Figure 5 - Mean shapes of specimens of *Papio* taxa: **a** - *Papio anubis* (black) superimposed with *Papio cynocephalus (sensu stricto)* (red and white); **b** - *Papio cynocephalus (sensu stricto)* (black) superimposed with *Papio kindae* (red and white)

Figure 6 shows the differences between the *Macaca* taxa. There were slight differences between the *Macaca* species (mean pairwise PrD: 0.099), which were largely found in the supraorbital trigones and superior frontal squama region. *Macaca fascicularis* was found to have the most anteriorly projecting supraorbital tori in the medial region, while the lateral aspects of the supraorbital tori in *Macaca fuscata* were more projecting. The orbits of *Macaca mulatta* showed a higher degree of orbital frontation than in the other two species, and the frontal squamae in this group were more vertically aligned. Differences between the *Macaca fuscata* subspecies were relatively low (mean pairwise PrD: 0.087). *Macaca fuscata yakui* specimens had slightly more laterally thickened supraorbital trigones and mediolaterally narrower frontal squamae, which were more vertically aligned than seen in *Macaca fuscata fuscata*.

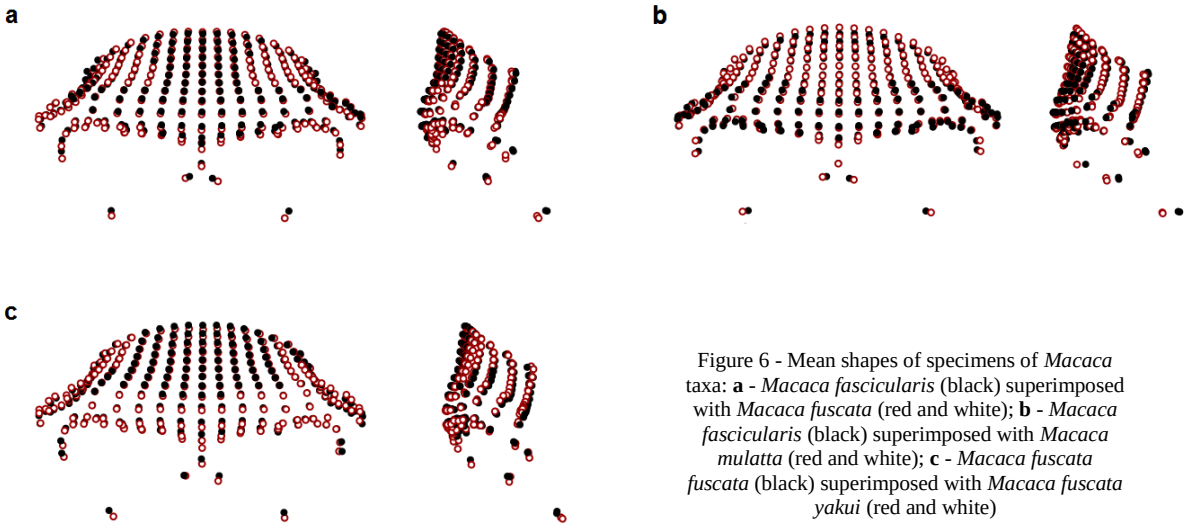

Figure 6 - Mean shapes of specimens of *Macaca* taxa: **a** - *Macaca fascicularis* (black) superimposed with *Macaca fuscata* (red and white); **b** - *Macaca fascicularis* (black) superimposed with *Macaca mulatta* (red and white); **c** - *Macaca fuscata fuscata* (black) superimposed with *Macaca fuscata yakui* (red and white)

Principal Component Analysis

Only the results of the tangent space analyses are presented here as they provide the most reliable levels of taxonomic differentiation (see Discriminant Analysis). The results of the form and allometry-free shape space analyses are available in Supplementary Information (SI-6).

Principal Component Analysis on the non-hominin primate dataset resulted in 46 principal components (PCs), with the first 32 accounting for >95% of the total sample variation combined, and the first 13 accounting for >1% of variation individually. The first PC accounted for 40.4% of sample variation. More negative values on PC1 were associated with less laterally flaring and anteriorly projecting supraorbital tori, a minimal postorbital sulcus, a higher degree of orbital frontation, a narrower nasal column, and a smaller degree of postorbital constriction (figure 7). The second PC accounted for 14.9% of sample variation. Negative values on this component were associated with superoinferiorly thicker supraorbital tori, a lack of a post-toral sulcus, and a particularly narrow nasal column.

The non-hominin primates were spread along two parallel trajectories in this plot, with one comprising the non-human apes, which had lower values on PC2, and the other the papionins. At genus level, *Gorilla* and *Pan* were separated along both PC1 and PC2, although with some overlap, with *Gorilla* having lower-values for PC1 and higher values for PC2 (figure S3). *Papio* and *Macaca* overlapped to a larger extent, with *Papio* having slightly lower values along PC1 and higher values on PC2.

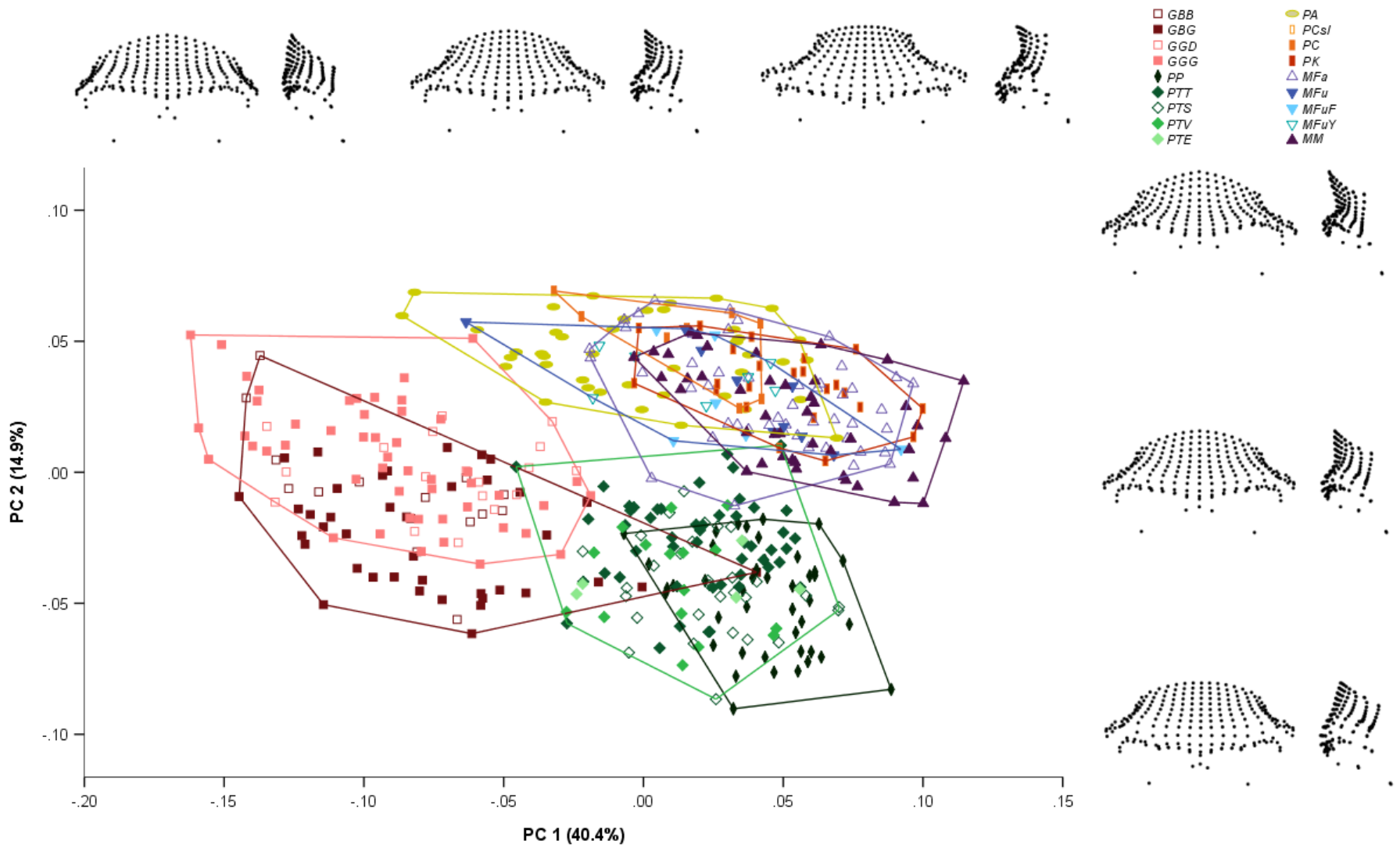

Figure 7 - Plot of PC1 (x-axis) and PC2 (y-axis), accounting for 55.4% of variation, for PCA in tangent space using dataset of 460 non-hominin primates. Specimens are identified by symbols shown in legend. See table 1 for list of abbreviations. Convex hulls are shown and correspond to species groups. Shape changes are shown for minimum, median, and maximum sample values for both axes, in frontal and left lateral view

At species level, *Gorilla beringei* specimens were found to have lower values along PC2 combined with slightly higher values on PC1 in comparison to *Gorilla gorilla* (figure S4). *Pan paniscus* was differentiated from *Pan troglodytes* by slightly higher values along PC1 and lower values on PC2. *Papio cynocephalus* was mostly encompassed by *Papio anubis*, while *Papio kindae* was somewhat differentiated by higher values for PC1. The three *Macaca* species showed considerable overlap for values on both PC1 and PC2.

In terms of subspecific differences, *Gorilla beringei beringei* had higher values along PC2, while *Gorilla beringei graueri* had lower values along this component, and a wider range of values along PC1 (figure S5). *Gorilla gorilla diehli* was almost fully encompassed by *Gorilla gorilla gorilla*, although they sat towards the lower end of this taxon's range for PC2. *Pan troglodytes verus* and *Pan troglodytes ellioti* were almost fully encompassed by the *Pan troglodytes schweinfurthii* specimens, while *Pan troglodytes troglodytes* was somewhat differentiated by lower values along PC1 and higher values along PC2. *Macaca fuscata yakui* was found to have slightly lower values along PC1 than *Macaca fuscata fuscata*.

Discriminant Analysis

Results of the discriminant analyses in the three shape spaces are shown in table 4. Primate taxa were found to have the highest biological distinctiveness using principal components from analyses in tangent space at the subspecies and species levels, and form space at the genus level (although biological distinctiveness was similar when using PCs from tangent space analysis at the genus level). Results of the discriminant analyses using principal components from PCA in form and allometry-free shape space can be found in SI-6. Using results from the PCA in tangent space, classification accuracy was highest for the genus-level analysis (97.5%), followed by the species-level analysis (75.4%), and the subspecies-level analysis (45.2%). Genus classification accuracy, taken to reflect biological distinctiveness, ranged from 96.6% in *Papio* to 98.9% in *Pan* (table 5). The range of biological distinctiveness for the species groups was broader; from 56.4% in *Papio cynocephalus* to 83.9% in *Gorilla gorilla* (table 6). Biological distinctiveness for the included subspecies showed a similarly broad range, with *Pan troglodytes ellioti* having the lowest classification accuracy at 30.7%, and *Gorilla beringei graueri* the highest at 63.3% (table 7).

Table 4 - Comparison of results of step-wise cross-validated discriminant analysis with subsampling using principal components that accounted for over 95% of total sample variance from PCA in tangent space, form space, and allometry-free shape space with dataset of 460 non-hominin primates. Percentage classification accuracy across the 1000 subsamples (n=16, for Genus; n=8 for Species; n=4 for Subspecies) is shown by taxon. See table 1 for list of abbreviations. See tables in SI-6 for detailed results for form and allometry-free shape space analysis

	Subspecies			Species			Genus		
	Tangent	Form	Allometry-free	Tangent	Form	Allometry-free	Tangent	Form	Allometry-free
GBB	42.7	25.3	29.7	83.8	70.5	57.2	97.1	95.4	69.4
GBG	63.3	35.9	47.7						
GGD	57.2	35.7	40.8	83.9	70.7	52.1			
GGG	49.3	38.1	34.8						
PP				81.6	82.8	76.3	98.9	98.3	94.7
PTT	44.6	33.1	38.0	78.3	76.4	72.2			
PTS	38.3	19.3	36.6						
PTV	35.5	20.4	34.7						
PTE	30.7	10.9	36.2						
PA				69.2	38.7	62.3	96.6	99.9	95.2
PC				56.4	35.2	56.9			
PK				85.9	80.0	86.9			
MFa				68.3	71.8	57.2	97.4	99.7	73.5
MFuF	36.1	57.9	30.5	72.1	48.5	63.6			
MFuY	54.6	55.6	45.4						
MM				74.8	66.4	63.9			
	45.2	33.2	37.4	75.4	64.1	64.9	97.5	98.3	83.2

Table 5 - Results of step-wise cross-validated discriminant analysis with subsampling using first 32 principal components that accounted for over 95% of total sample variance from PCA in tangent space with dataset of 460 non-hominin primates. Mean percentage classification accuracy across the 1000 subsamples (n=16) is shown by taxon. Specimens were classified by genus, and overall genus classification accuracy was 97.5%

	Gorilla	*Pan*	*Papio*	*Macaca*	Genus
Gorilla	97.1	2.5	0.4		97.1
Pan	0.5	98.9	0.1	0.5	98.9
Papio			96.6	3.4	96.6
Macaca		0.1	2.5	97.4	97.4

Table 6 - Results of step-wise cross-validated discriminant analysis with subsampling using first 32 principal components that accounted for over 95% of total sample variance from PCA in tangent space with dataset of 460 non-hominin primates. Mean percentage classification accuracy across the 1000 subsamples (n=8) is shown by taxon. Specimens were classified into species groups, and overall species classification accuracy was 75.4%. See table 1 for list of abbreviations

	GB	*GG*	*PP*	*PT*	*PA*	*PC*	*PK*	*MFa*	*MFu*	*MM*	Species
GB	83.8	10.8	1.2	4.1					0.1		83.8
GG	12.0	83.9	0.4	2.1	1.1	0.1	0.1		0.2	0.1	83.9
PP	0.3	0.1	81.6	17.7			0.2				81.6
PT	1.1	0.9	17.6	78.3	0.1	0.4	0.7	0.2	0.1	0.7	78.3
PA		0.5		0.1	69.2	15.5	12.2	0.6	0.8	1.2	69.2
PC					14.0	56.4	19.3	1.1	4.4	4.8	56.4
PK					4.8	6.9	85.9	0.8	0.3	1.2	85.9
MFa		0.1	0.1	0.2	0.8	1.2	1.4	68.3	13.8	14.1	68.3
MFu				0.1	0.7	2.3	0.4	14.2	72.1	10.2	72.1
MM	0.1	0.1		0.1	1.8	4.2	2.3	8.8	7.9	74.8	74.8

Table 7 - Results of step-wise cross-validated discriminant analysis with subsampling using first 32 principal components that accounted for over 95% of total sample variance from PCA in tangent space with dataset of 460 non-hominin primates. Mean percentage classification accuracy across the 1000 subsamples (n=4) is shown by taxon. Specimens were classified into subspecies groups where possible, and overall subspecies accuracy was 45.2%. See table 1 for list of abbreviations

	GBB	*GBG*	*GGD*	*GGG*	*PP*	*PTT*	*PTS*	*PTV*	*PTE*	*PA*	*PC*	*PK*	*MFa*	*MFuF*	*MFuY*	*MM*	Subspecies
GBB	42.7	24.5	11.5	11.0	0.8	1.9	1.0	1.8	1.6	0.2	0.3	0.3	0.6	0.6	0.7	0.7	42.7
GBG	12.6	63.3	5.0	5.8	1.1	2.0	2.1	2.7	3.7	0.2	0.2	0.1	0.3	0.3	0.3	0.6	63.3
GGD	10.3	5.5	57.2	17.6	0.4	2.3	0.7	1.1	0.6	1.7	0.4	0.5	0.4	0.4	0.4	0.8	57.2
GGG	11.7	7.9	20.5	49.3	0.6	1.8	0.7	1.8	1.0	1.7	0.5	0.9	0.4	0.3	0.4	0.7	49.3
PP	0.5	0.8	0.3	0.3	50.3	9.6	11.7	10.8	11.7	0.4	0.9	1.1	0.6	0.2	0.4	0.6	
PTT	1.0	1.3	1.6	1.3	7.9	44.6	13.7	10.4	12.1	0.7	1.4	0.4	0.8	0.9	0.6	1.4	44.6
PTS	0.3	1.2	0.6	0.3	10.3	15.0	38.3	13.2	17.4	0.5	1.1	0.4	0.6	0.2	0.3	0.5	38.3
PTV	0.7	1.6	0.9	0.9	10.0	11.4	13.9	35.5	22.4	0.8	0.7	0.3	0.3	0.3	0.2	0.3	35.5
PTE	0.3	1.8	0.3	0.5	14.7	10.4	14.9	22.4	30.7	0.7	0.7	0.3	0.9	0.6	0.5	0.6	30.7
PA	0.3	0.3	1.1	1.0	0.5	0.7	0.4	0.5	0.6	54.8	18.3	12.5	1.8	2.1	2.7	2.5	
PC	0.1	0.2	0.3	0.3	0.8	1.3	0.6	0.5	0.6	15.6	43.7	17.3	2.6	8.5	4.1	3.7	
PK	0.2	0.1	0.2	0.3	0.6	0.2	0.4	0.5	0.2	5.7	9.7	74.7	2.3	1.7	0.9	2.6	
MFa	0.5	0.3	0.3	0.4	0.8	1.3	0.6	0.2	0.5	2.8	3.4	3.5	47.6	12.3	11.4	14.0	
MFuF	0.9	0.1	0.2	0.5	0.2	1.3	0.2	0.1	0.3	1.8	3.2	2.3	13.7	36.1	27.6	11.5	36.1
MFuY	0.2	0.1	0.1	0.2	0.1	0.3	0.1	0.1	0.2	2.7	2.7	1.1	8.4	22.7	54.6	6.6	54.6
MM	0.7	0.4	0.7	0.7	0.6	1.2	0.4	0.2	0.4	2.5	5.1	4.6	10.5	11.9	8.1	52.2	

Hominins

Group Morphology

Large differences, reflected by a mean pairwise PrD of 0.127 (see table S23), were found between the average *Homo sapiens* and *Homo neanderthalensis* shapes (figure 8). *Homo sapiens* had taller frontal squamae, which were more vertically aligned, their orbits were more anteriorly placed, and their supraorbital tori were narrower mediolaterally. In addition, *Homo sapiens* had more superiorly placed nasion landmarks and thinner supraorbital trigones in comparison to *Homo neanderthalensis*. The shape differences were even larger between *Homo erectus sensu lato* and *Homo sapiens* (mean pairwise PrD: 0.172), with the latter having parallel frontal squamae and lateral aspects of the supraorbital tori, thin supraorbital trigones, high, vertical frontal squamae, more superiorly located nasion points, and less protruding supraorbital tori. The differences between the mean *Homo neanderthalensis* and *Homo erectus sensu lato* configurations were less visible (mean pairwise PrD: 0.117), with *Homo neanderthalensis* having slightly taller and more vertical frontal squamae, less anteriorly projecting supraorbital tori, and slightly thinner, less laterally flaring supraorbital trigones.

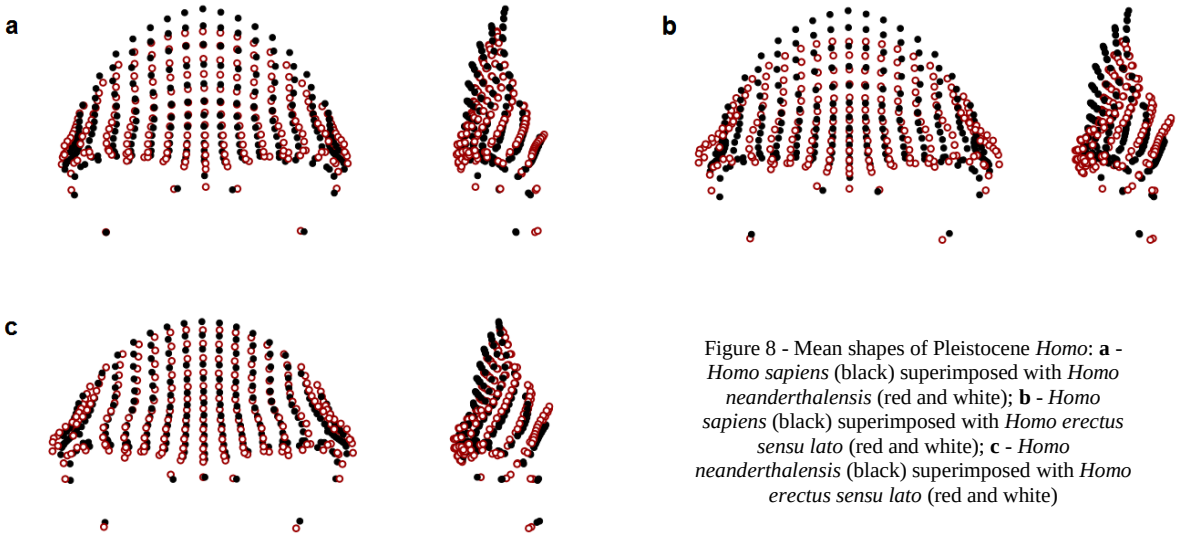

Figure 8 - Mean shapes of Pleistocene *Homo*: **a** - *Homo sapiens* (black) superimposed with *Homo neanderthalensis* (red and white); **b** - *Homo sapiens* (black) superimposed with *Homo erectus sensu lato* (red and white); **c** - *Homo neanderthalensis* (black) superimposed with *Homo erectus sensu lato* (red and white)

Comparisons between early *Homo* and related hominins are shown in figure 9. The *Homo rudolfensis* specimen (KNM-ER 1470) showed a more superoinferiorly bulging frontal squama in comparison to the *Homo habilis* specimens (mean pairwise PrD of 0.100), with more inferiorly placed orbits, and a more superiorly located nasion. *Homo naledi* showed closer affinities to early *Homo* in the PCA plots (and especially to KNM-ER 3733 and OH 24), and lower mean pairwise PrD to *Homo erectus sensu lato* and *Homo rudolfensis* (0.118 and 0.119, respectively) in particular despite its Middle Pleistocene age, so it is also considered here. DH1 had a slightly taller supraorbital torus than the mean *Homo*

habilis shape, with much more angled orbits which were also wider, and a shorter frontal squama. *Homo habilis* had a more angled frontal squama in this orientation (i.e. a narrower angle between mid-frontotemporale-nasion-orbitale) than that found in the *Australopithecus africanus* specimen (Sts 5; mean pairwise PrD of 0.114), as well as more superiorly placed orbits and inferior supraorbital torus, and a mediolaterally wider frontal squama.

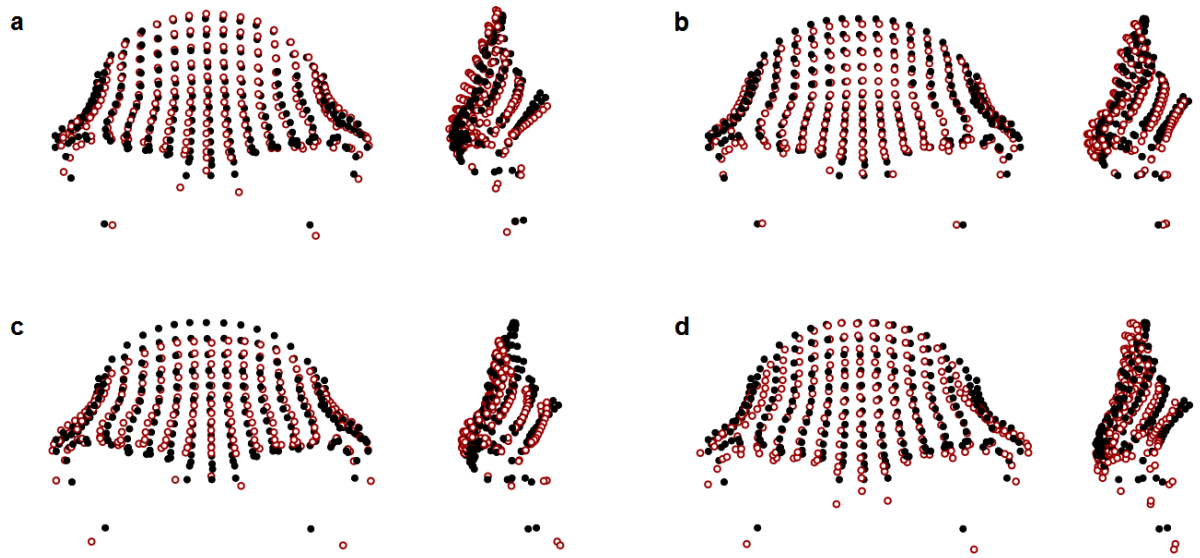

Figure 9 - Mean shapes of early *Homo* and related hominins: **a** - *Homo habilis* (black) superimposed with *Homo rudolfensis* (red and white); **b** - *Homo habilis* (black) superimposed with *Homo erectus sensu lato* (red and white); **c** - *Homo habilis* (black) superimposed with *Homo naledi* (red and white); **d** - *Homo habilis* (black) superimposed with *Australopithecus africanus* (red and white)

There are fairly large visible shape differences between Sts 5 and the *Paranthropus aethiopicus* specimen (KNM-WT 17000; figure 10), reflected in the mean pairwise PrD of 0.133. For instance, KNM-WT 17000 had thick, laterally flaring, and posteriorly rotated supraorbital trigones, and a lower frontal squama than Sts 5. Differences between the *Paranthropus* species were less pronounced (mean pairwise PrD: 0.116): *Paranthropus boisei* was found to have less posteriorly rotated supraorbital trigones, slightly more vertical frontal squamae, slightly wider orbits and nasal columns, and slightly more anteriorly projecting supraorbital tori than seen in *Paranthropus aethiopicus*. Caution must be taken when interpreting these results, due to the low sample sizes available for the earlier hominins.

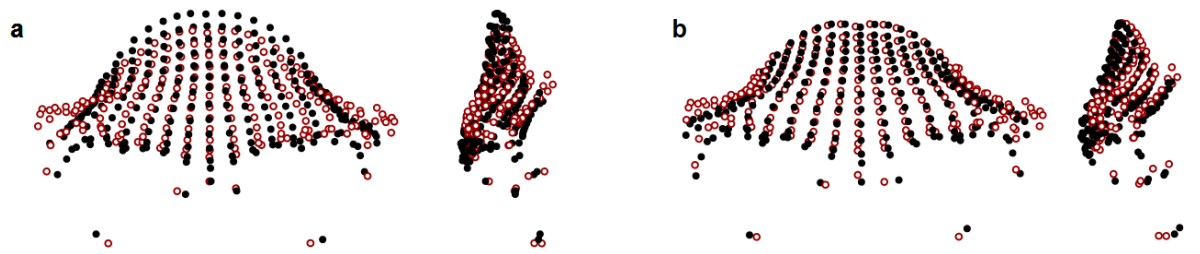

Figure 10 - Mean shapes of *Australopithecus* and *Paranthropus* specimens: **a** - *Australopithecus africanus* (black) superimposed with *Paranthropus aethiopicus* (red and white); **b** - *Paranthropus aethiopicus* (black) superimposed with *Paranthropus boisei* (red and white)

Principal Component Analysis

PCA in tangent space resulted in 54 principal components, with the first 17 accounting for over 95% of the total sample variance combined, and the first 10 accounting for >1% of variance individually. Figure 11 shows a plot of specimens by PC1 and PC2, accounting for 55.5% and 11.1% of variance, respectively. PC1 broadly corresponded with robusticity of the supraorbital region, with the more robust specimens (e.g. *Paranthropus*) having more negative values along this axis, and the more gracile *Homo sapiens* having the most positive values. Positive values corresponded to taller and more curved frontal squamae which occupied a larger area of the recorded morphology, minimal expression of the supraorbital tori in all dimensions, an absence of a supraorbital sulcus, a relatively superiorly positioned nasion, and a higher degree of orbital frontation. PC2 separated the early *Homo sapiens*, *Homo neanderthalensis*, MPH, and *Homo erectus sensu lato*, which had lower values along this axis, from the later *Homo sapiens* and earlier hominins. Specimens with higher values were associated with more laterally flaring supraorbital trigones, less projecting supraorbital tori with minimal post-toral sulci, more vertical frontal squamae, lower positions of dacryon points, and more vertically oriented orbits. *Homo sapiens* had the highest values along PC1 and PC2, with some earlier members (Omo 1, Jebel Irhoud 1, and Skhūl V) falling within the *Homo neanderthalensis* convex hull due to their lower values on PC1. The *Homo erectus sensu lato* specimens were separated from *Homo neanderthalensis* due to their relatively lower values along PC1. The MPH largely overlapped with the *Homo erectus sensu lato*, although they fell more towards the *Homo erectus sensu stricto* end of the convex hull, due to their higher values along PC1.

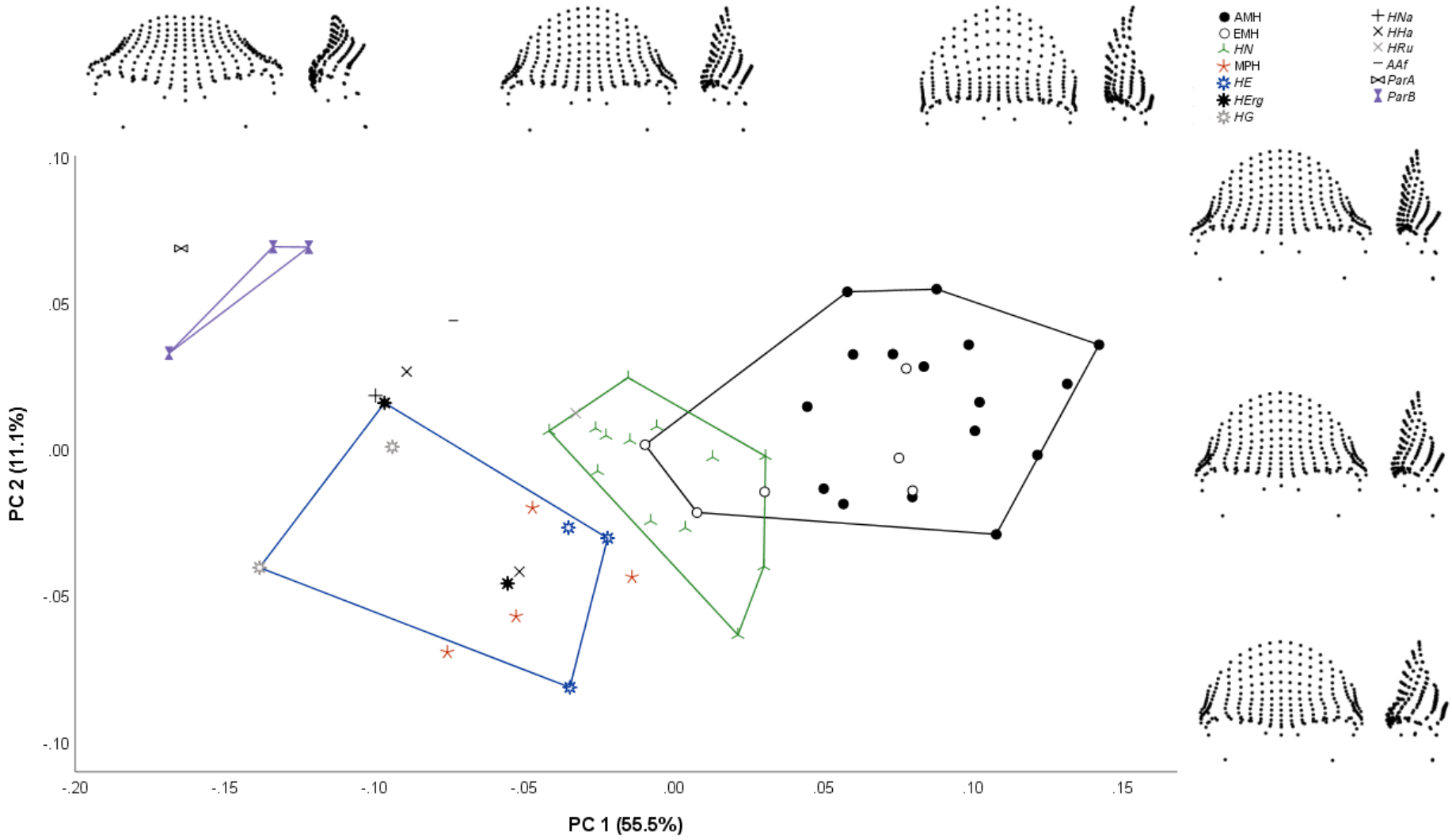

Figure 11 - Plot of PC1 (x-axis) and PC2 (y-axis), accounting for 66.3% of variation, for PCA in tangent space using sample of 55 Pleistocene hominin specimens. Specimens are identified by symbols shown in legend. See table 2 for list of abbreviations. Convex hulls are shown and correspond to species groups: black - *Homo sapiens*; green - *Homo neanderthalensis*; blue - *Homo erectus sensu lato*; purple - *Paranthropus boisei*. Shape changes are shown for minimum, median, and maximum sample values for both axes, in frontal and left lateral view

Discriminant Analysis

The results of the hominin tangent space discriminant analysis are shown in table 8. Species classification accuracy was 87.3% across the 1000 subsamples. Classification accuracy was highest for *Homo neanderthalensis* (92.2%) and *Homo sapiens* (87.6%), followed by *Homo erectus sensu lato* (82.3%). 20 of the 22 *Homo sapiens* were classified correctly in the majority of repeats (table S24), although Skhūl V was only correctly classified in 47.2% of subsamples in which it was randomly selected (and was classified as *Homo neanderthalensis* in 39.3% of cases). Jebel Irhoud 1 and Omo 1 were most frequently classified as *Homo neanderthalensis* (in 73.6% and 48.7% of cases, respectively). All of the *Homo neanderthalensis* and *Homo erectus sensu lato* were most frequently correctly classified when included in subsample repeats. OH 24 was classified as *Homo habilis* in 49.0% of subsamples, while KNM-ER 1813 was classified as *Homo erectus sensu lato* in 64.1% of cases, reflecting its placement in the PC plot.

Table 8 - Results of step-wise cross-validated discriminant analysis with sampling using first 17 principal components that accounted for over 95% of total sample variance from PCA in tangent space with dataset of 48 hominins. Mean percentage classification accuracy across the 1000 subsamples (n=7 except for the MPH where n=4 and *Homo habilis* where n=2) is shown. Specimens were classified into species groups, and overall species classification accuracy was 87.3%. MPH and *Homo habilis* were excluded from this figure due to uncertain taxonomic status and small sample size, respectively. See table 2 for list of abbreviations

	HS	*HN*	MPH	*HEsl*	*HHa*	Species
HS	87.6	9.1	2.1	0.9	0.3	87.6
HN	3.3	92.2	1.0	3.6		92.2
MPH	0.2	15.8	67.3	12.0	4.8	67.3
HEsl		7.3	5.2	82.3	5.2	
HHa		3.3	11.3	47.4	38.1	38.1

Discussion

A proper understanding of biological variation is fundamental to the study of evolutionary processes, however the accurate documentation of phenotypic variation in the fossil record is particularly challenging due to its fragmentary nature. Studies have found that different elements of the primate craniofacial complex have varying levels of effectiveness in differentiating groups at different taxonomic levels (Bjarnason, Chamberlain, & Lockwood, 2011; Bjarnason, Soligo, & Elton, 2015, 2017; Cardini & Elton, 2008a; Lockwood, Kimbel, & Lynch, 2004; von Cramon-Taubadel & Smith, 2012). As such, it is important to establish the extent to which aspects of the craniofacial morphology that are relatively well documented in the fossil record reflect taxonomic differentiation in extant primates. The supraorbital torus is one such region, being particularly well-preserved in the hominin fossil record, potentially due to the robusticity of this cranial superstructure.

This study identified notable differences between accepted non-hominin primate taxa in the recorded morphology, indicating that the primate supraorbital region can be used in taxonomic differentiation. Larger differences were noted at the genus level, although this varied between families and analyses; *Pan* and *Gorilla* were more separated in the principal component plots than *Papio* and *Macaca*, although all genera showed relatively high biological distinctiveness (97.5% in tangent space). Differences between species were less substantial (75.4% in tangent space), especially in the case of *Papio cynocephalus*, *Papio anubis*, and *Macaca fascicularis*. Differences between non-hominin primate subspecies were even more subtle, with several subspecies groups being fully encompassed within other closely-related subspecies in terms of key principal components, and with subspecies groups having lower biological distinctiveness (45.2% in tangent space).

This pattern of increasing biological distinctiveness with increasing taxonomic rank is not unexpected. Subspecies are considered by some to be incipient species, populations which have begun to diverge from their conspecifics but which have not achieved full speciation and are genetically reticulate (Boggs, 2001; Groves, 2004; Mayr, 1982; Simpson, 1961). As such, the morphological divergence between subspecies groups is predicted to be lower than that between fully diverged species. Species, in contrast, are considered by many researchers to reflect biological entities (Balakrishnan, 2005; Cracraft, 1983; Eldredge & Cracraft, 1980; Ghiselin, 1974; Tattersall, 1992), and should therefore be expected to have more distinct boundaries than those between subspecies (Simpson, 1961). Genera are classified among the higher taxa, and in turn are expected to show a greater degree of biological divergence (Tattersall, 2017).

It is important to put the biological distinctiveness of the catarrhine supraorbital region into its wider context. Genus-level results were very similar to those found for hairy armadillos (weighted average of 98.5% classification accuracy; Abba et al., 2015), although no comparable studies could be found within the primates. The values for species-level analyses were comparable to those found for marmots (87.4%; Cardini et al., 2009) and *Cercopithecus* (88.3%; Cardini & Elton, 2008b), at least for the non-hominin apes, but lower than those for red colobus monkeys (97.0%; Cardini & Elton, 2011) and hairy armadillos (94.1%; Abba et al., 2015). For subspecies-level analyses, the values of the present study lay between those for marmots (36.6%; Cardini et al., 2009) and red colobus monkeys (80.1%; Cardini & Elton, 2011). Nevertheless, comparisons to other studies are imperfect as some used anatomical landmarks across the cranium and mandible (Cardini & Elton, 2008b, 2011), rather than focusing on specific areas of the craniofacial complex. As studies indicate that different craniofacial regions may differentially preserve phylogenetic histories (Bjarnason et al., 2011; Bjarnason et al., 2015; von Cramon-Taubadel, 2009), it could be predicted that they may also preserve different taxonomic signals. Future research could investigate the taxonomic utility of other well-

represented regions, such as the temporal bone and basicranium, to further contextualise the results of the current study.

As shown by the group morphologies, differences between non-hominin primate and hominin taxa in supraorbital morphology are frequently subtle, especially in the case of the lower taxa (i.e. species and subspecies). Despite this, the above discriminant analyses resulted in relatively high classification accuracy in some groups. This contrasting result highlights the efficacy of geometric methods which allow quantitative analysis of morphology, especially when differences between taxa may be difficult to detect through qualitative assessment of craniofacial morphology. Regardless of whether primate subspecies are sufficiently biological distinct, at least in the supraorbital region, and the ability of geometric morphometric methods to distinguish between these groups, researchers have suggested that the likelihood of having sufficient samples of primate fossil specimens to identify subspecific distinctions is low (Kimbel, 1991; Simpson, 1943, 1961; Tattersall, 1986, 1992).

Analyses were performed in tangent, form (with size added as a variable), and allometry-free (with the effect of allometric scaling removed) shape space. Taxonomic differentiation was found to be highest in tangent space, as shown by the higher rates of biological distinctiveness of known taxa, indicating that tangent space may be more useful for primate taxonomic differentiation when considering the supraorbital region. This was somewhat unexpected, as form space has been hypothesised to be preferable when size is integral to the morphology under assessment, including classification studies such as this one which include organisms that vary in both size and shape (Mitteroecker and Gunz, 2009; Mitteroecker et al., 2013). The results of the present study did note comparable levels of taxonomic differentiation between form and tangent space analysis at the genus level, which could support this argument as size differences are less pronounced within the genera studied. However, several of the taxa analysed here are characterised by pronounced levels of sexual dimorphism and, hence, intraspecific size variation, which is likely to blur taxonomic distinctiveness based on size. As such, future work should explore the possibility that form space might more accurately distinguish between taxa that lack pronounced levels of sexual dimorphism.

The *Papio kindae* specimens were found to be more clearly separated from *Papio anubis* than *Papio cynocephalus* in principal component plots, and had higher biological distinctiveness. This may be partially affected by the relatively small size of the *Papio cynocephalus* sample, as research indicates that *Papio kindae* and *Papio cynocephalus* are more closely related to each other than they are to *Papio anubis* (Jolly, Burrell, Phillips-Conroy, Bergey, & Rogers, 2011; Zinner et al., 2009; Zinner et al., 2013), although this does not adequately explain the difference in biological distinctiveness as subsampling would have mitigated against differences in sample size. An alternative hypothesis is that this distinction is affected by the smaller physical size of *Papio kindae*, which are suggested to be

paedomorphic in comparison to *Papio cynocephalus* (Dunn, Cardini, & Elton, 2013; Frost et al., 2003; Singleton, Seitelman, Krecioch, & Frost, 2017). Tangent space, while unaffected by isometric scaling, can be influenced by allometry. *Papio kindae* specimens were distinguished in terms of the key components of morphology in both form and allometry-free shape space (see Supplementary Information), indicating that their biological distinctiveness in the supraorbital region may be unrelated to any allometric scaling.

Macaca fuscata yakui was found to have higher biological distinctiveness than *Macaca fuscata fuscata* overall (although not in form space), which is contrary to the fact that genetic data indicate low differentiation of this group relative to other populations of *Macaca fuscata* not currently given subspecific status (Marmi, Bertranpetit, Terradas, Takenaka, & Domingo-Roura, 2004). Biological distinctiveness was higher for the *Macaca fuscata* subspecies in form space, unlike all other non-hominin primate subspecies studied here. Research has shown that *Macaca fuscata yakui* is the smaller of the two subspecies (Napier, 1981; Yano, Egi, Takano, & Ogihara, 2018), indicating that further research into allometric differences between these taxa is required.

Of the *Pan troglodytes* subspecies, *Pan troglodytes troglodytes* was found to have the highest biological distinctiveness in supraorbital morphology, while *Pan troglodytes ellioti* had the lowest. Genetic analysis has indicated that the first phylogenetic split within *Pan troglodytes* was between *Pan troglodytes schweinfurthii* and *Pan troglodytes troglodytes* on the one hand, and *Pan troglodytes ellioti* and *Pan troglodytes verus* on the other (Prado-Martinez et al., 2013). This phylogenetic pattern was not reflected in the supraorbital morphology, with the largest distinction being found between *Pan troglodytes schweinfurthii* and *Pan troglodytes troglodytes*. These subspecies appear to have diverged later on than *Pan troglodytes ellioti* and *Pan troglodytes verus*, although there is more substantial genetic evidence to support their subspecific status, while the separation of *Pan troglodytes ellioti* is more debated (de Manuel et al., 2016; Lobon et al., 2016; Stone et al., 2010).

The largest differences between closely related species and subspecies, as measured by pairwise-Procrustes distances, were found within *Gorilla*. While genetic evidence indicates considerable differentiation between the two *Gorilla* species, it also shows that hybridisation between *Gorilla* taxa occurred until fairly recently (Ackermann & Bishop, 2010; Thalmann, Fischer, Lankester, Pääbo, & Vigilant, 2007; Thalmann et al., 2011). Lower levels of biological distinctiveness were found for *Gorilla beringei beringei* in comparison to *Gorilla beringei graueri* in all shape space analyses. While both subspecies are known to have complicated phylogenetic histories, including periods of hybridisation, previous analysis indicates that only the latter group show evidence of this in their craniodental morphology (Ackermann & Bishop, 2010). In addition, *Gorilla beringei beringei* have relatively small habitats with few remaining individuals, and show strong evidence of inbreeding

(Fossey, 1983; Xue et al., 2015), which would be expected to lead to higher homogeneity in craniofacial morphology. Further analysis is required to confirm whether this pattern of inter-subspecific biological distinctiveness is consistent across the craniofacial complex.

The biological distinctiveness of the supraorbital morphology of *Homo sapiens* and *Homo neanderthalensis* was higher than that of all of the non-hominin primate species, and the value for *Homo erectus sensu lato* was comparable to the highest of those for the non-hominin primate species. This is somewhat unexpected, as the inclusion of individuals from across the lifespan and geographical range of a species may blur the boundaries between species, although not in all cases (Baab, 2016). In addition, the inclusion of the Middle Pleistocene hominins, which may include transitional and early members of these middle and later *Homo* species, could have been predicted to reduce the biological distinctiveness of these taxa. The relatively high biological distinctiveness for *Homo erectus sensu lato* is also surprising due to the considerably wider time range from which these specimens were sampled, and the ongoing taxonomic debate around this group (Antón, 2003; Baab, 2008; Baab, 2016; Bilsborough, 2005; Etler, 2004; Lordkipanidze et al., 2013; Rightmire, Lordkipanidze, & Vekua, 2006). The effect of low sample sizes for early *Homo* limits interpretation of the frequent misclassification of the KNM-ER 1813 specimen.

The results of the present study would indicate that the hominin supraorbital region is particularly taxonomically informative relative to the wider catarrhine primates. This could be in part due to the higher variability, particularly in the supraorbital torus, in hominins, as well as the later changes in the frontal squama seen in modern *Homo sapiens*. The supraorbital torus has been acquired, lost, and modified in various populations of hominins (Lahr & Wright, 1996), and has been shown to document distinctive morphologies between species (Athreya, 2006, 2012; Fiscella & Smith, 2006; Gonzalez, Perez, & Bernal, 2010; Lahr & Wright, 1996; Lieberman, 2000; Moss & Young, 1960; Russell, 1985; Schwartz & Tattersall, 2010; Smith & Ranyard, 1980; Weidenreich, 1947). At present, few studies have assessed the evolutionary significance of the hominin brow ridge. The fossils included in the present study indicate that there may have been a transition from a more general hominid form (protruding, bar-like supraorbital tori that are short superoinferiorly) in earlier hominins such as *Australopithecus*, to a more variable form in *Homo* (e.g. the swollen, rounded tori in *Homo neanderthalensis* and MPH), potentially linked to the latter groups increased orthognathy, relatively high levels of craniofacial robusticity, and associated large cranial superstructures (Gonzalez et al., 2010; Lieberman, 2011; Weidenreich, 1941).

This study supported the suggestion of previous studies that *Homo sapiens* are particularly distinct in their frontal bone morphology (Athreya, 2009; Bruner, Athreya, de la Cuétara, & Marks, 2013; Godinho, Spikins, & O'Higgins, 2018; Kurten, 1979; Lieberman, 2000; Russell, 1985; Schwartz &

Tattersall, 2010; Smith & Ranyard, 1980). This distinction appears to be due to the minimally expressed supraorbital torus in our species, along with our tall, bulging frontal squamae. Nevertheless, earlier members of *Homo sapiens* were found to overlap with *Homo neanderthalensis*, and Jebel Irhoud 1 and Omo 1 were more frequently misclassified as *Homo neanderthalensis* in the discriminant analysis. This is likely due to the presence of more plesiomorphic browridges in earlier *Homo sapiens* (Hublin et al., 2017; Lahr & Wright, 1996; Lieberman, 2000; Russell, 1985; Tattersall & Schwartz, 2008), although the possibility of interbreeding has also been raised in the case of the Jebel Irhoud assemblage (Mounier & Mirazón Lahr, 2019).

Homo neanderthalensis has been described as one of the most clearly defined and delineated extinct hominin species (Tattersall, 1992; Tattersall & Schwartz, 2006; White, Gowlett, & Grove, 2014), and the results of this study would seem to support this conclusion. While DNA analyses have shown that *Homo neanderthalensis* and *Homo sapiens* interbred on a number of occasions (Green et al., 2010; Prüfer et al., 2014; Racimo, Sankararaman, Nielsen, & Huerta-Sanchez, 2015; Sankararaman et al., 2014; Sankararaman, Patterson, Li, Pääbo, & Reich, 2012), this interbreeding does not seem to have led to increased similarity in the supraorbital morphology of these taxa, at least in the specimens studied here. Indeed, the results of the current study would support the specific status of *Homo neanderthalensis* (White et al., 2014). This group had a biological distinctiveness comparable to, and even somewhat higher than, that of *Homo sapiens*, along with a higher proportion of the sample being most frequently correctly classified across the subsamples. These groups were also clearly separated in terms of key morphology.

Conclusion

This study found that supraorbital morphology can be used to differentiate between closely-related, extant non-hominin primate genera, species, and subspecies, although with a reduced accuracy in the latter taxon. Hypothesised late Middle-to-Late Pleistocene hominin species were found to have relatively higher biological distinctiveness in this region than the extant catarrhine non-hominin primate species, while the *Homo erectus sensu lato* specimens had biological distinctiveness which was comparable to the higher range of the non-hominin catarrhine species. Overall, the results support the use of supraorbital morphology to assess the taxonomic affiliation of fossil hominins and catarrhines of unknown or debated taxonomy, and suggest that hominin taxa may be more readily distinguished by their morphology in this region. Future studies should explore the different aspects of the supraorbital morphology recorded here to determine which are the most useful for taxonomic differentiation, and compare the efficacy of supraorbital morphology to that of other regions suggested to reflect phylogeny, such as the temporal bone and basicranium.

Acknowledgements

The authors would like to thank the following curators for allowing access to the specimens in their collections: C. Stringer, R. Kruszynski, and R. Ives (Natural History Museum, London); M. Mirazon-Lahr and M. Belatti (Duckworth Laboratory, University of Cambridge); G. Garcia and E. Hoeger (American Museum of Natural History, New York); E. Gilissen (Royal Museum for Central Africa, Tervuren); K. Hussey and C. Phillips (Royal College of Surgeons, London); I. Livne (Powell Cotton Museum, Kent); H. Hashimoto (Kyoto University Museum, Kyoto); D. Shimizu (Kyoto University Primate Research Institute, Kyoto); P. Semal (Royal Belgian Institute of Natural Sciences, Brussels); S. Bond (Institute of Archaeology, UCL, London); G. Price (Biological Anthropology Collection, UCL, London); K. Helgen (Division of Mammals, Smithsonian, Washington); M. Tocheri (Human Origins Program, Smithsonian, Washington). The authors are grateful to A. Gleeson for his assistance with the coding of statistical analyses, A. Gomez-Robles for her constructive advice on drafts of this manuscript, and to two anonymous reviewers for their insightful comments.

This study was supported by an AHRC/LAHP-funded studentship, grant reference number AH/L503873/1.

Data Availability Statement

The data that support the findings of this study are available from the corresponding author upon reasonable request.

References

Abba, A. M., Cassini, G. H., Valverde, G., Tilak, M.-K., Vizcaíno, S. F., Superina, M., & Delsuc, F. (2015). Systematics of hairy armadillos and the taxonomic status of the Andean hairy armadillo (Chaetophractus nationi). *Journal of Mammalogy, 96*(4), 673-689. doi:10.1093/jmammal/gyv082

Ackermann, R. R. (2002). Patterns of covariation in the hominoid craniofacial skeleton: Implications for paleoanthropological models. *Journal of Human Evolution, 43*(2), 167-187. doi:10.1006/jhev.2002.0569

Ackermann, R. R., & Bishop, J. M. (2010). Morphological and molecular evidence reveals recent hybridization between *Gorilla* taxa. *Evolution, 64*(1), 271-290. doi:10.1111/j.1558-5646.2009.00858.x

Adams, D. C., Otárola-Castillo, E., & Paradis, E. (2013). Geomorph: An R package for the collection and analysis of geometric morphometric shape data. *Methods in Ecology and Evolution, 4*(4), 393-399. doi:10.1111/2041-210x.12035

Aiello, L., & Dean, C. (1990). *Introduction to Human Evolutionary Anatomy*. London: Academic Press.

Alberts, S. C., & Altmann, J. (2001). Immigration and hybridization patterns of yellow and anubis baboons in and around Amboseli, Kenya. *American Journal of Primatology, 53*(4), 139-154. doi:10.1002/ajp.1

Antón, S. C. (2003). Natural history of *Homo erectus*. *American Journal of Physical Anthropology, 122*(S37), 126-170. doi:10.1002/ajpa.10399

Athreya, S. (2006). Patterning of geographic variation in Middle Pleistocene *Homo* frontal bone morphology. *Journal of Human Evolution, 50*(6), 627-643. doi:10.1016/j.jhevol.2005.11.005

Athreya, S. (2009). A comparative study of frontal bone morphology among Pleistocene hominin fossil groups. *Journal of Human Evolution, 57*(6), 786-804. doi:10.1016/j.jhevol.2009.09.003

Athreya, S. (2012). The frontal bone in the genus *Homo*: a survey of functional and phylogenetic sources of variation. *Journal of Anthropological Science, 90*, 59-80. doi:10.4436/jass.90008

Baab, K. L. (2008). The taxonomic implications of cranial shape variation in *Homo erectus*. *Journal of Human Evolution, 54*(6), 827-847. doi:10.1016/j.jhevol.2007.11.003

Baab, K. L. (2016). The role of neurocranial shape in defining the boundaries of an expanded *Homo erectus* hypodigm. *Journal of Human Evolution, 92*, 1-21. doi:10.1016/j.jhevol.2015.11.004

Balakrishnan, R. (2005). Species concepts, species boundaries and species identification: A view from the tropics. *Systematic Biology, 54*(4), 689-693. doi:10.1080/10635150590950308

Berger, L. R., Hawks, J., de Ruiter, D. J., Churchill, S. E., Schmid, P., Delezene, L. K., . . . Zipfel, B. (2015). *Homo naledi*, a new species of the genus *Homo* from the Dinaledi Chamber, South Africa. *eLife, 4*, e09560. doi:10.7554/eLife.09560

Bilsborough, A. (2005). *Homo erectus* revisited: Aspects of affinity and diversity in a Pleistocene hominin species. *Anthropologie, 43*(2-3), 129-158.

Bjarnason, A., Chamberlain, A. T., & Lockwood, C. A. (2011). A methodological investigation of hominoid craniodental morphology and phylogenetics. *Journal of Human Evolution, 60*(1), 47-57. doi:10.1016/j.jhevol.2010.08.005

Bjarnason, A., Soligo, C., & Elton, S. (2015). Phylogeny, ecology, and morphological evolution in the Atelid cranium. *International Journal of Primatology, 36*(3), 513-529. doi:10.1007/s10764-015-9839-z

Bjarnason, A., Soligo, C., & Elton, S. (2017). Phylogeny, phylogenetic inference, and cranial evolution in pitheciids and Aotus. *American Journal of Primatology, 79*(3), e22621. doi:10.1002/ajp.22621

Boggs, C. L. (2001). Species and speciation. In N. Smelser & P. Baltes (Eds.), *International Encyclopedia of the Social and Behavioral Sciences* (pp. 14855-14861). Oxford: Elsevier.

Bruner, E., Athreya, S., de la Cuétara, J. M., & Marks, T. (2013). Geometric variation of the frontal squama in the genus *Homo*: Frontal bulging and the origin of modern human morphology. *American Journal of Physical Anthropology, 150*(2), 313-323. doi:10.1002/ajpa.22202

Buck, L. T., & Stringer, C. B. (2014). *Homo heidelbergensis*. *Current Biology, 24*(6), R214-215. doi:10.1016/j.cub.2013.12.048

Cardini, A., & Elton, S. (2008a). Does the skull carry a phylogenetic signal? Evolution and modularity in the guenons. *Biological Journal of the Linnean Society, 93*(4), 813-834. doi:10.1111/j.1095-8312.2008.01011.x

Cardini, A., & Elton, S. (2008b). Variation in guenon skulls (I): Species divergence, ecological and genetic differences. *Journal of Human Evolution, 54*(5), 615-637. doi:10.1016/j.jhevol.2007.09.022

Cardini, A., & Elton, S. (2011). GeMBiD, a Geometric Morphometric Approach to the Study of Biological Diversity: An Example Study of the Red Colobus (Procolobus [Piliocolobus]) Species Complex. *International Journal of Primatology, 32*(2), 377-389. doi:10.1007/s10764-010-9475-6

Cardini, A., Nagorsen, D., O'Higgins, P., Polly, P. D., Thorington, R. W., & Tongiorgi, P. (2009). Detecting biological distinctiveness using geometric morphometrics: An example case from the Vancouver Island marmot. *Ethology Ecology & Evolution, 21*(3-4), 209-223. doi:10.1080/08927014.2009.9522476

Cracraft, J. (1983). Species concepts and speciation analysis. *Current Ornithology, 1*, 159-187. doi:10.1007/978-1-4615-6781-3_6

Cramon-Taubadel, N. v. (2013). Congruence of cranial and genetic estimates of Old World primate phylogeny. In L. E. John Wiley & Sons (Ed.), *eLS* (pp. doi:10.1002/9780470015902.a9780470024959).

de Manuel, M., Kuhlwilm, M., Frandsen, P., Sousa, V. C., Desai, T., Prado-Martinez, J., . . . Marques-Bonet, T. (2016). Chimpanzee genomic diversity reveals ancient admixture with bonobos. *354*(6311), 477-481. doi:10.1126/science.aag2602 %J Science

Delson, E. (1978). Models of early hominid phylogeny. In C. J. Jolly (Ed.), *Early Hominids of Africa* (pp. 517-541). London: Duckworth.

DeVore, I. W., S.I. (1963). Baboon ecology and human evolution. In F. Bourlière & F. C. Howell (Eds.), *African Ecology and Human Evolution* (pp. 335-367). Chicago: Aldine.

Dirks, P. H. G. M., Roberts, E. M., Hilbert-Wolf, H., Kramers, J. D., Hawks, J., Dosseto, A., . . . Berger, L. R. (2017). The age of *Homo naledi* and associated sediments in the Rising Star Cave, South Africa. *eLife, 6*, e24231. doi:10.7554/eLife.24231

Dos Reis, M., Gunnell, G. F., Barba-Montoya, J., Wilkins, A., Yang, Z., & Yoder, A. D. (2018). Using phylogenomic data to explore the effects of relaxed clocks and calibration strategies on divergence time estimation: Primates as a test case. *Systematic Biology, 67*(4), 594-615. doi:10.1093/sysbio/syy001

Dryden, I. L., & Mardia, K. V. (1998). *Statistical Shape Analysis*. Chichester: Wiley-Blackwell.

Dunn, J., Cardini, A., & Elton, S. (2013). Biogeographic variation in the baboon: Dissecting the cline. *Journal of Anatomy, 223*(4), 337-352. doi:10.1111/joa.12085

Eldredge, N., & Cracraft, J. (1980). *Phylogenetic Patterns and the Evolutionary Process*. New York: Columbia University Press.

Etler, D. A. (2004). *Homo erectus* in East Asia: Human ancestor or evolutionary dead-end? *Athena Review, 4*(1), 37-50.

Fedorov, A., Beichel, R., Kalpathy-Cramer, J., Finet, J., Fillion-Robin, J. C., Pujol, S., . . . Kikinis, R. (2012). 3D Slicer as an image computing platform for the Quantitative Imaging Network. *Magn Reson Imaging, 30*(9), 1323-1341. doi:10.1016/j.mri.2012.05.001

Fiscella, G. N., & Smith, F. H. (2006). Ontogenetic study of the supraorbital region in modern humans: A longitudinal test of the spatial model. *Anthropologischer Anzeiger, 64*(2), 147-160. doi:10.1127/anthranz/64/2006/147

Fossey, D. (1983). *Gorillas in the Mist*. Boston, Mass.: Houghton Mifflin.

Frost, S. R., Marcus, L. F., Bookstein, F. L., Reddy, D. P., & Delson, E. (2003). Cranial allometry, phylogeography, and systematics of large-bodied Papionins (Primates: Cercopithecinae) inferred from geometric morphometric analysis of landmark data. *The Anatomical Record Part A: Discoveries in Molecular, Cellular, and Evolutionary Biology, 275*(2), 1048-1072. doi:10.1002/ar.a.10112

Garvin, H. M., Elliott, M. C., Delezene, L. K., Hawks, J., Churchill, S. E., Berger, L. R., & Holliday, T. W. (2017). Body size, brain size, and sexual dimorphism in *Homo naledi* from the Dinaledi Chamber. *Journal of Human Evolution, 111*(Supplement C), 119-138. doi:10.1016/j.jhevol.2017.06.010

Ghiselin, M. T. (1974). A radical solution to the species problem. *Systematic Zoology, 23*(4), 536-544. doi:10.2307/2412471

Glazko, G. V., & Nei, M. (2003). Estimation of divergence times for major lineages of primate species. *Molecular Biology and Evolution, 20*(3), 424-434. doi:10.1093/molbev/msg050

Godinho, R. M., Spikins, P., & O'Higgins, P. (2018). Supraorbital morphology and social dynamics in human evolution. *Nature Ecology & Evolution, 2*(6), 956-961. doi:10.1038/s41559-018-0528-0

Gonzalez, P. N., Perez, S. I., & Bernal, V. (2010). Ontogeny of robusticity of craniofacial traits in modern humans: A study of South American populations. *American Journal of Physical Anthropology, 142*(3), 367-379. doi:10.1002/ajpa.21231

Green, R. E., Green, J., Krause, A. W., Briggs, T., Maricic, U., Stenzel, M., . . . Reich, S. (2010). A draft sequence of the Neandertal genome. *Science, 328*(5979), 710-722. doi:10.1126/science.1188021

Groves, C. (2004). The what, why and how of primate taxonomy. *International Journal of Primatology, 25*(5), 1105-1126. doi:10.1023/b:ijop.0000043354.36778.55

Gunz, P. (2005). *Statistical and geometric reconstruction of hominid crania: Reconstructing australopithecine ontogeny.* (PhD). University of Vienna, Vienna.

Gunz, P., & Mitteroecker, P. (2013). Semilandmarks: A method for quantifying curves and surfaces. *Hystrix, the Italian Journal of Mammalogy, 24*(1), 103-109. doi:10.4404/hystrix-24.1-6292

Harvati, K. (2007). 100 years of *Homo heidelbergensis* - Life and times of a controversial taxon. *Mitteilungen der Gesellschaft für Urgeschichte, 16*, 85-94.

Harvati, K., Frost, S. R., & McNulty, K. P. (2004). Neanderthal taxonomy reconsidered: Implications of 3D primate models of intra- and interspecific differences. *Proceedings of the National Academy of Sciences, 101*(5), 1147-1152. doi:10.1073/pnas.0308085100

Hawks, J., & Berger, L. R. (2016). The impact of a date for understanding the importance of *Homo naledi*. *Transactions of the Royal Society of South Africa, 71*(2), 125-128. doi:10.1080/0035919X.2016.1178186

Hublin, J. J. (2013). The Middle Pleistocene record. In *A Companion to Paleoanthropology* (pp. 517-537). Chichester: Blackwell Publishing Ltd.

Hublin, J. J., Ben-Ncer, A., Bailey, S. E., Freidline, S. E., Neubauer, S., Skinner, M. M., . . . Gunz, P. (2017). New fossils from Jebel Irhoud, Morocco and the pan-African origin of *Homo sapiens*. *Nature, 546*(7657), 289-292. doi:10.1038/nature22336

Jiménez-Arenas, J. M., Palmqvist, P., & Pérez-Claros, J. A. (2011). A probabilistic approach to the craniometric variability of the genus *Homo* and inferences on the taxonomic affinities of the first human population dispersing out of Africa. *Quaternary International, 243*(1), 219-230. doi:10.1016/j.quaint.2011.02.024

Jolly, C. (1970). The seed-eaters: A new model of hominid differentiation based on a baboon analogy. *Man, 5*(1), 5-26. doi:10.2307/2798801

Jolly, C. J. (2001). A proper study for mankind: Analogies from the papionin monkeys and their implications for human evolution. *American Journal of Physical Anthropology, 116*(S33), 177-204. doi:10.1002/ajpa.10021

Jolly, C. J., Burrell, A. S., Phillips-Conroy, J. E., Bergey, C., & Rogers, J. (2011). Kinda baboons (*Papio kindae*) and grayfoot chacma baboons (*P. ursinus griseipes*) hybridize in the Kafue river valley, Zambia. *American Journal of Primatology, 73*(3), 291-303. doi:10.1002/ajp.20896

Kimbel, W. H. (1991). Species, species concepts and hominid evolution. *Journal of Human Evolution, 20*(355-371). doi:10.1016/0047-2484(91)90016-O

Kurten, B. (1979). The shadow of the brow. *Current Anthropology, 20*(1), 229-230. doi:10.1086/202246

Lahr, M., & Wright, R. V. S. (1996). The question of robusticity and the relationship between cranial size and shape in *Homo sapiens*. *Journal of Human Evolution, 31*(2), 157-191. doi:10.1006/jhev.1996.0056

Laird, M. F., Schroeder, L., Garvin, H. M., Scott, J. E., Dembo, M., Radovčić, D., . . . de Ruiter, D. J. (2017). The skull of *Homo naledi*. *Journal of Human Evolution, 104*, 100-123. doi:10.1016/j.jhevol.2016.09.009

Langergraber, K. E., Prüfer, K., Rowney, C., Boesch, C., Crockford, C., Fawcett, K., . . . Vigilant, L. (2012). Generation times in wild chimpanzees and gorillas suggest earlier divergence times in great ape and human evolution. *Proceedings of the National Academy of Sciences, 109*(39), 15716-15721. doi:10.1073/pnas.1211740109

Lieberman, D. (2000). Ontogeny, homology, and phylogeny in the hominid craniofacial skeleton: The problem of the browridge. In P. O'Higgins & M. J. Cohn (Eds.), *Development, Growth and Evolution* (pp. 85-122). London: Academic Press.

Lieberman, D. E. (1995). Testing hypotheses about recent human evolution from skulls: Integrating morphology, function, development, and phylogeny. *Current Anthropology, 36*(2), 159-197. doi:10.1086/204348

Lieberman, D. E. (2011). *The Evolution of the Human Head*. United States of America: The Belknap Press of Harvard University Press.

Lobon, I., Tucci, S., de Manuel, M., Ghirotto, S., Benazzo, A., Prado-Martinez, J., . . . Marques-Bonet, T. (2016). Demographic history of the genus *Pan* inferred from whole mitochondrial genome reconstructions. *Genome Biology and Evolution, 8*(6), 2020-2030. doi:10.1093/gbe/evw124

Lockwood, C. A. (1996). Randomization procedures and sexual dimorphism in *Australopithecus afarensis*. *Journal of Human Evolution, 31*(6), 537-548. doi:10.1006/jhev.1996.0078

Lockwood, C. A. (1999). Sexual dimorphism in the face of *Australopithecus africanus*. *American Journal of Physical Anthropology, 108*(1), 97-127. doi:10.1002/(SICI)1096-8644(199901)108:1<97::AID-AJPA6>3.0.CO;2-O

Lockwood, C. A., Kimbel, W. H., & Lynch, J. M. (2004). Morphometrics and hominoid phylogeny: Support for a chimpanzee–human clade and differentiation among great ape subspecies. *Proceedings of the National Academy of Sciences, 101*(13), 4356-4360. doi:10.1073/pnas.0306235101

Lockwood, C. A., Lynch, J. M., & Kimbel, W. H. (2002). Quantifying temporal bone morphology of great apes and humans: An approach using geometric morphometrics. *Journal of Anatomy, 201*(6), 447-464. doi:10.1046/j.1469-7580.2002.00122.x

Lordkipanidze, D., Lordkipanidze, M. S., Margvelashvili, Y., Margvelashvili, Y., Rak, G. P., Rightmire, A., & Zollikofer. (2013). A complete skull from Dmanisi, Georgia, and the evolutionary biology of early *Homo*. *Science, 342*(6156), 326-331. doi:10.1126/science.1238484

Marmi, J., Bertranpetit, J., Terradas, J., Takenaka, O., & Domingo-Roura, X. (2004). Radiation and phylogeography in the Japanese macaque, *Macaca fuscata*. *Molecular Phylogenetics and Evolution, 30*(3), 676-685. doi:10.1016/S1055-7903(03)00247-1

Mayr, E. (1982). Of what use are subspecies? *The Auk, 99*(3), 593-595. doi:10.1093/auk/99.3.593a

McNulty, K. P. (2005). A geometric morphometric assessment of the hominoid supraorbital region: affinities of the Eurasian Miocene hominoids *Dryopithecus*, *Graecopithecus*, and *Sivapithecus*. In D. E. Slice (Ed.), *Modern Morphometrics in Physical Anthropology* (pp. 349-373). New York: Kluwer Academic/Plenum Publishers.

Mitteroecker, P., & Gunz, P. (2009). Advances in geometric morphometrics. *Evolutionary Biology, 36*(2), 235-247. doi:10.1007/s11692-009-9055-x

Mitteroecker, P., Gunz, P., Windhager, S., & Schaefer, K. (2013). A brief review of shape, form, and allometry in geometric morphometrics, with applications to human facial morphology. *Hystrix, the Italian Journal of Mammalogy, 24*(1), 59-66. doi:10.4404/hystrix-24.1-6369

Moss, M. L., & Young, R. W. (1960). A functional approach to craniology. *American Journal of Physical Anthropology, 18*(4), 281-292. doi:10.1002/ajpa.1330180406

Mounier, A., & Mirazón Lahr, M. (2019). Deciphering African late middle Pleistocene hominin diversity and the origin of our species. *Nature Communications, 10*(1), 3406. doi:10.1038/s41467-019-11213-w

Napier, P. H. (1981). *Catalogue of Primates in the British Museum (Natural History) and elsewhere in the British Isles. Part II: Family Cercopithecidae, Subfamily Cercopithecinae*. London: Natural History Museum Publications.

O'Higgins, P. (2000). The study of morphological variation in the hominid fossil record: Biology, landmarks and geometry. *Journal of Anatomy, 197*(1), 103-120. doi:10.1046/j.1469-7580.2000.19710103.x

O'Higgins, P., & Dryden, I. L. (1993). Sexual dimorphism in hominoids - Further studies of craniofacial shape differences in *Pan*, *Gorilla* and *Pongo*. *Journal of Human Evolution, 24*(3), 183-205. doi:10.1006/jhev.1993.1014

Pan, R., & Oxnard, C. (2004). Craniodental variation in the African macaque, with reference to various Asian species. *Folia Primatologica, 75*(6), 355-375. doi:10.1159/000081016

Pan, R., Oxnard, C., & Milne, N. (2002). Mandibular variation among Chinese macaques. *American Journal of Primatology, 56*(2), 99-115. doi:10.1002/ajp.1067

Pan, R., & Oxnard, C. E. (2002). Craniodental variation among Macaques (*Macaca*), nonhuman primates. *BMC Evolutionary Biology, 2*(1), 10. doi:10.1186/1471-2148-2-10

Perelman, P., Johnson, W. E., Roos, C., Seuánez, H. N., Horvath, J. E., Moreira, M. A. M., . . . Pecon-Slattery, J. (2011). A molecular phylogeny of living primates. *PLOS Genetics, 7*(3), e1001342. doi:10.1371/journal.pgen.1001342

Plavcan, J. M. (2012). Body size, size variation, and sexual size dimorphism in Early *Homo*. *Current Anthropology, 53*(S6), S409-S423. doi:10.1086/667605

Prado-Martinez, J., Sudmant, P. H., Kidd, J. M., Li, H., Kelley, J. L., Lorente-Galdos, B., . . . Marques-Bonet, T. (2013). Great ape genetic diversity and population history. *Nature, 499*, 471. doi:10.1038/nature12228

Prüfer, K., Racimo, F., Patterson, N., Jay, F., Sankararaman, S., Sawyer, S., . . . Paabo, S. (2014). The complete genome sequence of a Neanderthal from the Altai Mountains. *Nature, 505*(7481), 43-49. doi:10.1038/nature12886

Racimo, F., Sankararaman, S., Nielsen, R., & Huerta-Sanchez, E. (2015). Evidence for archaic adaptive introgression in humans. *Nature Reviews Genetics, 16*(6), 359-371. doi:10.1038/nrg3936

Richmond, B. G., & Jungers, W. L. (1995). Size variation and sexual dimorphism in *Australopithecus afarensis* and living hominoids. *Journal of Human Evolution, 29*(3), 229-245. doi:10.1006/jhev.1995.1058

Rightmire, G. P., Lordkipanidze, D., & Vekua, A. (2006). Anatomical descriptions, comparative studies and evolutionary significance of the hominin skulls from Dmanisi, Republic of Georgia. *Journal of Human Evolution, 50*(2), 115-141. doi:10.1016/j.jhevol.2005.07.009

Rohlf, F. J. (1999). Shape statistics: Procrustes superimposition and Tangent Space. *Journal of Classification, 16*, 197-223. doi:10.1007/s003579900054

Rohlf, F. J., & Slice, D. (1990). Extensions of the Procrustes method for the optimal superimposition of landmarks. *Systematic Zoology, 39*(1), 40-59. doi:10.2307/2992207

Royer, D. F., Lockwood, C. A., Scott, J. E., & Grine, F. E. (2009). Size variation in early human mandibles and molars from Klasies River, South Africa: Comparison with other middle and late Pleistocene assemblages and with modern humans. *American Journal of Physical Anthropology, 140*(2), 312-323. doi:10.1002/ajpa.21071

Russell, M. D. (1985). The supraorbital torus: "A most remarkable peculiarity". *Current Anthropology, 26*(3), 337-360. doi:10.1086/203279

Sankararaman, S., Mallick, S., Dannemann, M., Prufer, K., Kelso, J., Paabo, S., . . . Reich, D. (2014). The genomic landscape of Neanderthal ancestry in present-day humans. *Nature, 507*(7492), 354-357. doi:10.1038/nature12961

Sankararaman, S., Patterson, N., Li, H., Pääbo, S., & Reich, D. (2012). The date of interbreeding between Neandertals and Modern humans. *PLOS Genetics, 8*(10), e1002947. doi:10.1371/journal.pgen.1002947

Schaefer, K., Mitteroecker, P., Gunz, P., Bernhard, M., & Bookstein, F. L. (2004). Craniofacial sexual dimorphism patterns and allometry among extant hominids. *Annals of Anatomy - Anatomischer Anzeiger, 186*(5), 471-478. doi:10.1016/S0940-9602(04)80086-4

Schrago, C. G., & Voloch, C. M. (2013). The precision of the hominid timescale estimated by relaxed clock methods. *Journal of Evolutionary Biology, 26*(4), 746-755. doi:10.1111/jeb.12076

Schroeder, L., Scott, J. E., Garvin, H. M., Laird, M. F., Dembo, M., Radovčić, D., . . . Ackermann, R. R. (2017). Skull diversity in the *Homo* lineage and the relative position of *Homo naledi*. *Journal of Human Evolution, 104*, 124-135. doi:10.1016/j.jhevol.2016.09.014

Schwartz, J. H., & Tattersall, I. (2010). Fossil evidence for the origin of *Homo sapiens*. *American Journal of Physical Anthropology, 143*(Suppl 51), 94-121. doi:10.1002/ajpa.21443

Simpson, G. G. (1943). Criteria for genera, species, and subspecies in zoology and paleozoology. *Annals of the New York Academy of Sciences, 44*(2), 145-178. doi:10.1111/j.1749-6632.1943.tb31301.x

Simpson, G. G. (1961). *Principles of Animal Taxonomy*. New York: Columbia University Press

Singleton, M., Seitelman, B. C., Krecioch, J. R., & Frost, S. R. (2017). Cranial sexual dimorphism in the Kinda baboon (*Papio hamadryas kindae*). *American Journal of Physical Anthropology, 164*(4), 665-678. doi:10.1002/ajpa.23304

Smith, A. B. (1994). *Systematics and the Fossil Record: Documenting Evolutionary Patterns*. New York: Columbia University Press

Smith, F. H., & Ranyard, G. C. (1980). Evolution of the supraorbital region in Upper Pleistocene fossil hominids from south-central Europe. *American Journal of Physical Anthropology, 53*(4), 589-610. doi:10.1002/ajpa.1330530414

Smith, H. F. (2009). Which cranial regions reflect molecular distances reliably in humans? Evidence from three-dimensional morphology. *American Journal of Human Biology, 21*(1), 36-47. doi:10.1002/ajhb.20805

Stone, A. C., Battistuzzi, F. U., Kubatko, L. S., Perry, G. H., Trudeau, E., Lin, H., & Kumar, S. (2010). More reliable estimates of divergence times in *Pan* using complete mtDNA sequences and accounting for population structure. *Philosophical Transactions of the Royal Society B: Biological Sciences, 365*(1556), 3277-3288. doi:10.1098/rstb.2010.0096

Stringer, C. B. (2012). The status of *Homo heidelbergensis* (Schoetensack 1908). *Evolutionary Anthropology: Issues, News, and Reviews, 21*(3), 101-107. doi:10.1002/evan.21311

Stringer, C. B., Howell, F. C., & Melentis, J. K. (1979). The significance of the fossil hominid skull from Petralona, Greece. *American Journal of Physical Anthropology, 50*(3), 485. doi:10.1016/0305-4403(79)90002-5

Tattersall, I. (1986). Species recognition in human paleontology. *Journal of Human Evolution, 15*(3), 165-175. doi:10.1016/S0047-2484(86)80043-4

Tattersall, I. (1992). Species concepts and species identification in human evolution. *Journal of Human Evolution, 22*(4-5), 341-349. doi:10.1016/0047-2484(92)90064-G

Tattersall, I. (2005). Species concepts and hominid diversity in Later Pleistocene Europe. *Anthropologie (Brno), 43*(2-3), 207-213.

Tattersall, I. (2017). Species, genera, and phylogenetic structure in the human fossil record: a modest proposal. *Evolutionary Anthropology: Issues, News, and Reviews, 26*(3), 116-118. doi:10.1002/evan.21523

Tattersall, I., & Schwartz, J. H. (2006). The distinctiveness and systematic context of *Homo neanderthalensis*. In K. Harvati & T. Harrison (Eds.), *Neanderthals Revisited: New Approaches and Perspectives* (pp. 9-22). Dordrecht: Springer.

Tattersall, I., & Schwartz, J. H. (2008). The morphological distinctiveness of *Homo sapiens* and its recognition in the fossil record: Clarifying the problem. *Evolutionary Anthropology: Issues, News, and Reviews, 17*(1), 49-54. doi:10.1002/evan.20153

Thalmann, O., Fischer, A., Lankester, F., Pääbo, S., & Vigilant, L. (2007). The complex evolutionary history of gorillas: Insights from genomic data. *Molecular Biology and Evolution, 24*(1), 146-158. doi:10.1093/molbev/msl160

Thalmann, O., Wegmann, D., Spitzner, M., Arandjelovic, M., Guschanski, K., Leuenberger, C., . . . Vigilant, L. (2011). Historical sampling reveals dramatic demographic changes in western gorilla populations. *BMC Evolutionary Biology, 11*, 85-85. doi:10.1186/1471-2148-11-85

von Cramon-Taubadel, N. (2009). Congruence of individual cranial bone morphology and neutral molecular affinity patterns in modern humans. *American Journal of Physical Anthropology, 140*(2), 205-215. doi:10.1002/ajpa.21041

von Cramon-Taubadel, N., & Smith, H. F. (2012). The relative congruence of cranial and genetic estimates of hominoid taxon relationships: Implications for the reconstruction of hominin phylogeny. *Journal of Human Evolution, 62*(5), 640-653. doi:10.1016/j.jhevol.2012.02.007

Weidenreich, F. (1941). The brain and its role in the phylogenetic transformation of the human skull. *Transactions of the American Philosophical Society, 31*(5), 320-442. doi:10.2307/1005610

Weidenreich, F. (1947). Facts and speculations concerning the origin of *Homo sapiens*. *American Anthropologist, 49*(2), 187-203. doi:10.1525/aa.1947.49.2.02a00010

White, S., Gowlett, J. A. J., & Grove, M. (2014). The place of the Neanderthals in hominin phylogeny. *Journal of Anthropological Archaeology, 35*, 32-50. doi:10.1016/j.jaa.2014.04.004

Wilkinson, R. D., Steiper, M. E., Soligo, C., Martin, R. D., Yang, Z., & Tavaré, S. (2011). Dating primate divergences through an integrated analysis of palaeontological and molecular data. *Systematic Biology, 60*(1), 16-31. doi:10.1093/sysbio/syq054

Wood, B. A. (2010). Systematics, taxonomy, and phylogenetics: Ordering life, past and present. In *A Companion to Biological Anthropology* (pp. 56-73): Wiley-Blackwell.

Wood, B. A., Li, Y., & Willoughby, C. (1991). Intraspecific variation and sexual dimorphism in cranial and dental variables among higher primates and their bearing on the hominid fossil record. *Journal of Anatomy, 174*, 185-205.

Xue, Y., Prado-Martinez, J., Sudmant, P. H., Narasimhan, V., Ayub, Q., Szpak, M., . . . Scally, A. (2015). Mountain gorilla genomes reveal the impact of long-term population decline and inbreeding. *Science, 348*(6231), 242-245. doi:10.1126/science.aaa3952

Yano, W., Egi, N., Takano, T., & Ogihara, N. (2018). Subspecies and sexual craniofacial size and shape variations in Japanese macaques (*Macaca fuscata*). *bioRxiv*, 467456. doi:10.1101/467456

Zinner, D., Groeneveld, L. F., Keller, C., & Roos, C. (2009). Mitochondrial phylogeography of baboons (*Papio spp.*): Indication for introgressive hybridization? *BMC Evolutionary Biology, 9*, 83. doi:10.1186/1471-2148-9-83

Zinner, D., Wertheimer, J., Liedigk, R., Groeneveld, L. F., & Roos, C. (2013). Baboon phylogeny as inferred from complete mitochondrial genomes. *American Journal of Physical Anthropology, 150*(1), 133-140. doi:10.1002/ajpa.22185

Supplementary Information

SI-1: Details of Specimens

Non-Hominin Primate Specimens

Table S1 - Details of non-hominin primate specimens, showing taxonomic classification, institution, sex, type of data used, and whether the specimen required reconstruction for the purposes of this study

Reference	Taxonomic Classification	Institution	Sex	Cranium/CT	Reconstruction
RMCA 2263	*Gorilla beringei beringei*	RMCA	F	Cranium	N
USNM 545026	*Gorilla beringei beringei*	Smithsonian	F	Cranium	Y
USNM 545027	*Gorilla beringei beringei*	Smithsonian	F	Cranium	N
USNM 545029	*Gorilla beringei beringei*	Smithsonian	F	CT	Y
USNM 545030	*Gorilla beringei beringei*	Smithsonian	F	CT	Y
USNM 545031	*Gorilla beringei beringei*	Smithsonian	F	Cranium	N
RMCA 2257	*Gorilla beringei beringei*	RMCA	M	Cranium	N
RMCA 2260	*Gorilla beringei beringei*	RMCA	M	Cranium	N
USNM 395636	*Gorilla beringei beringei*	Smithsonian	M	Cranium	Y
USNM 396934	*Gorilla beringei beringei*	Smithsonian	M	Cranium	Y
USNM 545028	*Gorilla beringei beringei*	Smithsonian	M	Cranium	Y
USNM 545034	*Gorilla beringei beringei*	Smithsonian	M	Cranium	Y
USNM 545035	*Gorilla beringei beringei*	Smithsonian	M	Cranium	Y
ZD.1922.2.10.1	*Gorilla beringei beringei*	NHM	M?	Cranium	N
RMCA 812	*Gorilla beringei graueri*	RMCA	F	Cranium	Y
RMCA 995	*Gorilla beringei graueri*	RMCA	F	Cranium	N
RMCA 11725	*Gorilla beringei graueri*	RMCA	F	Cranium	N
RMCA 14769	*Gorilla beringei graueri*	RMCA	F	Cranium	N
RMCA 15352	*Gorilla beringei graueri*	RMCA	F	Cranium	N
RMCA 15353	*Gorilla beringei graueri*	RMCA	F	Cranium	N
RMCA 15355	*Gorilla beringei graueri*	RMCA	F	Cranium	N
RMCA 15356	*Gorilla beringei graueri*	RMCA	F	Cranium	N
RMCA 15357	*Gorilla beringei graueri*	RMCA	F	Cranium	N
RMCA 15363	*Gorilla beringei graueri*	RMCA	F	Cranium	N
RMCA 21533	*Gorilla beringei graueri*	RMCA	F	Cranium	N
RMCA 21534	*Gorilla beringei graueri*	RMCA	F	Cranium	N
RMCA 22904	*Gorilla beringei graueri*	RMCA	F	Cranium	N
RMCA 27839	*Gorilla beringei graueri*	RMCA	F	Cranium	N
RMCA 27840	*Gorilla beringei graueri*	RMCA	F	Cranium	N
RMCA 29102	*Gorilla beringei graueri*	RMCA	F	Cranium	N
RMCA 29104	*Gorilla beringei graueri*	RMCA	F	Cranium	Y
RMCA 29538	*Gorilla beringei graueri*	RMCA	F	Cranium	Y
RMCA 31132	*Gorilla beringei graueri*	RMCA	F	Cranium	N
RMCA 31133	*Gorilla beringei graueri*	RMCA	F	Cranium	N
RMCA 34476	*Gorilla beringei graueri*	RMCA	F	Cranium	N
USNM 260582	*Gorilla beringei graueri*	Smithsonian	F	CT	Y
RMCA 86.044 M13	*Gorilla beringei graueri*	RMCA	F?	Cranium	N
RMCA 804	*Gorilla beringei graueri*	RMCA	M	Cranium	N
RMCA 994	*Gorilla beringei graueri*	RMCA	M	Cranium	N
RMCA 999	*Gorilla beringei graueri*	RMCA	M	Cranium	N
RMCA 1000	*Gorilla beringei graueri*	RMCA	M	Cranium	N

RMCA 1001	*Gorilla beringei graueri*	RMCA	M	Cranium	N
RMCA 8187	*Gorilla beringei graueri*	RMCA	M	Cranium	N
RMCA 18739	*Gorilla beringei graueri*	RMCA	M	Cranium	N
RMCA 22762	*Gorilla beringei graueri*	RMCA	M	Cranium	N
RMCA 22763	*Gorilla beringei graueri*	RMCA	M	Cranium	N
RMCA 22905	*Gorilla beringei graueri*	RMCA	M	Cranium	N
RMCA 29099	*Gorilla beringei graueri*	RMCA	M	Cranium	N
RMCA 29100	*Gorilla beringei graueri*	RMCA	M	Cranium	N
RMCA 29103	*Gorilla beringei graueri*	RMCA	M	Cranium	N
RMCA 31131	*Gorilla beringei graueri*	RMCA	M	Cranium	N
RMCA 86.044-M-0014	*Gorilla beringei graueri*	RMCA	M	Cranium	N
RMCA 86.044-M-0016	*Gorilla beringei graueri*	RMCA	M	Cranium	N
RMCA 9220	*Gorilla beringei graueri*	RMCA	M	Cranium	Y
ZD.1929.11.29.1	*Gorilla beringei graueri*	NHM	M	Cranium	N
USNM 590946	*Gorilla gorilla diehli*	Smithsonian	F	Cranium	Y
USNM 590947	*Gorilla gorilla diehli*	Smithsonian	F	Cranium	Y
USNM 590948	*Gorilla gorilla diehli*	Smithsonian	F	Cranium	Y
USNM 590951	*Gorilla gorilla diehli*	Smithsonian	F	Cranium	Y
USNM 590956	*Gorilla gorilla diehli*	Smithsonian	F	Cranium	Y
USNM 590957	*Gorilla gorilla diehli*	Smithsonian	F	Cranium	N
USNM 590963	*Gorilla gorilla diehli*	Smithsonian	F	Cranium	Y
ZD.1986.758	*Gorilla gorilla diehli*	NHM	F	Cranium	N
ZD.1939.918	*Gorilla gorilla diehli*	NHM	F?	Cranium	N
USNM 590950	*Gorilla gorilla diehli*	Smithsonian	M	Cranium	Y
USNM 590953	*Gorilla gorilla diehli*	Smithsonian	M	Cranium	Y
USNM 590955	*Gorilla gorilla diehli*	Smithsonian	M	Cranium	Y
USNM 590958	*Gorilla gorilla diehli*	Smithsonian	M	Cranium	Y
USNM 590959	*Gorilla gorilla diehli*	Smithsonian	M	Cranium	Y
USNM 590967	*Gorilla gorilla diehli*	Smithsonian	M	Cranium	Y
USNM 590968	*Gorilla gorilla diehli*	Smithsonian	M	Cranium	Y
ZD.1939.913	*Gorilla gorilla diehli*	NHM	M	Cranium	N
ZD.1939.916	*Gorilla gorilla diehli*	NHM	M?	Cranium	N
Cameroon I 139	*Gorilla gorilla gorilla*	Powell Cotton Museum	F	Cranium	N
Cameroon I 96	*Gorilla gorilla gorilla*	Powell Cotton Museum	F	Cranium	N
French Congo 208	*Gorilla gorilla gorilla*	Powell Cotton Museum	F	Cranium	N
French Congo 217	*Gorilla gorilla gorilla*	Powell Cotton Museum	F	Cranium	N
Merfield 139	*Gorilla gorilla gorilla*	Powell Cotton Museum	F	Cranium	N
Merfield 786	*Gorilla gorilla gorilla*	Powell Cotton Museum	F	Cranium	Y
USNM 220380	*Gorilla gorilla gorilla*	Smithsonian	F	CT	Y
USNM 252575	*Gorilla gorilla gorilla*	Smithsonian	F	Cranium	Y
USNM 252576	*Gorilla gorilla gorilla*	Smithsonian	F	Cranium	Y
USNM 252577	*Gorilla gorilla gorilla*	Smithsonian	F	CT	Y
USNM 252579	*Gorilla gorilla gorilla*	Smithsonian	F	Cranium	Y
USNM 252580	*Gorilla gorilla gorilla*	Smithsonian	F	Cranium	Y
ZD.1857.11.2.3 1011c	*Gorilla gorilla gorilla*	NHM	F	Cranium	N
ZD.1907.1.8.4	*Gorilla gorilla gorilla*	NHM	F	Cranium	N
ZD.1907.1.8.5	*Gorilla gorilla gorilla*	NHM	F	Cranium	N
ZD.1907.1.8.7	*Gorilla gorilla gorilla*	NHM	F	Cranium	N
ZD.1923.11.29.8	*Gorilla gorilla gorilla*	NHM	F	Cranium	N
ZD.1939.907	*Gorilla gorilla gorilla*	NHM	F	Cranium	N
ZD.1939.927	*Gorilla gorilla gorilla*	NHM	F	Cranium	N
ZD.1939.935	*Gorilla gorilla gorilla*	NHM	F	Cranium	N
ZD.1939.936	*Gorilla gorilla gorilla*	NHM	F	Cranium	N
ZD.1948.3.31.1	*Gorilla gorilla gorilla*	NHM	F	Cranium	N

ZD.1949.664	*Gorilla gorilla gorilla*	NHM	F	Cranium	N
ZD.1951.9.27.14	*Gorilla gorilla gorilla*	NHM	F	Cranium	N
ZD.1989.329	*Gorilla gorilla gorilla*	NHM	F?	Cranium	N
F.C.130	*Gorilla gorilla gorilla*	Powell Cotton Museum	M	Cranium	Y
Merfield 28	*Gorilla gorilla gorilla*	Powell Cotton Museum	M	Cranium	N
Merfield 372	*Gorilla gorilla gorilla*	Powell Cotton Museum	M	Cranium	N
USNM 174714	*Gorilla gorilla gorilla*	Smithsonian	M	Cranium	Y
USNM 176207	*Gorilla gorilla gorilla*	Smithsonian	M	Cranium	Y
USNM 176209	*Gorilla gorilla gorilla*	Smithsonian	M	Cranium	Y
USNM 176213	*Gorilla gorilla gorilla*	Smithsonian	M	CT	Y
USNM 176215	*Gorilla gorilla gorilla*	Smithsonian	M	CT	N
USNM 176216	*Gorilla gorilla gorilla*	Smithsonian	M	Cranium	Y
USNM 220324	*Gorilla gorilla gorilla*	Smithsonian	M	CT	Y
ZD.1878.12.14.1	*Gorilla gorilla gorilla*	NHM	M	Cranium	N
ZD.1913.2.2.1	*Gorilla gorilla gorilla*	NHM	M	Cranium	N
ZD.1925.1.4.1	*Gorilla gorilla gorilla*	NHM	M	Cranium	N
ZD.1935.12.16.1	*Gorilla gorilla gorilla*	NHM	M	Cranium	N
ZD.1935.12.16.2	*Gorilla gorilla gorilla*	NHM	M	Cranium	N
ZD.1939.920	*Gorilla gorilla gorilla*	NHM	M	Cranium	N
ZD.1939.923	*Gorilla gorilla gorilla*	NHM	M	Cranium	N
ZD.1939.924	*Gorilla gorilla gorilla*	NHM	M	Cranium	N
ZD.1939.929	*Gorilla gorilla gorilla*	NHM	M	Cranium	N
ZD.1948.435	*Gorilla gorilla gorilla*	NHM	M	Cranium	N
ZD.1949.603	*Gorilla gorilla gorilla*	NHM	M	Cranium	N
ZD.1949.663	*Gorilla gorilla gorilla*	NHM	M	Cranium	N
Zenker VI 32	*Gorilla gorilla gorilla*	Powell Cotton Museum	M	Cranium	N
ZD.1925.1.4.2	*Gorilla gorilla gorilla*	NHM	M?	Cranium	N
ZD.1939.944	*Gorilla gorilla gorilla*	NHM	M?	Cranium	N
RMCA 28960	*Pan paniscus*	RMCA	?	Cranium	N
RMCA 888	*Pan paniscus*	RMCA	?	Cranium	N
RMCA 84.036-M-0009	*Pan paniscus*	RMCA	?	Cranium	N
RMCA 84.036-M-0010	*Pan paniscus*	RMCA	?	Cranium	N
RMCA 9338	*Pan paniscus*	RMCA	F	Cranium	N
RMCA 11351	*Pan paniscus*	RMCA	F	Cranium	N
RMCA 11352	*Pan paniscus*	RMCA	F	Cranium	N
RMCA 13201	*Pan paniscus*	RMCA	F	Cranium	N
RMCA 15296	*Pan paniscus*	RMCA	F	Cranium	N
RMCA 20882	*Pan paniscus*	RMCA	F	Cranium	N
RMCA 21697	*Pan paniscus*	RMCA	F	Cranium	N
RMCA 26945	*Pan paniscus*	RMCA	F	Cranium	N
RMCA 26947	*Pan paniscus*	RMCA	F	Cranium	N
RMCA 26963	*Pan paniscus*	RMCA	F	Cranium	N
RMCA 26991	*Pan paniscus*	RMCA	F	Cranium	N
RMCA 27012	*Pan paniscus*	RMCA	F	Cranium	N
RMCA 27698	*Pan paniscus*	RMCA	F	Cranium	N
RMCA 29034	*Pan paniscus*	RMCA	F	Cranium	N
RMCA 29035	*Pan paniscus*	RMCA	F	Cranium	N
RMCA 29040	*Pan paniscus*	RMCA	F	Cranium	N
RMCA 29042	*Pan paniscus*	RMCA	F	Cranium	N
RMCA 29045	*Pan paniscus*	RMCA	F	Cranium	N
RMCA 29059	*Pan paniscus*	RMCA	F	Cranium	N
RMCA 29060	*Pan paniscus*	RMCA	F	Cranium	N
RMCA 29065	*Pan paniscus*	RMCA	F	Cranium	N
RMCA 11149	*Pan paniscus*	RMCA	M	Cranium	N

RMCA 13202	*Pan paniscus*	RMCA	M	Cranium	N
RMCA 15294	*Pan paniscus*	RMCA	M	Cranium	N
RMCA 15295	*Pan paniscus*	RMCA	M	Cranium	N
RMCA 20881	*Pan paniscus*	RMCA	M	Cranium	N
RMCA 26939	*Pan paniscus*	RMCA	M	Cranium	N
RMCA 27005	*Pan paniscus*	RMCA	M	Cranium	N
RMCA 27696	*Pan paniscus*	RMCA	M	Cranium	N
RMCA 27699	*Pan paniscus*	RMCA	M	Cranium	N
RMCA 28712	*Pan paniscus*	RMCA	M	Cranium	N
RMCA 29036	*Pan paniscus*	RMCA	M	Cranium	N
RMCA 29037	*Pan paniscus*	RMCA	M	Cranium	N
RMCA 29038	*Pan paniscus*	RMCA	M	Cranium	N
RMCA 29039	*Pan paniscus*	RMCA	M	Cranium	N
RMCA 29050	*Pan paniscus*	RMCA	M	Cranium	N
RMCA 29052	*Pan paniscus*	RMCA	M	Cranium	N
RMCA 29063	*Pan paniscus*	RMCA	M	Cranium	N
RMCA 29064	*Pan paniscus*	RMCA	M	Cranium	N
Merfield 234	*Pan troglodytes ellioti*	Powell Cotton Museum	F	Cranium	N
ZD.1907.7.1.8.8	*Pan troglodytes ellioti*	NHM	F	Cranium	N
ZD.1917.12.16.1	*Pan troglodytes ellioti*	NHM	M	Cranium	N
ZD.1976.1797	*Pan troglodytes ellioti*	NHM	M	Cranium	N
ZD.1979.1798	*Pan troglodytes ellioti*	NHM	M	Cranium	N
M-51205	*Pan troglodytes schweinfurthii*	AMNH	?	Cranium	N
RMCA 12014	*Pan troglodytes schweinfurthii*	RMCA	?	Cranium	N
RMCA 12089	*Pan troglodytes schweinfurthii*	RMCA	?	Cranium	N
RMCA 8341	*Pan troglodytes schweinfurthii*	RMCA	F	Cranium	N
RMCA 9289	*Pan troglodytes schweinfurthii*	RMCA	F	Cranium	N
RMCA 9655	*Pan troglodytes schweinfurthii*	RMCA	F	Cranium	N
RMCA 26989	*Pan troglodytes schweinfurthii*	RMCA	F	Cranium	N
RMCA 29074	*Pan troglodytes schweinfurthii*	RMCA	F	Cranium	N
RMCA 29079	*Pan troglodytes schweinfurthii*	RMCA	F	Cranium	N
RMCA 29080	*Pan troglodytes schweinfurthii*	RMCA	F	Cranium	N
RMCA 29086	*Pan troglodytes schweinfurthii*	RMCA	F	Cranium	N
RMCA 29088	*Pan troglodytes schweinfurthii*	RMCA	F	Cranium	N
RMCA 83.006-M-0032	*Pan troglodytes schweinfurthii*	RMCA	F	Cranium	N
RMCA 83.006-M-0034	*Pan troglodytes schweinfurthii*	RMCA	F	Cranium	N
USNM 236971	*Pan troglodytes schweinfurthii*	Smithsonian	F	Cranium	Y
ZD.1887.12.2.1	*Pan troglodytes schweinfurthii*	NHM	F	Cranium	N
ZD.1920.10.21.4	*Pan troglodytes schweinfurthii*	NHM	F	Cranium	N
ZD.1920.4.13.2	*Pan troglodytes schweinfurthii*	NHM	F	Cranium	N
ZD.1927.1.4.1	*Pan troglodytes schweinfurthii*	NHM	F	Cranium	N
M-51203	*Pan troglodytes schweinfurthii*	AMNH	M	Cranium	N
M-51209	*Pan troglodytes schweinfurthii*	AMNH	M	Cranium	N
M-51278	*Pan troglodytes schweinfurthii*	AMNH	M	Cranium	N
M-51377	*Pan troglodytes schweinfurthii*	AMNH	M	Cranium	N
M-51379	*Pan troglodytes schweinfurthii*	AMNH	M	Cranium	N
M-51381	*Pan troglodytes schweinfurthii*	AMNH	M	Cranium	N
M-51382	*Pan troglodytes schweinfurthii*	AMNH	M	Cranium	N
M-81854	*Pan troglodytes schweinfurthii*	AMNH	M	Cranium	N
Merfield C259	*Pan troglodytes schweinfurthii*	Powell Cotton Museum	M	Cranium	N
ZD.1901.8.9.10	*Pan troglodytes schweinfurthii*	NHM	M	Cranium	N
ZD.1922.12.19.1	*Pan troglodytes schweinfurthii*	NHM	M	Cranium	N
Cameroon 147	*Pan troglodytes troglodytes*	Powell Cotton Museum	F	Cranium	N
Cameroon 204	*Pan troglodytes troglodytes*	Powell Cotton Museum	F	Cranium	N

Cameroon 216	*Pan troglodytes troglodytes*	Powell Cotton Museum	F	Cranium	N
Merfield 169	*Pan troglodytes troglodytes*	Powell Cotton Museum	F	Cranium	N
Merfield 181	*Pan troglodytes troglodytes*	Powell Cotton Museum	F	Cranium	N
Merfield 273	*Pan troglodytes troglodytes*	Powell Cotton Museum	F	Cranium	N
Merfield 352	*Pan troglodytes troglodytes*	Powell Cotton Museum	F	Cranium	N
Merfield 450	*Pan troglodytes troglodytes*	Powell Cotton Museum	F	Cranium	N
Merfield 467	*Pan troglodytes troglodytes*	Powell Cotton Museum	F	Cranium	N
Merfield 475 1st	*Pan troglodytes troglodytes*	Powell Cotton Museum	F	Cranium	N
Merfield 803	*Pan troglodytes troglodytes*	Powell Cotton Museum	F	Cranium	N
Merfield 873	*Pan troglodytes troglodytes*	Powell Cotton Museum	F	Cranium	N
USNM 174701	*Pan troglodytes troglodytes*	Smithsonian	F	CT	Y
USNM 174702	*Pan troglodytes troglodytes*	Smithsonian	F	CT	Y
USNM 174707	*Pan troglodytes troglodytes*	Smithsonian	F	CT	Y
USNM 174710	*Pan troglodytes troglodytes*	Smithsonian	F	CT	Y
USNM 220062	*Pan troglodytes troglodytes*	Smithsonian	F	CT	Y
ZD.1864.12.1.7	*Pan troglodytes troglodytes*	NHM	F	Cranium	N
ZD.1883.7.28.17	*Pan troglodytes troglodytes*	NHM	F	Cranium	N
ZD.1936.7.7.2	*Pan troglodytes troglodytes*	NHM	F	Cranium	N
ZD.1939.3366	*Pan troglodytes troglodytes*	NHM	F	Cranium	N
ZD.1939.3367	*Pan troglodytes troglodytes*	NHM	F	Cranium	N
ZD.1939.3383	*Pan troglodytes troglodytes*	NHM	F	Cranium	N
ZD.1939.957	*Pan troglodytes troglodytes*	NHM	F	Cranium	N
ZD.1939.965	*Pan troglodytes troglodytes*	NHM	F	Cranium	N
Cameroon 200	*Pan troglodytes troglodytes*	Powell Cotton Museum	M	Cranium	N
Cameroon 74	*Pan troglodytes troglodytes*	Powell Cotton Museum	M	Cranium	N
Cameroon II 62	*Pan troglodytes troglodytes*	Powell Cotton Museum	M	Cranium	N
Merfield 254 3rd	*Pan troglodytes troglodytes*	Powell Cotton Museum	M	Cranium	N
Merfield 440	*Pan troglodytes troglodytes*	Powell Cotton Museum	M	Cranium	N
Merfield 984	*Pan troglodytes troglodytes*	Powell Cotton Museum	M	Cranium	N
Merfield 988	*Pan troglodytes troglodytes*	Powell Cotton Museum	M	Cranium	N
USNM 174704	*Pan troglodytes troglodytes*	Smithsonian	M	Cranium	Y
USNM 176228	*Pan troglodytes troglodytes*	Smithsonian	M	Cranium	Y
USNM 176240	*Pan troglodytes troglodytes*	Smithsonian	M	Cranium	Y
USNM 176242	*Pan troglodytes troglodytes*	Smithsonian	M	CT	Y
USNM 220065	*Pan troglodytes troglodytes*	Smithsonian	M	CT	Y
USNM 220326	*Pan troglodytes troglodytes*	Smithsonian	M	CT	Y
USNM 220327	*Pan troglodytes troglodytes*	Smithsonian	M	CT	Y
USNM 599172	*Pan troglodytes troglodytes*	Smithsonian	M	CT	Y
ZD.1924.8.6.1	*Pan troglodytes troglodytes*	NHM	M	Cranium	N
ZD.1939.3362	*Pan troglodytes troglodytes*	NHM	M	Cranium	N
ZD.1939.3363	*Pan troglodytes troglodytes*	NHM	M	Cranium	N
ZD.1939.3365	*Pan troglodytes troglodytes*	NHM	M	Cranium	N
ZD.1939.3369	*Pan troglodytes troglodytes*	NHM	M	Cranium	N
ZD.1939.3370	*Pan troglodytes troglodytes*	NHM	M	Cranium	N
ZD.1986.214	*Pan troglodytes troglodytes*	NHM	M	Cranium	N
Zenker VI 34	*Pan troglodytes troglodytes*	Powell Cotton Museum	M	Cranium	N
Zenker VII 0.2	*Pan troglodytes troglodytes*	Powell Cotton Museum	M	Cranium	N
Zenker VII 24	*Pan troglodytes troglodytes*	Powell Cotton Museum	M	Cranium	N
M-89351	*Pan troglodytes verus*	AMNH	F	Cranium	N
M-89354	*Pan troglodytes verus*	AMNH	F	Cranium	N
USNM 477333	*Pan troglodytes verus*	Smithsonian	F	Cranium	Y
USNM 481803	*Pan troglodytes verus*	Smithsonian	F	Cranium	Y
ZE.1968.7.5.10	*Pan troglodytes verus*	NHM	F	Cranium	N
ZE.1968.7.5.11	*Pan troglodytes verus*	NHM	F	Cranium	N

M-89353	*Pan troglodytes verus*	AMNH	M	Cranium	N
M-89355	*Pan troglodytes verus*	AMNH	M	Cranium	N
M-89406	*Pan troglodytes verus*	AMNH	M	Cranium	N
M-89407	*Pan troglodytes verus*	AMNH	M	Cranium	N
RMCA 31489	*Pan troglodytes verus*	RMCA	M	Cranium	N
RMCA 35122	*Pan troglodytes verus*	RMCA	M	Cranium	N
USNM 481804	*Pan troglodytes verus*	Smithsonian	M	Cranium	N
ZD.1986.213	*Pan troglodytes verus*	NHM	M	Cranium	N
ZE.1968.7.5.7	*Pan troglodytes verus*	NHM	M	Cranium	N
ZE.1968.7.5.8	*Pan troglodytes verus*	NHM	M	Cranium	N
C.139	*Papio anubis*	Powell Cotton Museum	F	Cranium	N
C.438	*Papio anubis*	Powell Cotton Museum	F	Cranium	N
M-161115	*Papio anubis*	AMNH	F	Cranium	Y
M-82097	*Papio anubis*	AMNH	F	Cranium	Y
N.N.304	*Papio anubis*	Powell Cotton Museum	F	Cranium	N
RCS(OM) A92.28	*Papio anubis*	RCS	F	Cranium	N
U.222	*Papio anubis*	Powell Cotton Museum	F	Cranium	N
USNM 397476	*Papio anubis*	Smithsonian	F	Cranium	N
ZD.1901.8.9.23	*Papio anubis*	NHM	F	Cranium	N
ZD.1908.8.9.41	*Papio anubis*	NHM	F	Cranium	Y
ZD.1908.8.9.42	*Papio anubis*	NHM	F	Cranium	N
ZD.1914.3.8.2	*Papio anubis*	NHM	F	Cranium	N
ZD.1923.3.4.3	*Papio anubis*	NHM	F	Cranium	N
ZD.1924.8.6.16	*Papio anubis*	NHM	F	Cranium	Y
ZD.1930.12.1.2	*Papio anubis*	NHM	F	Cranium	Y
ZD.1962.25	*Papio anubis*	NHM	F	Cranium	N
ZD.1964.2194	*Papio anubis*	NHM	F	Cranium	Y
Cam.II.85	*Papio anubis*	Powell Cotton Museum	M	Cranium	Y
M-52678	*Papio anubis*	AMNH	M	Cranium	N
M-55446	*Papio anubis*	AMNH	M	Cranium	Y
M-70064	*Papio anubis*	AMNH	M	Cranium	N
U.144	*Papio anubis*	Powell Cotton Museum	M	Cranium	N
ZD.1899.7.8.1	*Papio anubis*	NHM	M	Cranium	Y
ZD.1900.3.18.1	*Papio anubis*	NHM	M	Cranium	Y
ZD.1902.9.2.1	*Papio anubis*	NHM	M	Cranium	Y
ZD.1904.11.5.2	*Papio anubis*	NHM	M	Cranium	N
ZD.1906.11.1.6	*Papio anubis*	NHM	M	Cranium	N
ZD.1913.10.18.2	*Papio anubis*	NHM	M	Cranium	N
ZD.1913.10.18.3	*Papio anubis*	NHM	M	Cranium	N
ZD.1918.11.8.1	*Papio anubis*	NHM	M	Cranium	N
ZD.1922.12.19.6	*Papio anubis*	NHM	M	Cranium	Y
ZD.1924.2.25.1	*Papio anubis*	NHM	M	Cranium	Y
ZD.1925.5.12.1	*Papio anubis*	NHM	M	Cranium	N
ZD.1930.12.1.1	*Papio anubis*	NHM	M	Cranium	N
ZD.1935.2.14.1	*Papio anubis*	NHM	M	Cranium	N
ZD.1939.1021	*Papio anubis*	NHM	M	Cranium	N
ZD.1939.1033	*Papio anubis*	NHM	M	Cranium	Y
ZD.1947.586	*Papio anubis*	NHM	M	Cranium	N
ZD.1951.532	*Papio anubis*	NHM	M	Cranium	N
ZD.1971.2352	*Papio anubis*	NHM	M	Cranium	N
ZD.1971.2355	*Papio anubis*	NHM	M	Cranium	N
ZD.1973.1291	*Papio anubis*	NHM	M	Cranium	Y
ZD.1939.1035	*Papio cynocephalus sensu lato*	NHM	F	Cranium	Y
ZD.1966.769	*Papio cynocephalus sensu lato*	NHM	F	Cranium	N

ZD.1966.770	*Papio cynocephalus sensu lato*	NHM	F	Cranium	N
M-161734	*Papio cynocephalus sensu lato*	AMNH	M	Cranium	N
ZD.1966.491	*Papio cynocephalus sensu lato*	NHM	M	Cranium	N
RMCA 2168	*Papio cynocephalus*	RMCA	F	Cranium	N
ZD.1924.1.1.6	*Papio cynocephalus*	NHM	F	Cranium	N
M-161737	*Papio cynocephalus*	AMNH	M	Cranium	N
RMCA 2167	*Papio cynocephalus*	RMCA	M	Cranium	N
ZD.1897.10.1.11	*Papio cynocephalus*	NHM	M	Cranium	Y
ZD.1924.1.1.4	*Papio cynocephalus*	NHM	M	Cranium	N
ZD.1924.1.1.7	*Papio cynocephalus*	NHM	M	Cranium	Y
ZD.1972.1291	*Papio cynocephalus*	NHM	M	Cranium	N
ZD.1961.737	*Papio kindae*	NHM	F	Cranium	Y
ZD.1961.758	*Papio kindae*	NHM	F	Cranium	Y
ZD.1961.762	*Papio kindae*	NHM	F	Cranium	N
ZD.1961.768	*Papio kindae*	NHM	F	Cranium	Y
ZD.1961.772	*Papio kindae*	NHM	F	Cranium	N
ZD.1961.773	*Papio kindae*	NHM	F	Cranium	N
ZD.1961.784	*Papio kindae*	NHM	F	Cranium	N
ZD.1961.785	*Papio kindae*	NHM	F	Cranium	N
ZD.1961.790	*Papio kindae*	NHM	F	Cranium	N
ZD.1967.1659	*Papio kindae*	NHM	F	Cranium	N
RMCA 17979	*Papio kindae*	RMCA	M	Cranium	N
RMCA 19283	*Papio kindae*	RMCA	M	Cranium	N
ZD.1916.2.26.2	*Papio kindae*	NHM	M	Cranium	N
ZD.1961.734	*Papio kindae*	NHM	M	Cranium	N
ZD.1961.753	*Papio kindae*	NHM	M	Cranium	N
ZD.1961.756	*Papio kindae*	NHM	M	Cranium	N
ZD.1961.764	*Papio kindae*	NHM	M	Cranium	N
ZD.1961.775	*Papio kindae*	NHM	M	Cranium	N
ZD.1961.782	*Papio kindae*	NHM	M	Cranium	Y
ZD.1967.1658	*Papio kindae*	NHM	M	Cranium	Y
ZD.1969.555	*Papio kindae*	NHM	M	Cranium	N
ZD.1969.556	*Papio kindae*	NHM	M	Cranium	N
ZD.1969.561	*Papio kindae*	NHM	M	Cranium	N
M-102018	*Macaca fascicularis*	AMNH	F	Cranium	Y
M-103652	*Macaca fascicularis*	AMNH	F	Cranium	Y
M-103662	*Macaca fascicularis*	AMNH	F	Cranium	N
M-106285	*Macaca fascicularis*	AMNH	F	Cranium	N
M-107094	*Macaca fascicularis*	AMNH	F	Cranium	N
M-107095	*Macaca fascicularis*	AMNH	F	Cranium	Y
M-107096	*Macaca fascicularis*	AMNH	F	Cranium	N
M-107100	*Macaca fascicularis*	AMNH	F	Cranium	Y
M-107556	*Macaca fascicularis*	AMNH	F	Cranium	N
M-30622	*Macaca fascicularis*	AMNH	F	Cranium	N
ZD.1894.6.12.13	*Macaca fascicularis*	NHM	F	Cranium	Y
ZD.1903.2.6.4	*Macaca fascicularis*	NHM	F	Cranium	N
ZD.1908.1.25.1	*Macaca fascicularis*	NHM	F	Cranium	N
ZD.1909.4.1.26	*Macaca fascicularis*	NHM	F	Cranium	N
ZD.1909.4.1.35	*Macaca fascicularis*	NHM	F	Cranium	N
ZD.1910.12.24.1	*Macaca fascicularis*	NHM	F	Cranium	N
ZD.1910.4.5.20	*Macaca fascicularis*	NHM	F	Cranium	N
ZD.1914.12.8.11	*Macaca fascicularis*	NHM	F	Cranium	N
ZD.1914.12.8.17	*Macaca fascicularis*	NHM	F	Cranium	N
ZD.1939.181	*Macaca fascicularis*	NHM	F	Cranium	N

ZD.1939.892	*Macaca fascicularis*	NHM	F	Cranium	N
ZD.1939.894	*Macaca fascicularis*	NHM	F	Cranium	N
ZD.1951.67	*Macaca fascicularis*	NHM	F	Cranium	Y
ZD.1955.1523	*Macaca fascicularis*	NHM	F	Cranium	N
M-102015	*Macaca fascicularis*	AMNH	M	Cranium	Y
M-102763	*Macaca fascicularis*	AMNH	M	Cranium	N
M-103644	*Macaca fascicularis*	AMNH	M	Cranium	N
M-106565	*Macaca fascicularis*	AMNH	M	Cranium	Y
M-107559	*Macaca fascicularis*	AMNH	M	Cranium	Y
M-107562	*Macaca fascicularis*	AMNH	M	Cranium	N
M-187215	*Macaca fascicularis*	AMNH	M	Cranium	N
ZD.1876.10.4.9	*Macaca fascicularis*	NHM	M	Cranium	Y
ZD.1909.1.5.24	*Macaca fascicularis*	NHM	M	Cranium	N
ZD.1909.11.1.2	*Macaca fascicularis*	NHM	M	Cranium	Y
ZD.1909.4.1.31	*Macaca fascicularis*	NHM	M	Cranium	N
ZD.1914.8.22.3	*Macaca fascicularis*	NHM	M	Cranium	N
ZD.1919.11.12.8	*Macaca fascicularis*	NHM	M	Cranium	N
ZD.1939.180	*Macaca fascicularis*	NHM	M	Cranium	N
ZD.1939.891	*Macaca fascicularis*	NHM	M	Cranium	N
ZD.1955.1508	*Macaca fascicularis*	NHM	M	Cranium	Y
ZD.1955.1510	*Macaca fascicularis*	NHM	M	Cranium	N
ZD.1955.1511	*Macaca fascicularis*	NHM	M	Cranium	N
ZD.1955.1513	*Macaca fascicularis*	NHM	M	Cranium	N
ZD.1955.1518	*Macaca fascicularis*	NHM	M	Cranium	Y
ZD.1955.1519	*Macaca fascicularis*	NHM	M	Cranium	N
ZD.1955.1520	*Macaca fascicularis*	NHM	M	Cranium	N
ZD.1955.1522	*Macaca fascicularis*	NHM	M	Cranium	N
ZD.1955.1524	*Macaca fascicularis*	NHM	M	Cranium	N
ZD.1955.1527	*Macaca fascicularis*	NHM	M	Cranium	N
ZD.1905.11.3.4	*Macaca fuscata*	NHM	F	Cranium	Y
ZD.1905.11.8.5	*Macaca fuscata*	NHM	F	Cranium	N
ZD.1906.1.4.3	*Macaca fuscata*	NHM	F	Cranium	N
M-201287	*Macaca fuscata*	AMNH	M	Cranium	N
ZD.1842.1.19.95	*Macaca fuscata*	NHM	M	Cranium	Y
ZD.1905.11.3.1	*Macaca fuscata*	NHM	M	Cranium	Y
ZD.1905.11.3.2	*Macaca fuscata*	NHM	M	Cranium	N
ZD.1905.11.3.3	*Macaca fuscata*	NHM	M	Cranium	Y
ZD.1939.1050	*Macaca fuscata*	NHM	M	Cranium	N
KAS-19	*Macaca fuscata fuscata*	KUM	?	Cranium	N
KAS-26	*Macaca fuscata fuscata*	KUM	?	Cranium	N
KAS-218	*Macaca fuscata fuscata*	KUM	F	Cranium	N
KAS-23	*Macaca fuscata fuscata*	KUM	F	Cranium	N
KAS-245	*Macaca fuscata fuscata*	KUM	F	Cranium	N
KAS-20	*Macaca fuscata fuscata*	KUM	M	Cranium	N
KAS-288	*Macaca fuscata yakui*	KUM	F	Cranium	N
KAS-290	*Macaca fuscata yakui*	KUM	F	Cranium	N
KAS-294	*Macaca fuscata yakui*	KUM	F	Cranium	N
KAS-302	*Macaca fuscata yakui*	KUM	F	Cranium	Y
KAS-303	*Macaca fuscata yakui*	KUM	F	Cranium	Y
KAS-24	*Macaca fuscata yakui*	KUM	M	Cranium	N
KAS-279	*Macaca fuscata yakui*	KUM	M	Cranium	Y
M-112740	*Macaca mulatta*	AMNH	F	Cranium	N
M-112971	*Macaca mulatta*	AMNH	F	Cranium	N
M-112972	*Macaca mulatta*	AMNH	F	Cranium	N

M-27573	*Macaca mulatta*	AMNH	F	Cranium	N
M-27574	*Macaca mulatta*	AMNH	F	Cranium	N
M-27578	*Macaca mulatta*	AMNH	F	Cranium	N
M-54679	*Macaca mulatta*	AMNH	F	Cranium	N
M-60038	*Macaca mulatta*	AMNH	F	Cranium	N
ZD.1845.1.8.5	*Macaca mulatta*	NHM	F	Cranium	N
ZD.1856.5.6.18	*Macaca mulatta*	NHM	F	Cranium	N
ZD.1897.6.5.2	*Macaca mulatta*	NHM	F	Cranium	N
ZD.1914.7.10.3	*Macaca mulatta*	NHM	F	Cranium	N
ZD.1914.7.10.4	*Macaca mulatta*	NHM	F	Cranium	N
ZD.1914.7.10.6	*Macaca mulatta*	NHM	F	Cranium	N
ZD.1915.5.5.5	*Macaca mulatta*	NHM	F	Cranium	N
ZD.1915.9.1.1	*Macaca mulatta*	NHM	F	Cranium	N
ZD.1921.7.9.4	*Macaca mulatta*	NHM	F	Cranium	N
ZD.1931.1.11.12	*Macaca mulatta*	NHM	F	Cranium	N
ZD.1931.1.11.13	*Macaca mulatta*	NHM	F	Cranium	N
ZD.1931.1.11.14	*Macaca mulatta*	NHM	F	Cranium	N
ZD.1931.1.11.26	*Macaca mulatta*	NHM	F	Cranium	Y
ZD.1931.1.11.3	*Macaca mulatta*	NHM	F	Cranium	N
ZD.1937.12.3.75	*Macaca mulatta*	NHM	F	Cranium	N
ZD.1956.5.6.18	*Macaca mulatta*	NHM	F	Cranium	N
ZD.1972.1333	*Macaca mulatta*	NHM	F	Cranium	N
M-26646	*Macaca mulatta*	AMNH	M	Cranium	N
M-43086	*Macaca mulatta*	AMNH	M	Cranium	N
M-54816	*Macaca mulatta*	AMNH	M	Cranium	Y
M-57039	*Macaca mulatta*	AMNH	M	Cranium	N
M-84474	*Macaca mulatta*	AMNH	M	Cranium	N
T4/8	*Macaca mulatta*	Powell Cotton Museum	M	Cranium	Y
ZD.1841.12.25.1	*Macaca mulatta*	NHM	M	Cranium	N
ZD.1843.5.27.2	*Macaca mulatta*	NHM	M	Cranium	N
ZD.1845.1.8.223	*Macaca mulatta*	NHM	M	Cranium	N
ZD.1910.10.19.5	*Macaca mulatta*	NHM	M	Cranium	N
ZD.1914.7.10.1	*Macaca mulatta*	NHM	M	Cranium	N
ZD.1921.7.9.3	*Macaca mulatta*	NHM	M	Cranium	Y
ZD.1922.5.16.2	*Macaca mulatta*	NHM	M	Cranium	N
ZD.1923.11.4.1	*Macaca mulatta*	NHM	M	Cranium	Y
ZD.1923.9.1.118	*Macaca mulatta*	NHM	M	Cranium	N
ZD.1926.10.8.7	*Macaca mulatta*	NHM	M	Cranium	N
ZD.1931.1.11.8	*Macaca mulatta*	NHM	M	Cranium	N
ZD.1937.12.3.76	*Macaca mulatta*	NHM	M	Cranium	N
ZD.1950.377	*Macaca mulatta*	NHM	M	Cranium	N

Hominin Specimens

Table S2 - Details of hominin specimens, showing taxonomic classification, subgroup, institution, type of data used, and whether the specimen required reconstruction for the purposes of this study

Reference	Name	Taxonomic Classification	Subgroup	Institution	Cast/Fossil/CT	Reconstruction
PA 23	Chancelade	*Homo sapiens*	AMH	BioAnth (UCL)	Cast	N
99.1/2308	Furfooz I	*Homo sapiens*	AMH	AMNH	Cast	N
EM 235	Keilor	*Homo sapiens*	AMH	NHM (Pal)	Cast	Y
99.1/2293	Oberkassel I	*Homo sapiens*	AMH	AMNH	Cast	N
99.1/2294	Oberkassel II	*Homo sapiens*	AMH	AMNH	Cast	N
-	Abri Pataud	*Homo sapiens*	AMH	NHM (Pal)	Cast	Y
99.1/3256	Brno II	*Homo sapiens*	AMH	AMNH	Cast	Y
PA 28	Cro-Magnon I	*Homo sapiens*	AMH	BioAnth (UCL)	Cast	N
PA 179	Cro-Magnon II	*Homo sapiens*	AMH	BioAnth (UCL)	Cast	Y
EM 268	Dolní Věstonice III	*Homo sapiens*	AMH	NHM (Pal)	Cast	Y
-	Mladeč 1	*Homo sapiens*	AMH	Vienna	CT	N
-	Mladeč 2	*Homo sapiens*	AMH	NHM (Pal)	Cast	Y
PA 85	Předmostí III	*Homo sapiens*	AMH	BioAnth (UCL)	Cast	N
M 16631	Předmostí IV	*Homo sapiens*	AMH	NHM (Pal)	Cast	Y
99.1/2094	Zhoukoudian UC.101	*Homo sapiens*	AMH	AMNH	Cast	N
99.1/2095	Zhoukoudian UC.102	*Homo sapiens*	AMH	AMNH	Cast	N
EM 2455	Border Cave 1	*Homo sapiens*	EMH	NHM (Pal)	Cast	N
PA 2168a	Qafzeh 9	*Homo sapiens*	EMH	BioAnth (UCL)	Cast	Y
-	Skhūl V	*Homo sapiens*	EMH	Peabody	CT	Y
EM 2442	Liujiang	*Homo sapiens*	EMH	NHM (Pal)	Cast	Y
EM 2345	Omo 1	*Homo sapiens*	EMH	NHM (Pal)	Cast	Y
EM 1805	Jebel Irhoud 1	*Homo sapiens*	EMH	NHM (Pal)	Cast	Y
99.1/3210	Tabun I	*Homo neanderthalensis*		AMNH	Cast	Y
99.1/3199	La Quina H5	*Homo neanderthalensis*		AMNH	Cast	Y
-	Spy 1	*Homo neanderthalensis*		NESPOS	CT	Y
PA 25a	La Chapelle	*Homo neanderthalensis*		BioAnth (UCL)	Cast	Y
EM 2864	Guattari	*Homo neanderthalensis*		NHM (Pal)	Cast	Y
-	Gibraltar 1	*Homo neanderthalensis*		NHM (Pal)	Fossil	Y
PA 122a	Le Moustier 1	*Homo neanderthalensis*		BioAnth (UCL)	Cast	Y
PA 1496	Amud 1	*Homo neanderthalensis*		BioAnth (UCL)	Cast	N
EM 2312	Krapina C	*Homo neanderthalensis*		NHM (Pal)	Cast	Y
99.1/3204	Krapina E	*Homo neanderthalensis*		AMNH	Cast	Y
99.1/3198	Saint-Césaire I	*Homo neanderthalensis*		AMNH	Cast	Y
99.1/3188	Shanidar I	*Homo neanderthalensis*		AMNH	Cast	N
99.1/3275	Shanidar V	*Homo neanderthalensis*		AMNH	Cast	Y

-	Bodo	Middle Pleistocene hominin	MPH	Vienna	CT	Y
-	Kabwe (Broken Hill) 1	Middle Pleistocene hominin	MPH	NHM (Pal)	Fossil	N
PA 1455	Petralona	Middle Pleistocene hominin	MPH	BioAnth (UCL)	Cast	N
EM 4365	Sima de los Huesos 5 (SH5)	Middle Pleistocene hominin	MPH	NHM (Pal)	Cast	Y
M 15728	Solo VI	*Homo erectus (sensu stricto)*	*HEss*	NHM (Pal)	Cast	Y
-	Sangiran 17	*Homo erectus (sensu stricto)*	*HEss*	MorphoSource	Cast	Y
-	Zhoukoudian XII	*Homo erectus (sensu stricto)*	*HEss*	BioAnth (UCL)	Cast	Y
-	KNM-ER 3773	*Homo ergaster*	*HEr*	NHM (Pal)	Cast	Y
EM 1533	KNM-ER 3883	*Homo ergaster*	*HEr*	NHM (Pal)	Cast	Y
-	Dmanisi D4500	*Homo georgicus*	*HG*	NHM (Pal)	Cast	Y
-	Dmanisi D2282	*Homo georgicus*	*HG*	NHM (Pal)	Cast	Y
-	Dinaledi hominin 1 (DH1)	*Homo naledi*		MorphoSource	Reconstruction	N
PA 1221	KNM-ER 1813	*Homo habilis*		BioAnth (UCL)	Cast	Y
PA 349	OH 24	*Homo habilis*		BioAnth (UCL)	Cast	N
PA 2146	KNM-ER 1470	*Homo rudolfensis*		BioAnth (UCL)	Cast	Y
-	Sts 5	*Australopithecus africanus*		Vienna	CT	Y
-	KNM-WT 17000	*Paranthropus aethiopicus*		AfricanFossils.org	Cast	Y
-	KNM-ER 406	*Paranthropus boisei*		AfricanFossils.org	Cast	Y
-	KNM-ER 732	*Paranthropus boisei*		AfricanFossils.org	Cast	Y
-	OH 5	*Paranthropus boisei*		BioAnth (UCL)	Cast	N

SI-2: Laser and CT Scan Parameters

Details of the scanning parameters for the hominin specimens for which CT data were acquired are shown in table S3. Unfortunately, this information was not available for the non-hominin primate specimens.

Table S3 - CT scanning parameters for hominin specimens

Specimen	CT Scanner	Slice thickness (mm)	Voxel size (mm)
Mladeč 1	Phillips Mx8000IDT	0.75	0.4668 x 0.4668
Skhūl V	Siemens multidetector scanner	0.50	0.488281 x 0.488281
Spy 1	Siemens Somatom 64	0.60	0.465 x 0.465
Sts 5	Siemens Somatom Plus 4	1.00	0.390625 x 0.390625

A set protocol was used to collect non-CT data (from both casts and crania) using the NextEngine 3D laser scanner. Crania were placed on the NextEngine rotating platform which was positioned at a distance of 17 inches from the scanner itself, to maximise performance (see NextEngine user manual). The software was set to collect surface scans at 10,000 points/inch^2 to achieve sufficiently detailed meshes at a reasonable speed, given the size of the required sample. Different combinations of scans were collected based on the type of specimen being examined. These were then aligned using the Align function in ScanStudio.

SI-3: Details of Reconstruction Methods

This study used a combination of reconstruction methods, with each specimen being assessed individually in order to apply the most appropriate method.

Geometric Reconstruction

When only a few points required reconstruction, geometric reconstruction methods were applied using the estimate.missing function in the Geomorph package in R, using reference samples that were matched by sex and species for non-hominin primates, and for time period and taxon for the hominins (Adams, Otárola-Castillo, & Paradis, 2013; see table S4). 49 of the specimens (45 of the non-hominin primates and four of the hominins) required this type of reconstruction (table S5).

Table S4 - Details of reference specimens used in Geometric Reconstruction procedure. * - Female members of *Papio cynocephalus* and *Papio kindae* were used as reference specimens for the *Papio cynocephalus sensu lato* individual, following reconstruction of members of these groups

Taxon	Sex	No. of Reference Specimens	Taxa of Reference Specimens
Gorilla beringei beringei	F	6	*Gorilla beringei beringei*
Gorilla beringei graueri	F	23	*Gorilla beringei graueri*
Gorilla gorilla gorilla	F	25	*Gorilla gorilla gorilla*
Gorilla gorilla gorilla	M	25	*Gorilla gorilla gorilla*
Pan troglodytes schweinfurthii	F	15	*Pan troglodytes schweinfurthii*
Pan troglodytes troglodytes	M	25	*Pan troglodytes troglodytes*
Papio anubis	F	17	*Papio anubis*
Papio anubis	M	25	*Papio anubis*
Papio cynocephalus sensu lato	F	15	*Papio cynocephalus sensu lato*, *Papio cynocephalus*, *Papio kindae**
Papio cynocephalus	M	6	*Papio cynocephalus*
Papio kindae	F	10	*Papio kindae*
Papio kindae	M	13	*Papio kindae*
Macaca fascicularis	F	24	*Macaca fascicularis*
Macaca fascicularis	M	25	*Macaca fascicularis*
Macaca fuscata	M	9	*Macaca fuscata* (*fuscata* and *yakui*)
Macaca mulatta	F	25	*Macaca mulatta*
Macaca mulatta	M	19	*Macaca mulatta*
Homo neanderthalensis	-	12	*Homo neanderthalensis*

Table S5 - Details of 49 specimens for which points were reconstructed using geometric method. # indicates the number of points that needed to be reconstructed for each specimen

Specimen	#	Group	Sex
USNM 545030	1	*Gorilla beringei beringei*	F
RMCA 29538	1	*Gorilla beringei graueri*	F
RMCA 29104	1	*Gorilla gorilla graueri*	F
USNM 252575	4	*Gorilla gorilla gorilla*	F
F.C. 130	4	*Gorilla gorilla gorilla*	M
USNM 599172	3	*Pan troglodytes troglodytes*	M
USNM 236971	4	*Pan troglodytes schweinfurthii*	F
M-16115	2	*Papio anubis*	F
M-82097	1	*Papio anubis*	F
ZD.1908.8.9.41	6	*Papio anubis*	F
ZD31924.8.6.16	6	*Papio anubis*	F
ZD.1930.12.1.2	2	*Papio anubis*	F
ZD.1964.2194	4	*Papio anubis*	F
USNM 397476	1	*Papio anubis*	F
M-55446	2	*Papio anubis*	M
ZD.1899.7.8.1	2	*Papio anubis*	M
ZD.1900.3.18.1	1	*Papio anubis*	M
ZD.1902.9.2.1	2	*Papio anubis*	M
ZD.1922.12.19.6	3	*Papio anubis*	M
ZD.1924.2.25.1	1	*Papio anubis*	M
ZD.1939.1033	3	*Papio anubis*	M
ZD.1973.1291	2	*Papio anubis*	M
Cam.II.85	2	*Papio anubis*	M
ZD.1939.1035	3	*Papio cynocephalus sensu lato*	F
ZD.1897.10.1.11	2	*Papio cynocephalus*	M
ZD.1924.1.1.7	2	*Papio cynocephalus*	M
ZD.1961.758	3	*Papio kindae*	F
ZD.1961.768	5	*Papio kindae*	F
ZD.1961.782	1	*Papio kindae*	M
ZD.1967.1658	1	*Papio kindae*	M
M-107100	1	*Macaca fascicularis*	F
ZD.1894.6.12.13	4	*Macaca fascicularis*	F
ZD.1951.67	2	*Macaca fascicularis*	F
M-102015	1	*Macaca fascicularis*	M
M-106565	1	*Macaca fascicularis*	M
ZD.1876.10.4.9	1	*Macaca fascicularis*	M
ZD.1909.11.1.2	1	*Macaca fascicularis*	M
ZD.1955.1508	1	*Macaca fascicularis*	M
ZD.1955.1518	1	*Macaca fascicularis*	M
ZD.1842.1.19.95	6	*Macaca fuscata*	M
ZD.1931.1.11.26	1	*Macaca mulatta*	F
M-54816	3	*Macaca mulatta*	M
ZD.1921.7.9.3	1	*Macaca mulatta*	M
ZD.1923.11.4.1	1	*Macaca mulatta*	M
T4-8	6	*Macaca mulatta*	M
Tabun	4	*Homo neanderthalensis*	U
La Quina H5	3	*Homo neanderthalensis*	U
La Chapelle	2	*Homo neanderthalensis*	U
Shanidar V	5	*Homo neanderthalensis*	U

Manual Virtual Reconstruction

A peculiarity of the process of generating 3D models from CT data meant that some automatic semilandmarks were placed on endocranial surfaces in the Checkpoint Stratovan software. 3D models generated from CT data, including all of the specimens from the Smithsonian collection, were therefore put through the Mesh Doctor function in Geomagic (uk.3dsystems.com). This automatically detects any errors in the polygon mesh and was used to fill holes, remove non-manifold edges, and smooth the mesh, which reduced the number of semilandmarks that fell through the ectocranial surface of the frontal bone during the landmarking process. The remaining misplaced semilandmarks were reconstructed manually in the Checkpoint software by using the surrounding points and the grid template to place single landmarks in the appropriate location. The exported landmark file was then amended, with the affected semilandmarks being replaced with the reconstructed coordinates. The process of sliding removed any effects this reconstruction method may have had on the homology of the semilandmarks (Gunz & Mitteroecker, 2013; Mitteroecker & Gunz, 2009). A total of 59 specimens (52 non-hominin primates and seven hominins) required this type of reconstruction (Table S6).

Table S6 - Details of 59 specimens for which points were reconstructed using manual virtual reconstruction. # indicates the number of points that were reconstructed for each specimen

Specimen	#	Group	Sex
USNM 545030	10	*Gorilla beringei beringei*	F
USNM 545026	6	*Gorilla beringei beringei*	F
USNM 545029	10	*Gorilla beringei beringei*	F
USNM 395636	6	*Gorilla beringei beringei*	M
USNM 396934	8	*Gorilla beringei beringei*	M
USNM 545028	1	*Gorilla beringei beringei*	M
USNM 545034	19	*Gorilla beringei beringei*	M
USNM 545035	17	*Gorilla beringei beringei*	M
USNM 260582	11	*Gorilla beringei graueri*	F
USNM 590946	1	*Gorilla gorilla diehli*	F
USNM 590947	1	*Gorilla gorilla diehli*	F
USNM 590948	5	*Gorilla gorilla diehli*	F
USNM 590951	3	*Gorilla gorilla diehli*	F
USNM 590956	4	*Gorilla gorilla diehli*	F
USNM 590963	12	*Gorilla gorilla diehli*	F
USNM 590950	5	*Gorilla gorilla diehli*	M
USNM 590953	3	*Gorilla gorilla diehli*	M
USNM 590955	9	*Gorilla gorilla diehli*	M
USNM 590958	5	*Gorilla gorilla diehli*	M
USNM 590959	6	*Gorilla gorilla diehli*	M
USNM 590967	10	*Gorilla gorilla diehli*	M
USNM 590968	15	*Gorilla gorilla diehli*	M
USNM 252575	1	*Gorilla gorilla gorilla*	F
USNM 220380	10	*Gorilla gorilla gorilla*	F
USNM 252576	7	*Gorilla gorilla gorilla*	F

USNM 252579	10	*Gorilla gorilla gorilla*	F
USNM 252580	12	*Gorilla gorilla gorilla*	F
USNM 252577	19	*Gorilla gorilla gorilla*	F
USNM 174714	21	*Gorilla gorilla gorilla*	M
USNM 176206	33	*Gorilla gorilla gorilla*	M
USNM 176207	8	*Gorilla gorilla gorilla*	M
USNM 176209	13	*Gorilla gorilla gorilla*	M
USNM 176213	18	*Gorilla gorilla gorilla*	M
USNM 176216	21	*Gorilla gorilla gorilla*	M
USNM 220324	10	*Gorilla gorilla gorilla*	M
USNM 174701	1	*Pan troglodytes troglodytes*	F
USNM 174702	3	*Pan troglodytes troglodytes*	F
USNM 174707	3	*Pan troglodytes troglodytes*	F
USNM 174710	1	*Pan troglodytes troglodytes*	F
USNM 220062	4	*Pan troglodytes troglodytes*	F
USNM 599172	6	*Pan troglodytes troglodytes*	M
USNM 220327	11	*Pan troglodytes troglodytes*	M
USNM 220326	1	*Pan troglodytes troglodytes*	M
USNM 220065	4	*Pan troglodytes troglodytes*	M
USNM 176242	3	*Pan troglodytes troglodytes*	M
USNM 176240	1	*Pan troglodytes troglodytes*	M
USNM 176228	2	*Pan troglodytes troglodytes*	M
USNM 174704	2	*Pan troglodytes troglodytes*	M
USNM 236971	7	*Pan troglodytes schweinfurthii*	F
USNM 477333	2	*Pan troglodytes verus*	F
USNM 481803	3	*Pan troglodytes verus*	F
USNM 162899	11	*Papio anubis*	M
Liujiang	5	*Homo sapiens*	U
Skhūl V	8	*Homo sapiens*	U
Spy 1	12	*Homo neanderthalensis*	U
D2282	5	*Homo georgicus*	U
Sangiran 17	1	*Homo erectus sensu lato*	U
KNM-ER 1813	12	*Homo habilis*	U
Sts 5	8	*Australopithecus africanus*	U

Reconstruction by Mirroring Across an Empirical Midplane

The method of mirroring landmarks across an empirical midplane, estimated with orthogonal regression, was applied to specimens which were missing one of a pair of bilateral single landmarks. This method was used on six specimens (five non-hominin primates and one hominin; Table S7). The midplane was estimated by placing a curve of semilandmarks using three control landmarks: nasion, glabella, and post-toral sulcus. These points were used to generate a plane in Checkpoint software, and were manipulated until this plane estimated the midsagittal plane. The process of orthogonal regression was performed in R and Microsoft Excel.

Table S7 - Details of six specimens for which single points were reconstructed using reflection across an empirical midplane. # indicates the number of points that were reconstructed for each

Specimen	#	Group	Sex
ZD.1961.737	1	*Papio kindae*	F
M-102018	1	*Macaca fascicularis*	F
M-103652	1	*Macaca fascicularis*	F
M-107095	1	*Macaca fascicularis*	F
M-107559	1	*Macaca fascicularis*	M
Tabun	1	*Homo neanderthalensis*	U

Digital Reconstruction

Specimens with larger areas of damage or distortion were reconstructed by digital reconstruction methods. 27 of the hominin specimens (Table S8) required digital reconstruction, either due to their fragmentary nature or because of taphonomic distortion. Fossil reference specimens were chosen based on species, geographic region, time period, and overall similarity of morphology, which was visually assessed. In cases where areas were missing on only one side of the cranium, a reflection of the specimen was also used as a reference for digital reconstruction. Homologous, standard craniofacial landmarks were placed on the target and reference specimen crania, after which one of two methods were used. In the first, the reference and target surface models were aligned using a Generalised Procrustes Analysis in Evan Toolbox (Phillips, O'Higgins, & Bookstein, 2010). In the second, the reference surface model was warped onto the target specimen in Evan Toolbox using the homologous landmarks and a mesh of semilandmarks covering the frontal bone. In both cases, the resulting reference and target surfaces were then exported and loaded into CloudCompare (version 2; www.cloudcompare.org). Distorted and damaged areas were removed on the target specimen, and superfluous areas were removed on the reference specimen. The alignment of the two surface models was refined using manual manipulation. The surface models were then exported and merged in Geomagic, and the Mesh Doctor function was used to correct for any defects in the merged surface model. Finally, the reconstructed model was scaled back to its original size in Meshlab in an iterative process where distances between two homologous points were measured on the original and reconstruction, and the reconstruction was scaled until the distances were approximately equal (to 0.01mm). Details of reconstruction methods and points affected can be found below.

Table S8 - Details of 27 fossil specimens which were digitally reconstructed, including reference specimen(s) used to guide reconstruction. Number and percentage (%) of landmarks and semilandmarks affected by digital reconstruction are shown. *See SI-4 for tests of effect of reference specimen on Brno II

Specimen	Group	Reference Specimen(s)	Landmarks affected		Semilandmarks affected	
Brno II	*Homo sapiens*	Brno II, Brno III*	7	35.0%	27	12.9%
Předmostí IV	*Homo sapiens*	Předmostí III	0	0.0%	8	3.8%
Cro-Magnon II	*Homo sapiens*	Cro-Magnon II	2	10.0%	7	3.3%
Mladeč 2	*Homo sapiens*	Mladeč 1	4	20.0%	0	0.0%
Liujiang	*Homo sapiens*	Liujiang	0	0.0%	11	5.2%
Qafzeh 9	*Homo sapiens*	Qafzeh 9	8	40.0%	114	54.3%
Jebel Irhoud 1	*Homo sapiens*	Jebel Irhoud 1	2	10.0%	54	25.7%
Gibraltar 1	*Homo neanderthalensis*	Gibraltar 1	2	10.0%	35	16.7%
Guattari	*Homo neanderthalensis*	Guattari	7	35.0%	35	16.7%
Krapina C	*Homo neanderthalensis*	Krapina C, Shanidar 1	4	20.0%	25	11.9%
Krapina E	*Homo neanderthalensis*	Krapina E, Shanidar 1	5	25.0%	17	8.1%
Le Moustier 1	*Homo neanderthalensis*	Le Moustier 1	0	0.0%	22	10.5%
Saint Césaire I	*Homo neanderthalensis*	Sainte Césaire I, Shanidar 1	9	45.0%	85	40.5%
Shanidar V	*Homo neanderthalensis*	Shanidar V	3	15.0%	5	2.4%
Spy 1	*Homo neanderthalensis*	Spy 1, La Chapelle	6	30.0%	0	0.0%
Bodo	Middle Pleistocene hominin	Bodo, Kabwe 1	1	5.0%	35	16.7%
SH5	Middle Pleistocene hominin	SH5	3	15.0%	45	21.4%
Solo VI	*Homo erectus sensu stricto*	Solo VI, Sangiran 17	7	35.0%	15	7.1%
Zhoukoudian XII	*Homo erectus sensu stricto*	Zhoukoudian XII	6	30.0%	0	0.0%
KNM-ER 3733	*Homo ergaster*	KNM-ER 3733	0	0.0%	15	7.1%
KNM-ER 3883	*Homo ergaster*	KNM-ER 3883	3	15.0%	22	10.5%
D2282	*Homo georgicus*	D2282, D4500	13	65.0%	29	13.8%
KNM-ER 1813	*Homo habilis*	KNM-ER 1813	4	20.0%	5	2.4%
KNM-ER 1470	*Homo habilis*	KNM-ER 1470	1	5.0%	9	4.3%
KNM-WT 17000	*Paranthropus aethiopicus*	KNM-WT 17000	0	0.0%	2	1.0%
KNM-ER 406	*Paranthropus boisei*	KNM-ER 406	1	5.0%	7	3.3%
KNM-ER 732	*Paranthropus boisei*	KNM-ER 732	8	40.0%	123	58.6%

Brno II

Brno II was missing regions of the left and right frontal squama interior to the temporal lines, as well as the nasal region of the frontal bone inferior to glabella, both maxillae, and the left zygomatic. There was also a depression to the right lateral side of the frontal squama. First, Brno II was reflected missing regions of the original were taken and merged with the original model in Geomagic. Brunn III was then warped on to the Brno II reconstruction, and parts of the warped Brunn III surface model were used to reconstruct the missing regions in the lateral frontal bone. The reconstructed areas affected seven landmarks and 27 semilandmarks. The effect of the reference specimen was tested for Brno II, and results are shown in SI-4.

Předmostí IV

Předmostí IV was missing a section of bone in the right lateral trigone region. This was reconstructed by merging the original model with the corresponding region of the reflected model, with eight semilandmarks affected by digital reconstruction.

Cro-Magnon II

Cro Magnon II had a mediolateral depression to the superior right frontal squama. It was also missing the inferior orbital margin on the left zygomatic, the frontal process of the left maxilla, and the left lacrymal. The affected regions of the original model were reconstructed using the corresponding areas of the reflected model. This affected two landmarks and seven semilandmarks.

Mladeč 2

The original fossil of Mladeč 2 was missing both zygoma, maxillae and lacrymals, as well as the inferior border of the lateral frontal squama on both sides. The lower face of Mladeč 1 was transformed, aligned and merged with Mladeč 2, affecting four of the landmarks.

Liujiang

Liujiang had a defect in the left frontal squama, superior to the midorbit, extending medially to be parallel with the left medial orbital rim. This was reconstructed by using corresponding regions of the reflected aligned surface model and affected 11 of the semilandmarks.

Qafzeh 9

Qafzeh 9 was missing areas of the left frontal squamous surface superior to the lateral aspects of the orbit, as well as some of the midsagittal region on the superior part of the squama extending to laterally to the left. There were also small missing regions in the left superior orbital margin (towards the trigone) and the right superior orbital margin (above midorbit). The depressed regions of the frontal squamous were raised to the level of the surrounding bone and merged in Geomagic. The reconstruction was then aligned with its reflection to reconstruct missing regions of the left and right supraorbital margin. Nasion was estimated using the reconstructed region on the cast. Finally, the reflected model was warped onto the reconstruction to patch the missing area of bone superior to the left trigone. This affected one of the landmarks and 24 of the semilandmarks.

Jebel Irhoud 1

Jebel Irhoud 1 had a depressed region in the left lateral frontal squama superior to midorbit extending laterally, which also affected the supraorbital trigone. This was reconstructed by using the relevant region from the right side of the specimen. This affected two landmarks and 54 semilandmarks.

Gibraltar 1

Gibraltar 1 was missing lateral portions of the left frontal squama, along with the left trigone region. This was reconstructed by using the appropriate areas of the reflected model. Two landmarks and 35 semilandmarks were affected by the reconstruction.

Guattari

The original Guattari model was missing the right anterolateral aspect of the frontal including all of right trigone. It was also missing the right zygomatic and the lateral aspect of the right inferior orbital rim. Missing areas were reconstructed by aligning the original model with its reflection and merging the two. In total, seven landmarks and 35 semilandmarks were affected by reconstruction.

Krapina C

Krapina C was missing most of the left half of the frontal squama, superior to the supraorbital torus. This extended into the midsagittal region on the superior aspect of the squama. It was also missing part of the left maxilla, affecting the inferior orbital rim, and the right zygomatic was displaced anterolaterally. The original model and its reflection were aligned with Shanidar I to aid realignment of the zygoma. The reflected model was then used to reconstruct the missing regions of the left frontal squama and maxilla. Shanidar I was then warped on to the reconstruction to reconstruct the missing superior midsagittal region of the frontal squama. Four landmarks and 25 semilandmarks were affected.

Krapina E

Krapina E was missing a large region of the left frontal squama, superior to the supraorbital torus, and some of the right supraorbital torus in the trigone area. It was also missing the right zygomatic, the right nasal bone and both maxillae, and the left zygomatic was misaligned. The alignment of the left zygomatic was corrected by aligning the original model with Shanidar I. The frontal bone and the right zygomatic were then reconstructed by aligning the original model, with the corrected zygomatic, with its reflection. The lower face was reconstructed by using the aligned Shanidar I model. This reconstruction affected five of the landmarks and 17 of the semilandmarks.

Le Moustier 1

Le Moustier 1 had a defect on the left supraciliary region, lateral to glabella and extending medially to affect the superomedial orbital rim. There was also a depression in the right trigone. These areas were reconstructed by using the corresponding regions from the reflected model. 22 semilandmarks were affected by the reconstruction.

Saint Césaire

The Saint Césaire fossil was missing all of the left frontal squama up to midsagittal region, as well as the left lateral supraorbital torus. The left zygomatic, and all of the left orbital margin. There was also a defect in the right frontal squama. This specimen was reconstructed firstly by using the relevant sections of its aligned reflection, followed by merging the resulting model with the lower face of the Shanidar 1 fossil, and finally by warping the frontal squama of Shanidar I on to the reconstructed model's surface to reconstruct the remaining defects. This affected nine landmarks and 85 semilandmarks.

Shanidar V

There was some erosion of the nasal region on Shanidar V, extending to the frontal processes of the maxillae. This specimen also had a defect on the left frontal squama, on the superior aspect above midorbit. It was reconstructed by using the corresponding regions from the reflected model. Three landmarks and five semilandmarks were affected by the reconstruction.

Spy 1

Spy 1 was missing both maxillae and nasal bones as well as the left zygomatic. The right zygomatic, while present, was displaced. First, the right zygomatic was aligned using La Chapelle as a reference. Then, the model was reflected to reconstruct the left zygomatic. Finally, the model was aligned with La Chapelle again to reconstruct the lower face. Six landmarks were affected.

Bodo

Bodo was missing the right zygomatic, the right lateral maxilla, affecting the inferior orbital margin, and sections of the frontal squama in the right and posterosuperior midsagittal region. It was also missing a section of bone around the left temporal line, and there was a crack of missing bone in the right temporal line region. These areas were reconstructed by using the corresponding regions of the reflected model to create a composite surface, then by warping the frontal squama of Kabwe 1 on to this model to reconstruct the missing areas. One landmark and 35 semilandmarks were affected

Sima de los Huesos

There was damage to the right lateral supraorbital torus and trigone region of Sima de los Huesos 5, which also affected the frontal squama posterior to this area. This specimen was reconstructed by using the corresponding morphology of the reflected model. Three landmarks and 45 semilandmarks were affected.

Solo VI

The Solo VI fossil was missing the left lateral supraorbital torus region, extending onto the frontal squama in the lateral aspect. There was also damage to the lateral part of the right trigone, and it was missing both zygomatics and maxillae. The trigone and frontal squama were reconstructed by using a reflected surface model, while the face and the anterior aspects of the zygomatic processes of the frontal were reconstructed by using Sangiran. Seven landmarks and 15 semilandmarks were affected by the reconstruction

Zhoukoudian XII

Zhoukoudian XII was missing both maxillae, the right zygomatic, and the inferomedial portion of the left zygomatic. These areas were reconstructed by using the reflected right zygomatic, and raising the preserved inferomedial portion to the level of the inferior orbital rim. Six landmarks were affected.

KNM-ER 3733

KNM-ER 3733 had a defect in the region of the supratoral sulcus, superior to glabella and extending to the left midorbit. There was also a slight defect in the left superior orbital rim on the medial side. This was reconstructed by using the corresponding regions from the reflected model. 15 semilandmarks were affected.

KNM-ER 3883

There was a depression on the left frontal squama of KNM-ER 3883. This specimen was also missing the left frontal process of maxilla and most of the left zygomatic, with the preserved areas being somewhat misaligned. This specimen was reconstructed by using the aligned reflected model. Three landmarks and 22 semilandmarks were affected.

D2282

D2282 showed some post-depositional changes. The lower face was misaligned, being shifted to the left. This specimen was missing the anteroinferior aspect of the supraorbital torus in the glabella region, the medial aspects of the supraciliary region, the nasal region, and the frontal processes of both maxillae. The right lateral frontal squama appeared to be deformed in the area of the temporal line region. To reconstruct this specimen, first the left zygomatic process of the frontal was moved medially into its correct alignment. Then the model was reflected to reconstruct the right lateral squama in the area of the temporal line and the posterior region of the zygomatic process. Next, the lower face, including the zygomatics, was moved to the right to be aligned with the calvarium. Finally, D4500 was used to reconstruct the nasal column, anterior glabella region, and inferomedial orbital rim. In total, 13 landmarks and 29 semilandmarks were affected.

KNM-ER 1813

KNM-ER 1813 was missing the left zygomatic, left inferior orbital margin on the maxilla, and the left lateral trigone region. These areas were reconstructed by using an aligned reflected model of the specimen. Four landmarks and five semilandmarks were affected by the digital reconstruction.

KNM-ER 1470

KNM-ER 1470 was missing some of the frontal process of the right zygomatic, and a section of the right supraorbital torus area above midorbit, affecting the supraorbital rim. This specimen was reconstructed by using the corresponding morphology of its own reflection, affecting one landmark and nine semilandmarks.

KNM-WT 17000

There was a slight circular defect in the frontal squama of KNM-ER 17000, isolated on the right hand side, inferior to the temporal line. This defect was reconstructed by using an aligned reflection of the specimen, with two landmarks being affected in total.

KNM-ER 406

KNM-ER 406 had a circular defect along the left temporal line on the frontal squama. It was also missing the left inferior orbital rim on the left maxilla. Both areas were reconstructed by using the corresponding areas of a reflection of the specimen. One landmark and seven semilandmarks were affected.

KNM-ER 732

KNM-ER 732 had a defect in the left supraciliary region, as well as some on the right squama between the midsagittal region and the temporal line. In addition, it was missing the lateral portion of the left frontal squama, the left supraorbital trigone, and the left zygomatic and maxilla. This specimen was therefore reconstructed by using the reflected left frontal squama to reconstruct the defects in the right squama, then by reflecting the reconstructed right side to reconstruct the majority of the left side. All of the left bilateral landmarks (eight in total) were affected, along with all left semilandmarks and 24 of those on the right side of the specimen (123 in total).

Reconstruction in ScanStudio

One non-hominin primate specimen required reconstruction by manipulation of the original ScanStudio file. RMCA 9220, a male *Gorilla beringei graueri*, had a small defect which was removed using the Trim function, after which the Fill function was used to fill in the area. This method only works for suitably small areas and uses the surrounding morphology to generate gaps in the 3D surface model. Sliding of semilandmarks in later analysis removed any effect on the homology of the affected points.

SI-4: Testing the Effect of Digital Reconstruction

Effect of Reference Specimen: Brno II

To test the effect of choice of reference specimen on the reconstructed morphology, one specimen, Brno II (*Homo sapiens*), was reconstructed using five different reference specimens: Brno III (taken as the control reconstruction, as Brno III was not included in the entire *Homo sapiens* sample), Mladeč 1, Předmostí IV, Dolní Věstonice III, and Abri Pataud. These specimens are from a similar time period (Upper Palaeolithic) and region (Europe), and are therefore suitable reference specimens for Brno II. The configuration of landmarks and semilandmarks for all five reconstructions was included in a dataset containing the remaining 54 Pleistocene hominins. The dataset was aligned using GPA, and PCA was used on the resulting Procrustes coordinates (see Materials and Methods).

Figure S1 shows a plot of PC1 and PC2 (67.5% of total sample variance combined) for the Brno II reconstruction dataset, in which the Brno II reconstructions are tightly clustered. Examination of Procrustes distances showed that the Brno II reconstruction using Mladeč 1 as a reference was closer to the reference specimen than the control reconstruction (table S9). For the other reconstructions of Brno II (using Dolní Věstonice III, Předmostí III, and Abri Pataud as references), the distance to the reference specimen was larger in comparison to the distance between the control Brno II reconstruction and the respective reference specimens. A one-way ANOVA with post-hoc Tukey HSD tests in SPSS 25 (table S10) showed that the Procrustes distances between the Brno II reconstructions and their reference specimens were not significantly different than either the distance between the Brno II control reconstruction and the other reference specimens (p=0.991), or between the other *Homo sapiens* specimens and the four Brno II reference specimens (p=0.132). A second one-way ANOVA (table S11) showed that the Procrustes distances between the five Brno II reconstructions was significantly lower (p=0.031) than the intraobserver error distances (see SI-5), and the intra-specific distances for the other *Homo sapiens* specimens (p<0.001). It was therefore concluded that the choice of reference specimen for digital reconstructions did not have an effect on the results of this study. The Brno II reconstruction which used Brno III as a reference was used in all subsequent analyses.

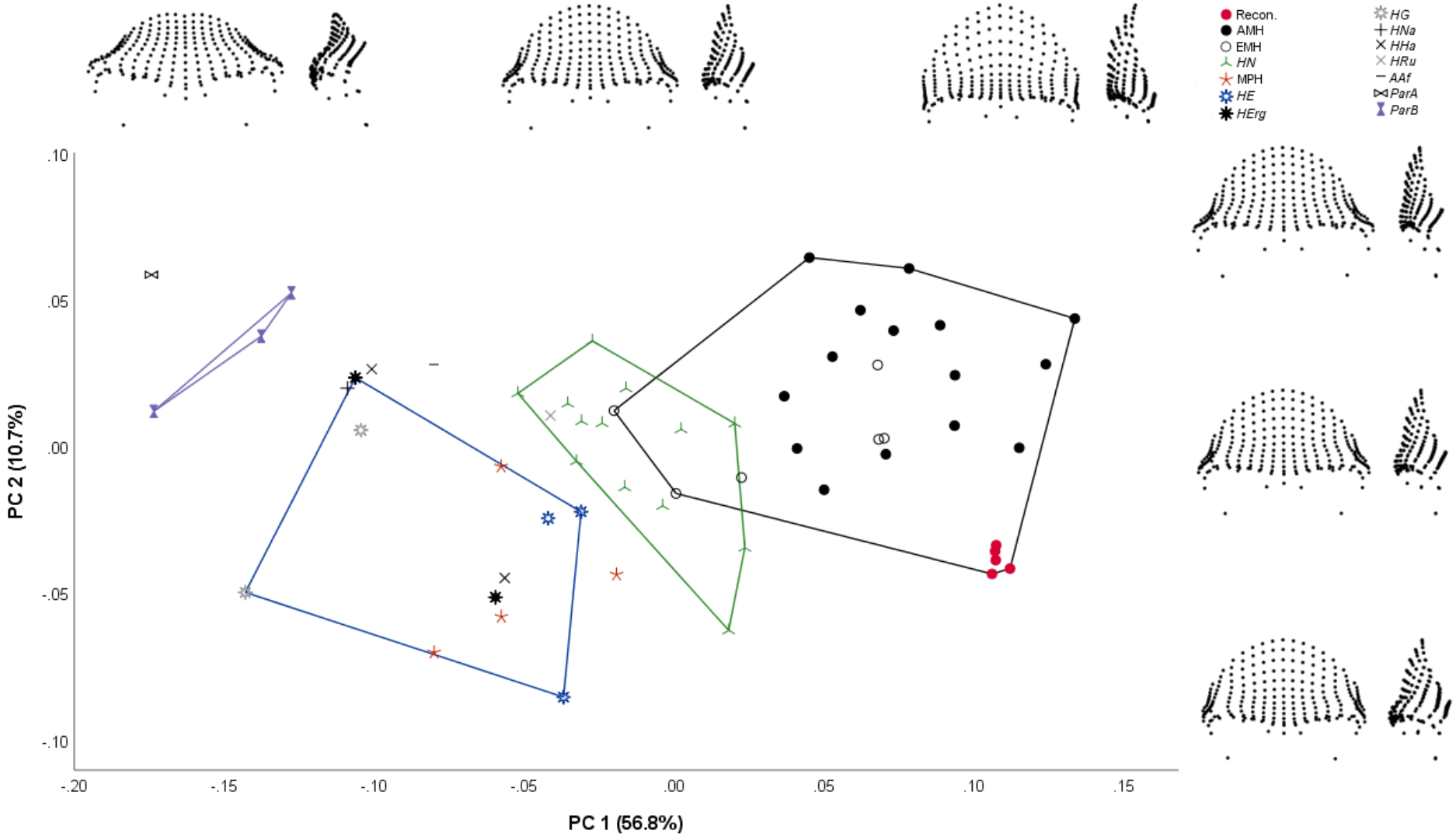

Figure S1 - Plot of PC1 (x-axis) and PC2 (y-axis), accounting for 67.5% of variation combined, for PCA in tangent space using dataset of 54 Pleistocene hominins combined with the five reconstructions of Brno II. See table 2 for list of abbreviations, and legend for identification of specimens. Convex hulls are shown and correspond to species; see figure 11 for identification

Table S9 - Procrustes distances between control reconstruction (using Brno III as a reference) and other reference specimens, and between reconstructions and their references

	Control - Reference	Recon. - Reference	Difference
Abri Pataud	0.117	0.121	0.004
Dolní Věstonice III	0.100	0.104	0.003
Mladeč 1	0.109	0.108	-0.001
Předmostí III	0.112	0.114	0.001

Table S10 - Results of Post-Hoc Tukey HSD comparisons of Procrustes distances between the Brno II reconstructions and their reference specimens compared to those between the control Brno II reconstruction and the reference specimens, and between the other *Homo sapiens* (*HS*) and the reference specimens

		Mean Difference	Std. Error	*p*	95% Confidence Interval	
					Lower Bound	Upper Bound
Recon. vs. Reference	Control vs. Reference	0.002	0.015	0.990	-0.034	0.038
	HS vs. Reference	0.021	0.011	0.135	-0.005	0.047

Table S11 - Results of Post-Hoc Tukey HSD comparisons of Procrustes distances within the five Brno II reconstructions, versus those within intraobserver error (IOE) repeats (see SI-5) and intra-*Homo sapiens* (*HS*) distances

		Mean Difference	Std. Error	*p*	95% Confidence Interval	
					Lower Bound	Upper Bound
Intra-Recon.	Intra-IOE	-0.021	0.008	0.031	-0.041	-0.001
	Intra-*HS*	-0.061	0.008	<0.001	-0.079	-0.043

Exclusion of a Specimen: Saint Césaire I

Saint Césaire I required approximately half of the frontal bone to be reconstructed (see SI-3); as such, it was one of the specimens which required the most extensive digital reconstruction. To test that the reconstruction method did not impact the overall results, analyses were run with a dataset where Saint Césaire I was excluded, and results were compared to those for the full dataset. Figure S2 shows a plot of PC1 and PC2 (66.9% of total variation combined) for the dataset where Saint Césaire I was excluded. As can be seen, the exclusion of this specimen has a negligible effect on the plot when compared to figure 11. Saint Césaire I's exclusion also had minimal effect on the results of the discriminant analysis (table S12), and the Procrustes distance between the Saint Césaire I reconstruction and the *Homo neanderthalensis* centroid (0.056) was very close to the mean distance to the centroid for the other *Homo neanderthalensis* specimens (0.055; st. dev. = 0.016).

Table S12 - Results of step-wise cross-validated discriminant analysis with subsampling (n=7, except for MPH where n=4 and *Homo habilis* where n=2 due to sample size) using first 17 principal components that accounted for over 95% of total sample variance from PCA in tangent space with dataset of 54 hominins (with Saint Césaire I excluded). Percentage classification accuracy is shown across 1000 repeats. Specimens were classified into species groups, and overall weighted species classification accuracy (excluding MPH and *Homo habilis*) was 87.5%. See table 2 for list of abbreviations

	HS	*HN*	MPH	*HE*	*HHa*	Species
HS	87.4	8.5	2.5	0.8	0.8	87.4
HN	4.8	89.8	0.8	4.6		89.8
MPH	0.1	12.4	72.6	14.2	0.8	
HE		7.2	3.3	85.5	4.0	85.5
HHa		0.4	8.2	47.8	43.8	

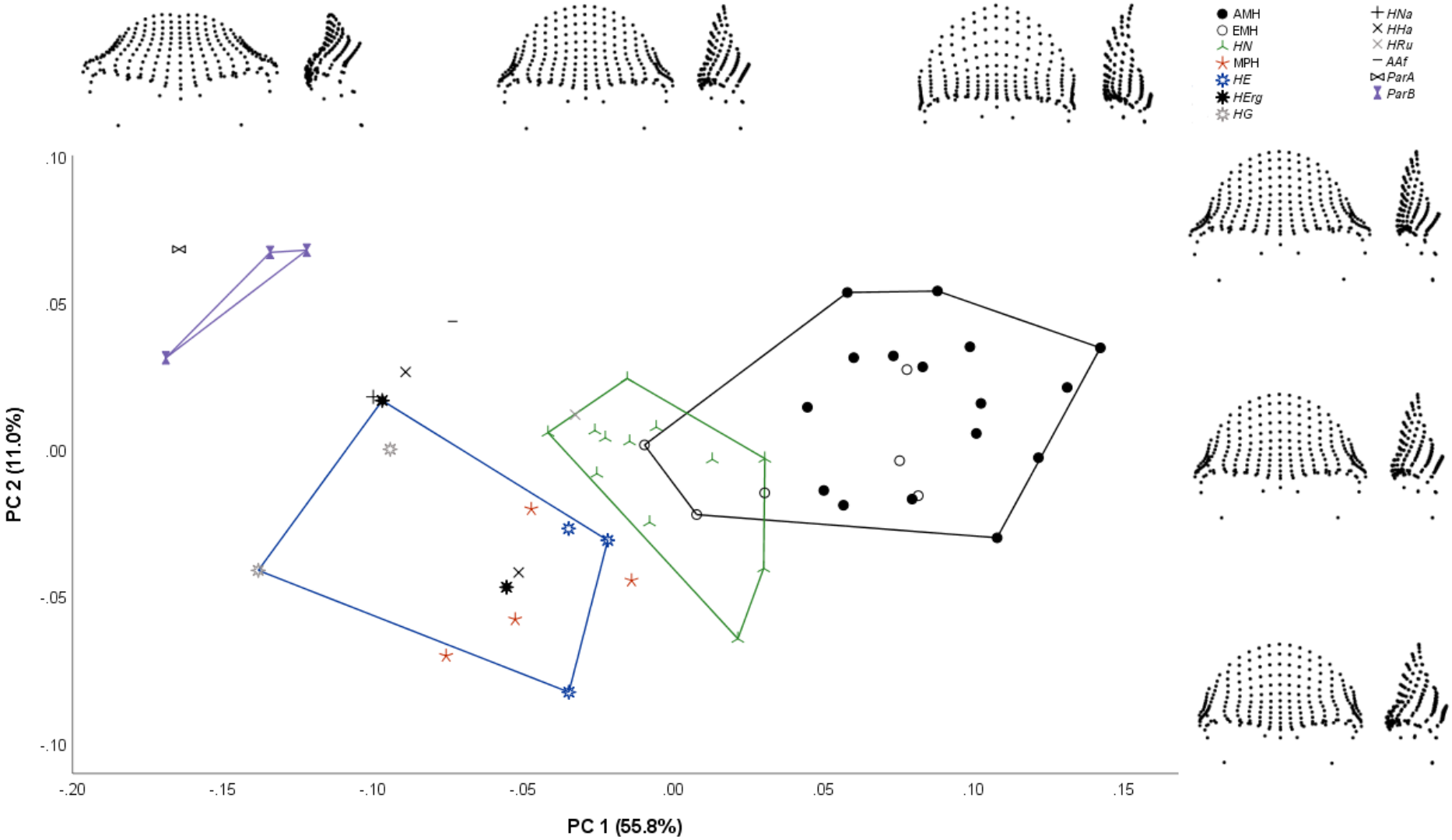

Figure S2 - Plot of PC1 (x-axis) and PC2 (y-axis), accounting for 66.9% of variation, for PCA in tangent space using dataset of 54 Pleistocene hominins (with Saint Césaire I excluded). See table 2 for list of abbreviations, and legend for identification of specimens. Convex hulls are shown and correspond to species; see figure S11 for identification

SI-5: Intra-observer Error

Details of Specimens

Table S13 - Details of 26 specimens used for intra-observer error assessment

Specimen	Species	Sex
RMCA 2260	*Gorilla beringei beringei*	Male
RMCA 27840	*Gorilla beringei graueri*	Female
USNM 590946	*Gorilla gorilla diehli*	Female
ZD.1878.12.14.1	*Gorilla gorilla gorilla*	Male
RMCA 27012	*Pan paniscus*	Female
RMCA 29036	*Pan paniscus*	Male
RMCA 29074	*Pan troglodytes schweinfurthii*	Female
ZD.1939.3365	*Pan troglodytes troglodytes*	Male
ZD.1908.8.9.42	*Papio anubis*	Female
ZD.1925.5.12.1	*Papio anubis*	Male
ZD.1961.772	*Papio kindae*	Female
ZD.1961.734	*Papio kindae*	Male
M-30622	*Macaca fascicularis*	Female
ZD.1919.11.12.8	*Macaca fascicularis*	Male
ZD.1905.11.3.2	*Macaca fuscata*	Male
KAS-290	*Macaca fuscata yakui*	Female
ZD.1914.7.10.3	*Macaca mulatta*	Female
ZD.1931.1.11.8	*Macaca mulatta*	Male
Zhoukoudian UC 102	*Homo sapiens*	
Border Cave 1	*Homo sapiens*	
Gibraltar 1	*Homo neanderthalensis*	
Bodo	MPH	
KNM-ER 3733	*Homo ergaster*	
D4500	*Homo georgicus*	
OH 24	*Homo habilis*	
KNM-ER 732	*Paranthropus boisei*	

Results

Table S14 - Descriptive statistics for within-group Procrustes distances for analysis of intra-observer error (IOE) for non-hominin primate and hominin datasets. All values reported to 3 decimal places

		Mean	Median	Min.	Max.	St. Dev.
Non-Hominin Primates	IOE	0.046	0.043	0.025	0.081	0.011
	Intra-subspecies	0.101	0.098	0.040	0.216	0.025
	Inter-subspecies	0.098	0.095	0.044	0.222	0.023
	Intra-species	0.097	0.094	0.034	0.222	0.024
	Inter-species	0.105	0.102	0.043	0.246	0.026
	Intra-genus	0.101	0.097	0.034	0.246	0.025
	Inter-genus	0.142	0.137	0.053	0.307	0.038
Hominins	IOE	0.056	0.048	0.025	0.151	0.028
	Intra-species	0.096	0.093	0.017	0.181	0.025
	Inter-species	0.141	0.135	0.057	0.305	0.044
	Intra-genus	0.131	0.123	0.017	0.305	0.045
	Inter-genus	0.156	0.148	0.097	0.240	0.033

Table S15 - Results of Post-Hoc Tukey HSD comparisons of intra-observer Procrustes distances to intra- and inter-taxonomic Procrustes distances for the non-hominin primate and hominin datasets

			Mean Difference	Std. Error	*p*	95% Confidence Interval	
						Lower Bound	Upper Bound
Non-Hominin Primates	IOE	Intra-subspecies	-0.055	0.003	<0.001	-0.064	-0.047
		Inter-subspecies	-0.052	0.003	<0.001	-0.060	-0.044
		Intra-species	-0.051	0.003	<0.001	-0.059	-0.043
		Inter-species	-0.059	0.003	<0.001	-0.067	-0.051
		Intra-genus	-0.055	0.003	<0.001	-0.063	-0.047
		Inter-genus	-0.096	0.003	<0.001	-0.104	-0.088
Hominins	IOE	Intra-species	-0.039	0.006	<0.001	-0.057	-0.022
		Inter-species	-0.085	0.006	<0.001	-0.102	-0.068
		Intra-genus	-0.074	0.006	<0.001	-0.091	-0.058
		Inter-genus	-0.099	0.008	<0.001	-0.122	-0.077

SI-6: Non-Hominin Primates - Additional Results

Mean Pairwise Procrustes Distances

Table S16 - Mean pairwise Procrustes distances (PrD) for inter-taxon comparisons for non-hominin primate dataset. See table 1 for list of abbreviations. PrD shown to 3 decimal places

		Pairwise PrD
Genus	*Gorilla-Pan*	0.155
	Papio-Macaca	0.117
Species	*GB-GG*	0.123
	PP-PT	0.096
	PA-PC	0.098
	PA-PK	0.106
	PK-PC	0.094
	MFa-MM	0.100
	MFa-MFu	0.098
	MFu-MM	0.097
Subspecies	*GBB-GBG*	0.119
	GGG-GGD	0.112
	PTT-PTS	0.090
	PTT-PTV	0.091
	PTT-PTE	0.094
	PTS-PTV	0.088
	PTS-PTE	0.091
	PTV-PTE	0.088
	MFuF-MFuY	0.087

Principal Component Analysis: Tangent Space - Additional Figures

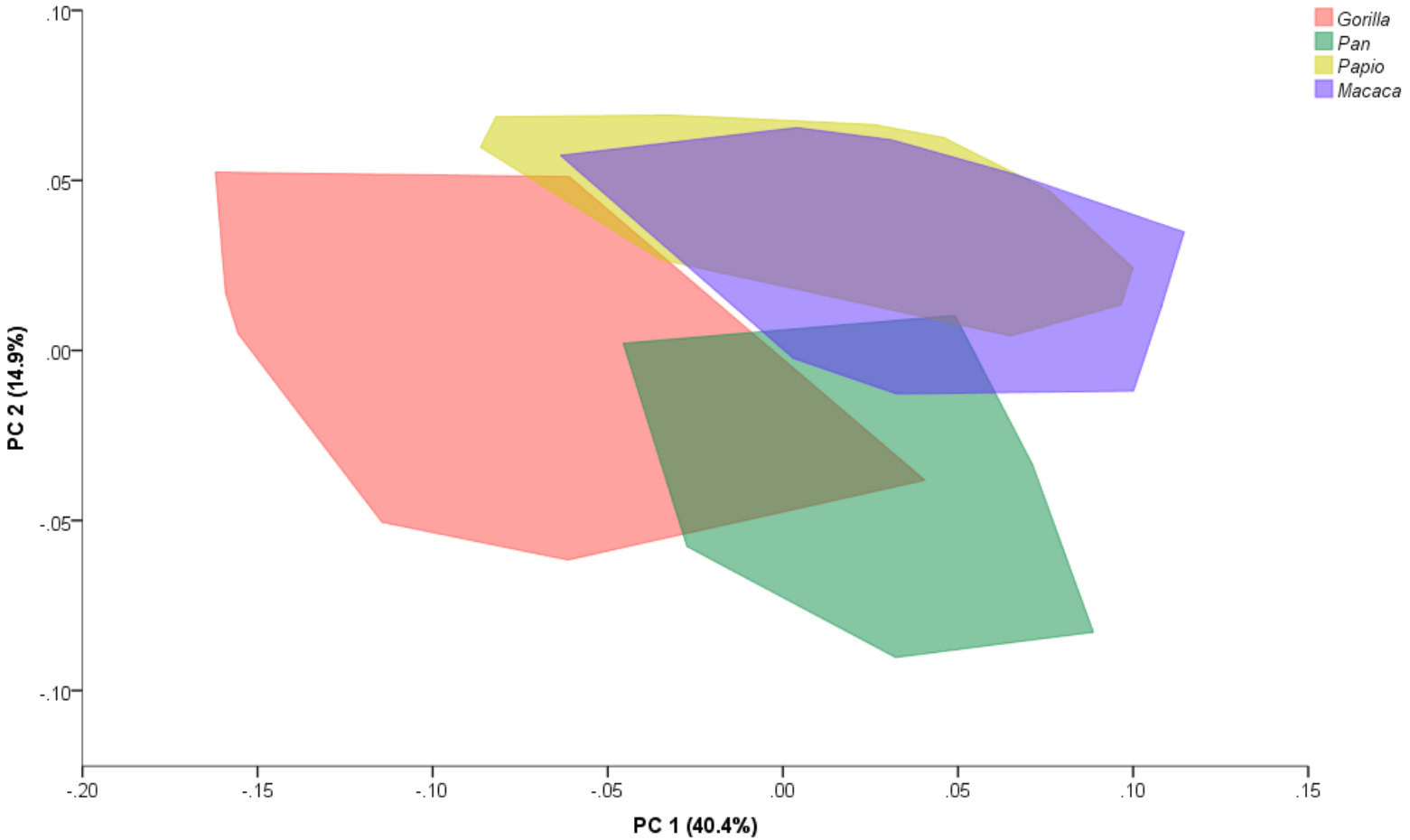

Figure S3 - Plot of PC1 (x-axis) and PC2 (y-axis), accounting for 55.4% of variation, for PCA in tangent space using dataset of 460 non-hominin primates. See table 1 for list of abbreviations. Convex hulls are shown and correspond to genus; see legend for identification

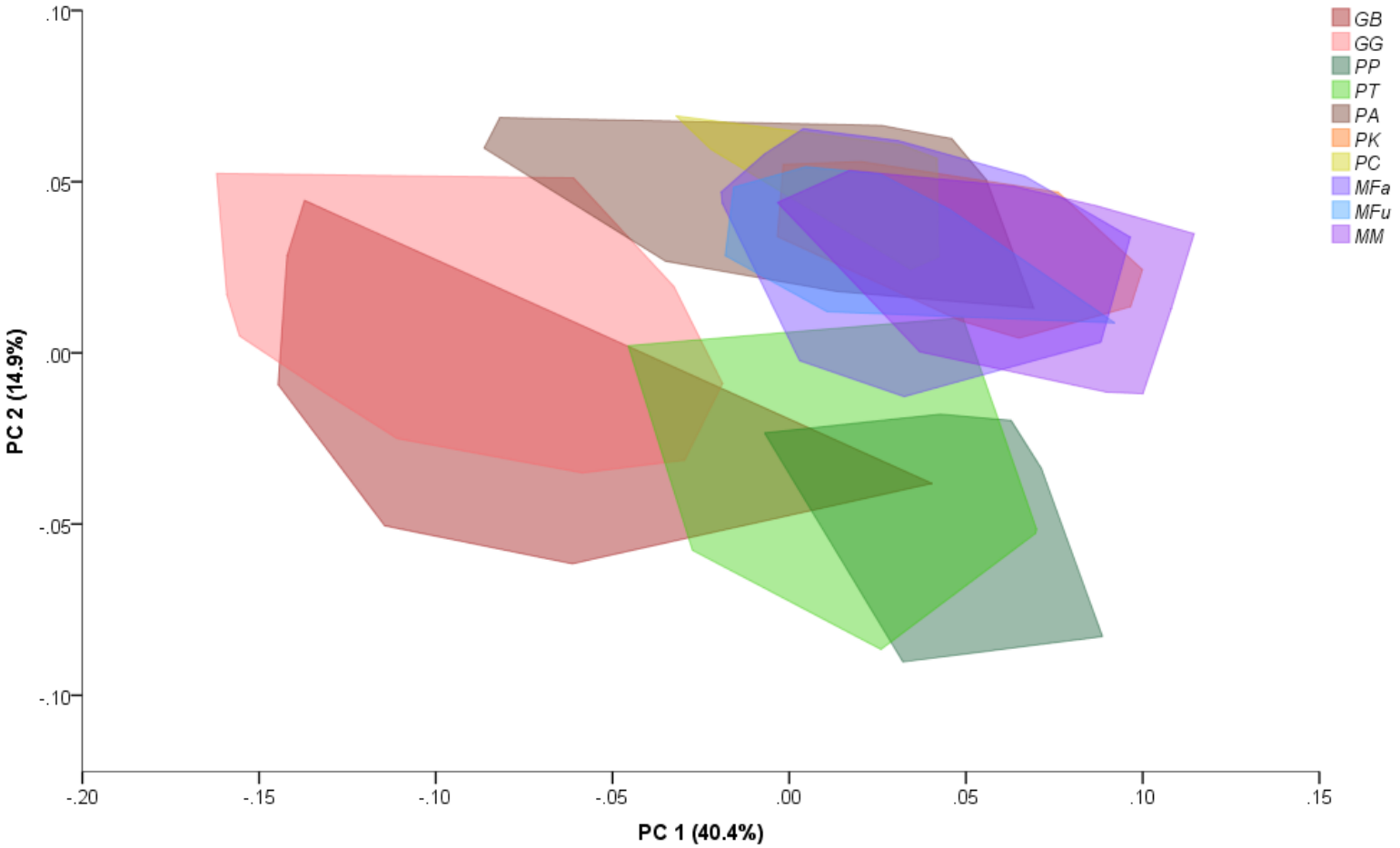

Figure S4 - Plot of PC1 (x-axis) and PC2 (y-axis), accounting for 55.4% of variation, for PCA in tangent space using dataset of 460 non-hominin primates. See table 1 for list of abbreviations. Convex hulls are shown and correspond to species; see legend for identification

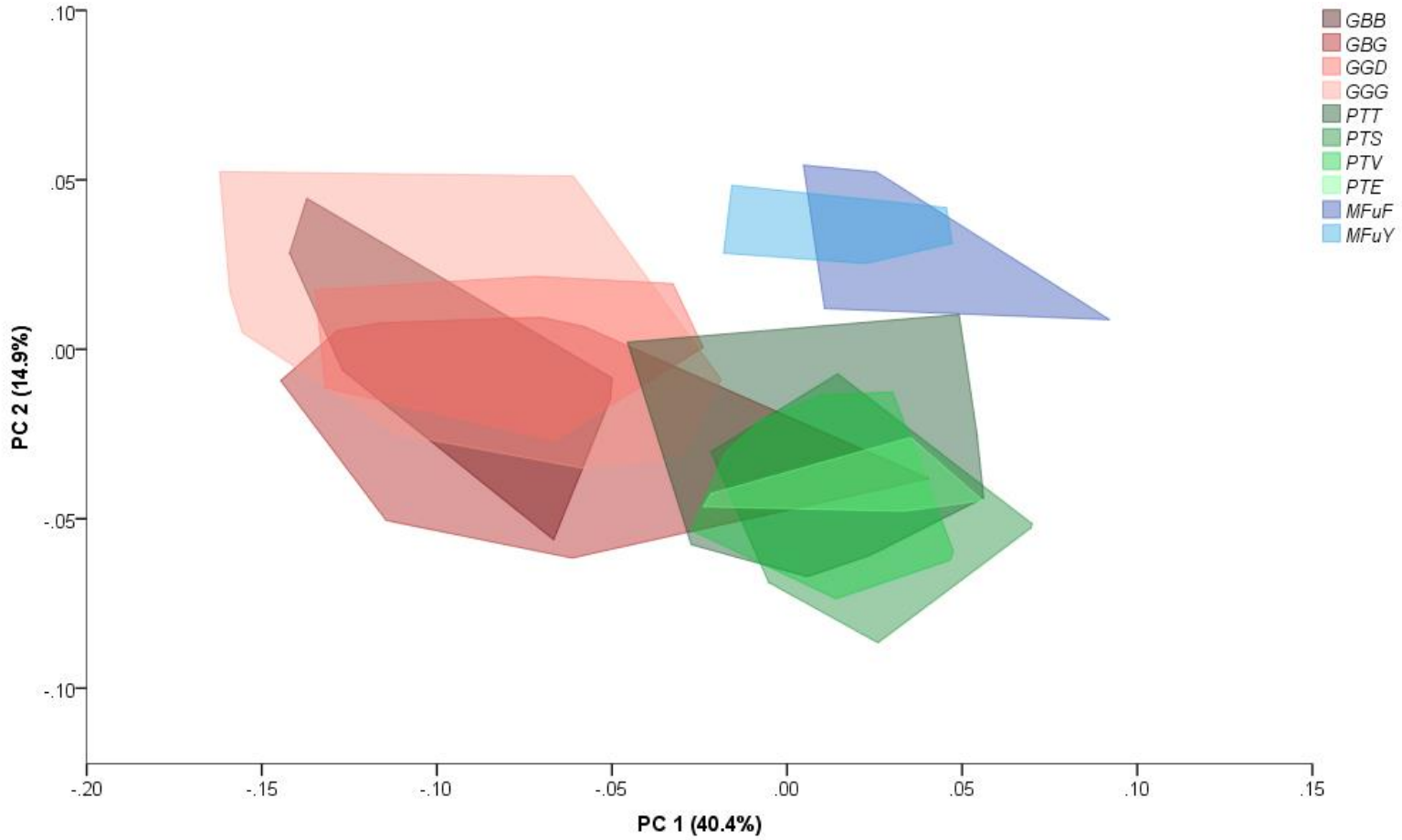

Figure S5 - Plot of PC1 (x-axis) and PC2 (y-axis), accounting for 55.4% of variation, for PCA in tangent space using dataset of 460 non-hominin primates. See table 1 for list of abbreviations. Convex hulls are shown and correspond to subspecies; see legend for identification

Principal Component Analysis: Form Space

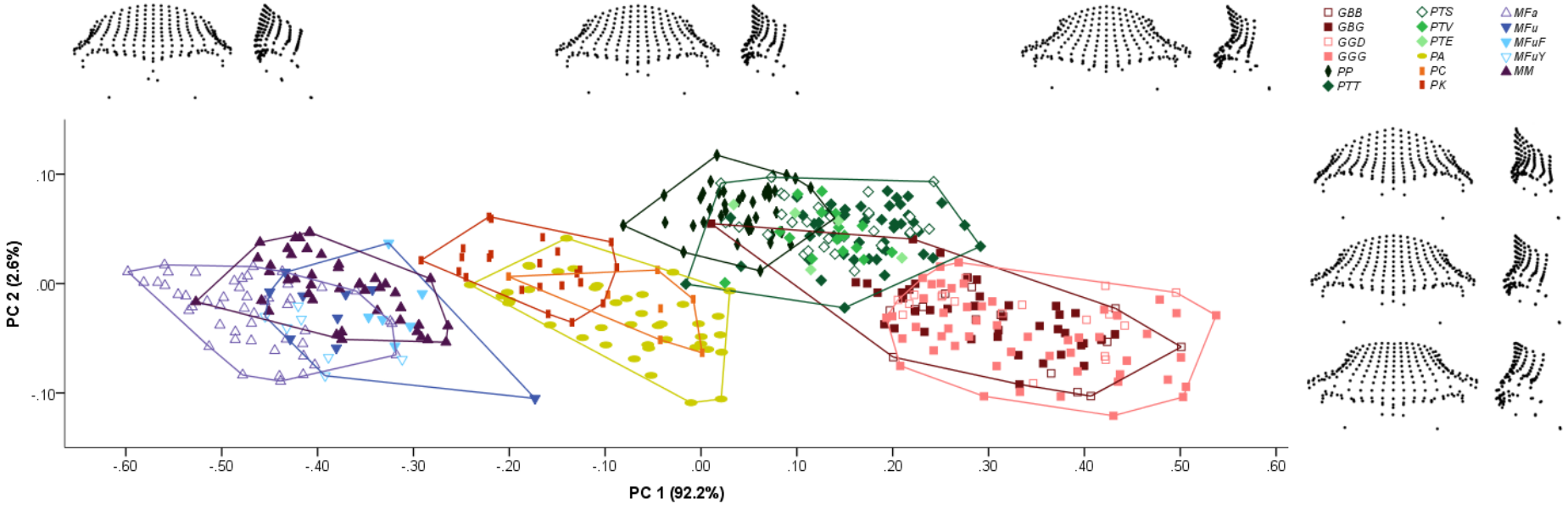

Figure S6 - Plot of PC1 (x-axis) and PC2 (y-axis), accounting for 94.8% of variation, for PCA in form space using dataset of 460 non-hominin primates. Specimens are identified by symbols shown in legend. See table 1 for list of abbreviations. Convex hulls are shown and correspond to species groups. Shape changes are shown for minimum, median, and maximum sample values for both axes, in frontal and left lateral view

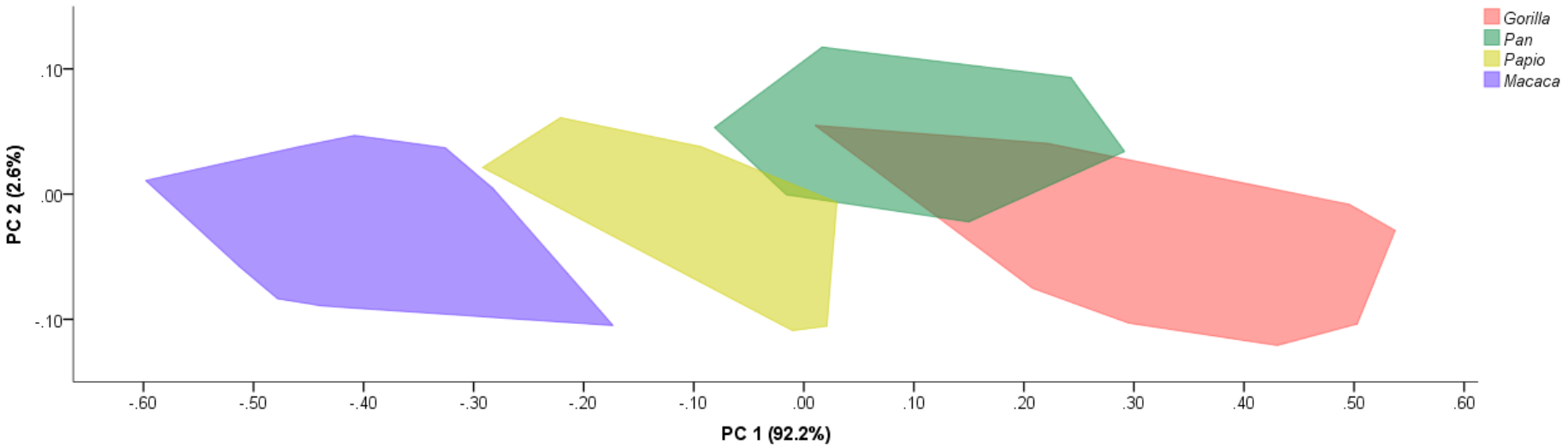

Figure S7 - Plot of PC1 (x-axis) and PC2 (y-axis), accounting for 94.8% of variation, for PCA in form space using dataset of 460 non-hominin primates. Convex hulls are shown and correspond to genera; see legend for identification

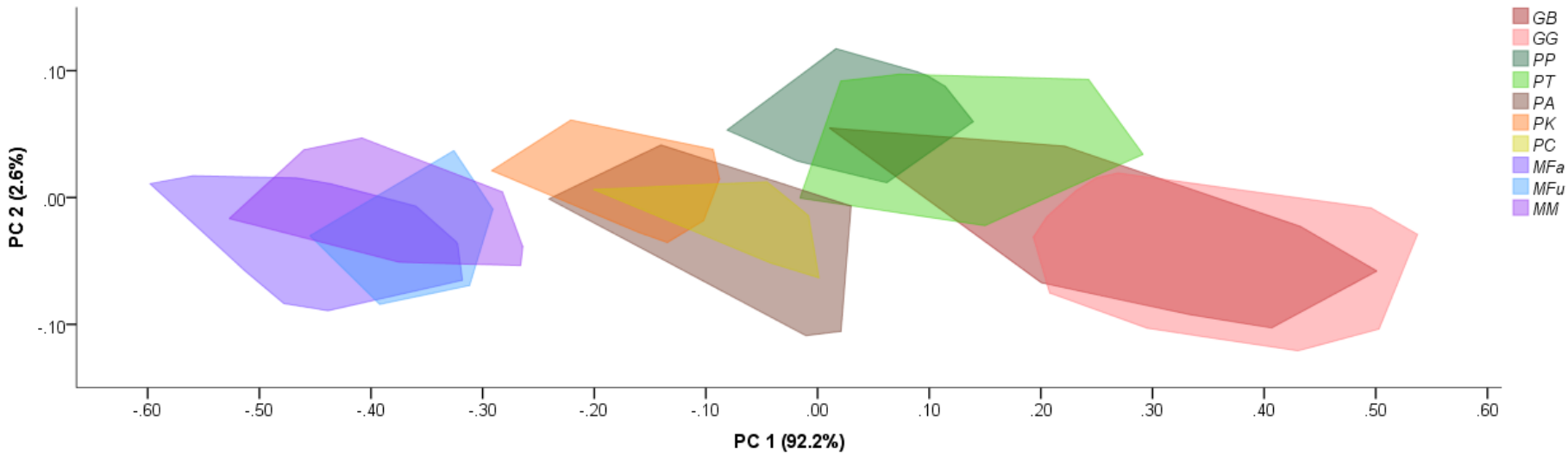

Figure S8 - Plot of PC1 (x-axis) and PC2 (y-axis), accounting for 94.8% of variation, for PCA in form space using dataset of 460 non-hominin primates. See table 1 for list of abbreviations. Convex hulls are shown and correspond to species; see legend for identification

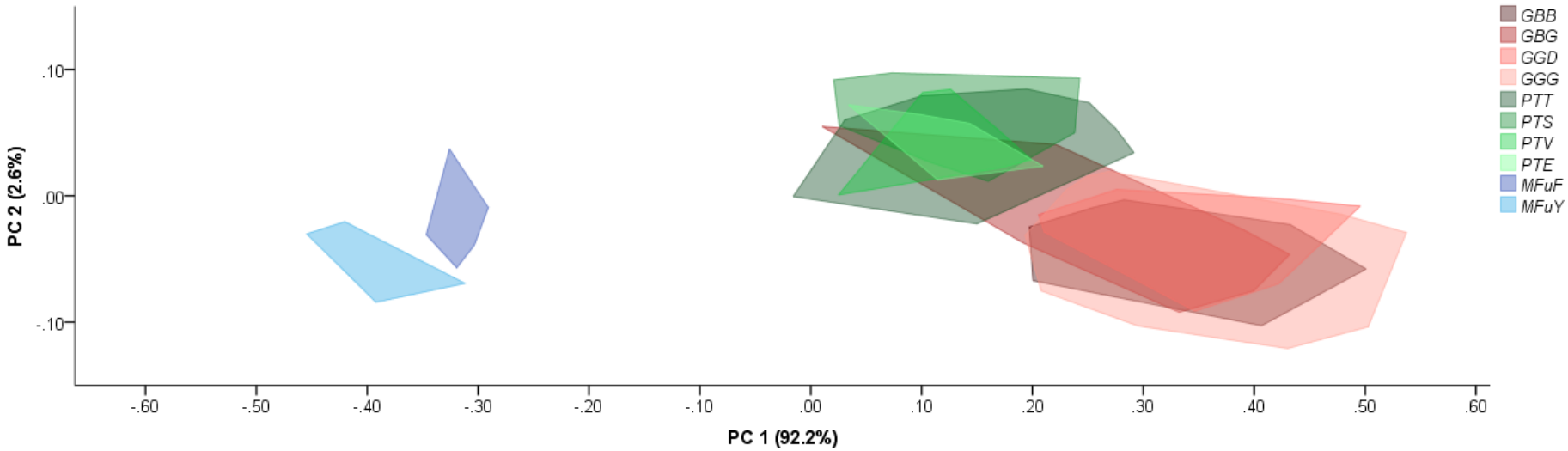

Figure S9 - Plot of PC1 (x-axis) and PC2 (y-axis), accounting for 94.8% of variation, for PCA in form space using dataset of 460 non-hominin primates. Only subspecies are shown. See table 1 for list of abbreviations. Convex hulls are shown and correspond to subspecies; see legend for identification

Discriminant Analysis: Form Space

Table S17 - Table showing results of step-wise cross-validated discriminant analysis with subsampling (n=16) using first three principal components that accounted for over 95% of total sample variance from PCA in form space with dataset of 460 non-hominin primates. Mean percentage classification accuracy across the 1000 subsamples is shown by taxon. Specimens were classified by genus, and overall genus classification accuracy was 99.2%

	Gorilla	*Pan*	*Papio*	*Macaca*	Genus
Gorilla	95.4	4.6			95.4
Pan	1.1	98.3	0.6		98.3
Papio			99.9	0.1	99.9
Macaca			0.3	99.7	99.7

S18 - Table showing results of step-wise cross-validated discriminant analysis with subsampling (n=8) using first three principal components that accounted for over 95% of total sample variance from PCA in form space with dataset of 460 non-hominin primates. Mean percentage classification accuracy across the 1000 subsamples is shown by taxon. Specimens were classified by species, and overall species classification accuracy was 64.1%. See table 1 for list of abbreviations

	GB	*GG*	*PP*	*PT*	*PA*	*PC*	*PK*	*MFa*	*MFu*	*MM*	Species
GB	70.5	22.1	2.2	5.2							70.5
GG	25.2	70.7		4.0		0.1					70.7
PP			82.8	16.8	0.1	0.2	0.1				82.8
PT	1.9	1.4	19.9	76.4	0.1	0.4					76.4
PA			0.6		38.7	35.1	25.6				38.7
PC			0.3		34.1	35.2	30.4				35.2
PK					9.3	10.4	80.0			0.3	80.0
MFa								71.8	14.3	14.0	71.8
MFu					0.2		0.5	25.5	48.5	25.3	48.5
MM							0.3	8.4	24.9	66.4	66.4

S19 - Table showing results of step-wise cross-validated discriminant analysis with subsampling (n=4) using first three principal components that accounted for over 95% of total sample variance from PCA in form space with dataset of 460 non-hominin primates. Mean percentage classification accuracy across the 1000 subsamples is shown by taxon. Specimens were classified by subspecies, and overall subspecies classification accuracy was 33.2%. See table 1 for list of abbreviations

	GBB	*GBG*	*GGD*	*GGG*	*PP*	*PTT*	*PTS*	*PTV*	*PTE*	*PA*	*PC*	*PK*	*MFa*	*MFuF*	*MFuY*	*MM*	Subspecies
GBB	25.3	38.6	14.5	16.9	0.5	1.5	0.8	0.8	1.1								25.3
GBG	31.5	35.9	11.9	8.8	1.7	3.4	1.7	2.3	2.9								35.9
GGD	15.9	14.7	35.7	28.3		3.7	0.6	1.1	0.1						0.1		35.7
GGG	16.3	10.9	29.5	38.1		3.8	0.6	0.6	0.3	0.1							38.1
PP					56.3	5.7	13.2	10.3	13.5	0.3	0.5	0.2					
PTT	0.3	2.0	2.0	1.1	4.8	33.1	23.4	18.4	14.4	0.1	0.5						33.1
PTS	0.3	0.8	0.3	0.1	15.3	24.3	19.3	19.1	20.5	0.2							19.3
PTV		0.4	0.5	0.1	6.0	20.0	21.1	20.4	30.3	0.2	1.1						20.4
PTE	0.4	2.5	0.1	0.1	19.0	18.3	21.9	27.0	10.9			0.1					10.9
PA					1.0			0.1		35.6	38.3	24.5		0.5		0.1	
PC					0.7	0.1				37.7	35.7	25.8					
PK					0.1					11.6	14.7	72.7		0.6		0.5	
MFa													52.3	4.0	30.0	13.7	
MFuF												2.0	1.1	57.9	13.3	25.7	57.9
MFuY													28.9	8.3	55.6	7.2	55.6
MM	0.1											0.6	10.2	30.1	9.6	49.5	

Principal Component Analysis: Allometry-free Shape Space

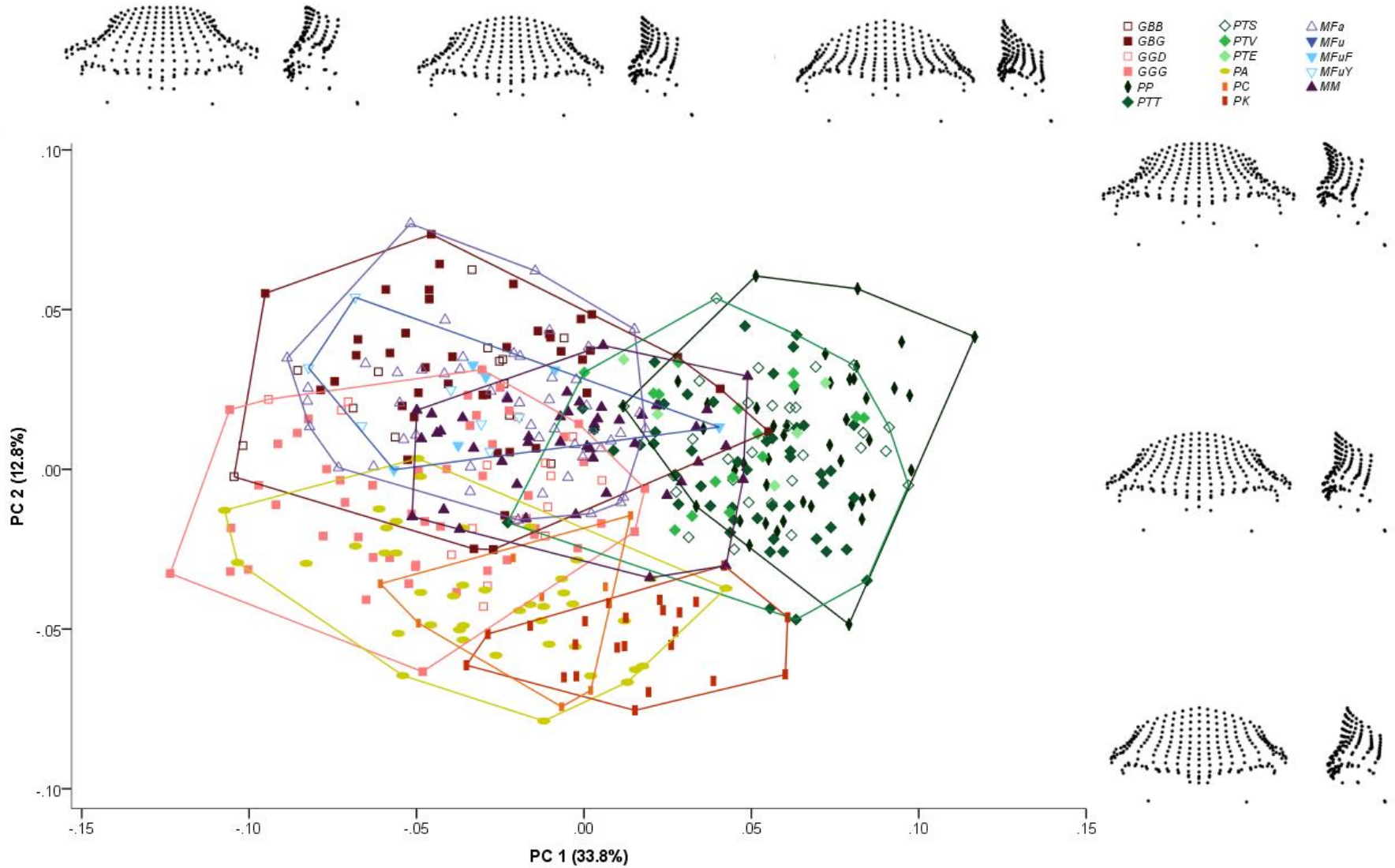

Figure S10 - Plot of PC1 (x-axis) and PC2 (y-axis), accounting for 46.6% of variation, for PCA in allometry-free shape space using dataset of 460 non-hominin primates. Specimens are identified by symbols shown in legend. See table 1 for list of abbreviations. Convex hulls are shown and correspond to species groups. Shape changes are shown for minimum, median, and maximum sample values for both axes, in frontal and left lateral view

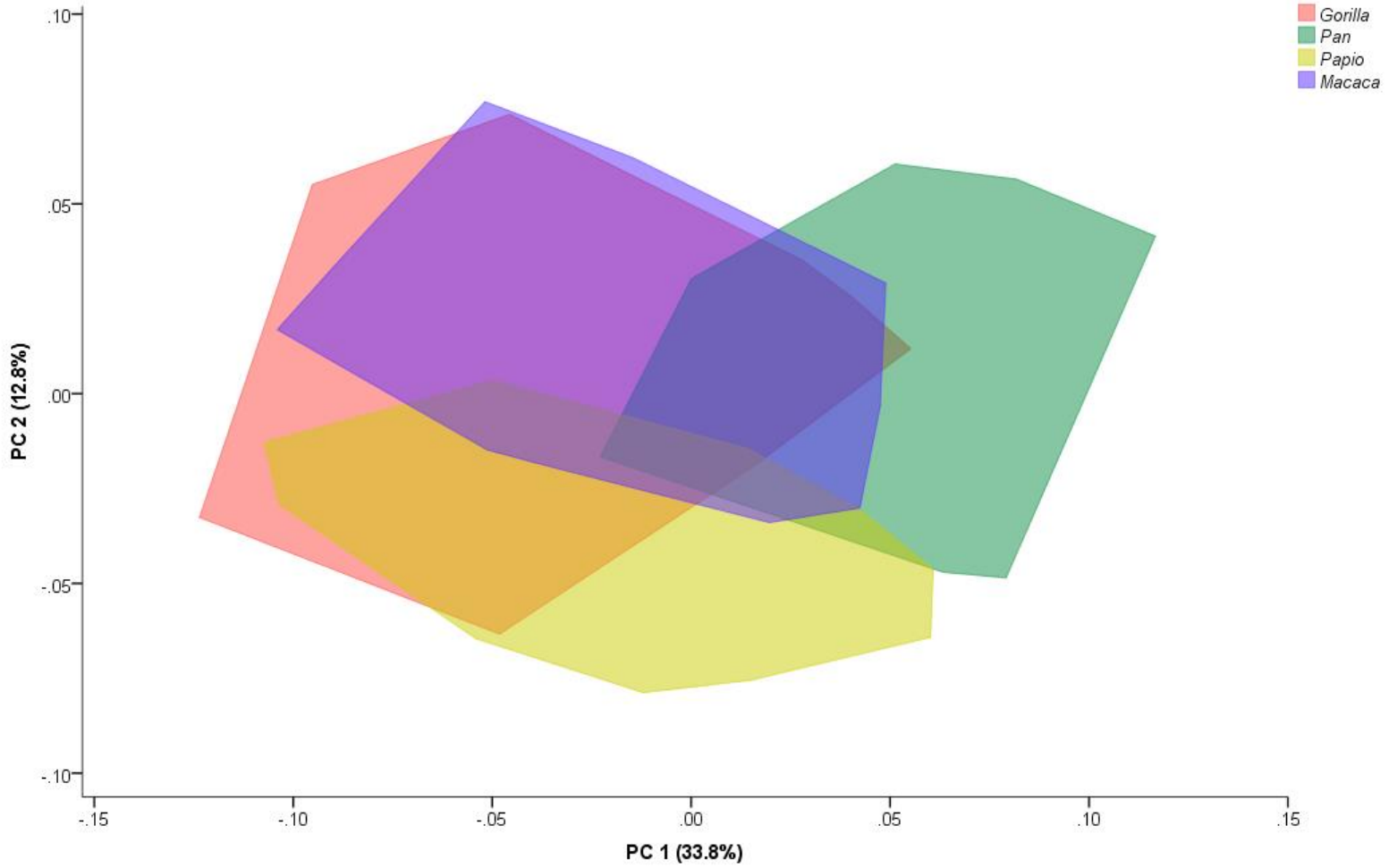

Figure S11 - Plot of PC1 (x-axis) and PC2 (y-axis), accounting for 46.6% of variation, for PCA in allometry-free shape space using dataset of 460 non-hominin primates. Convex hulls are shown and correspond to genera; see legend for identification

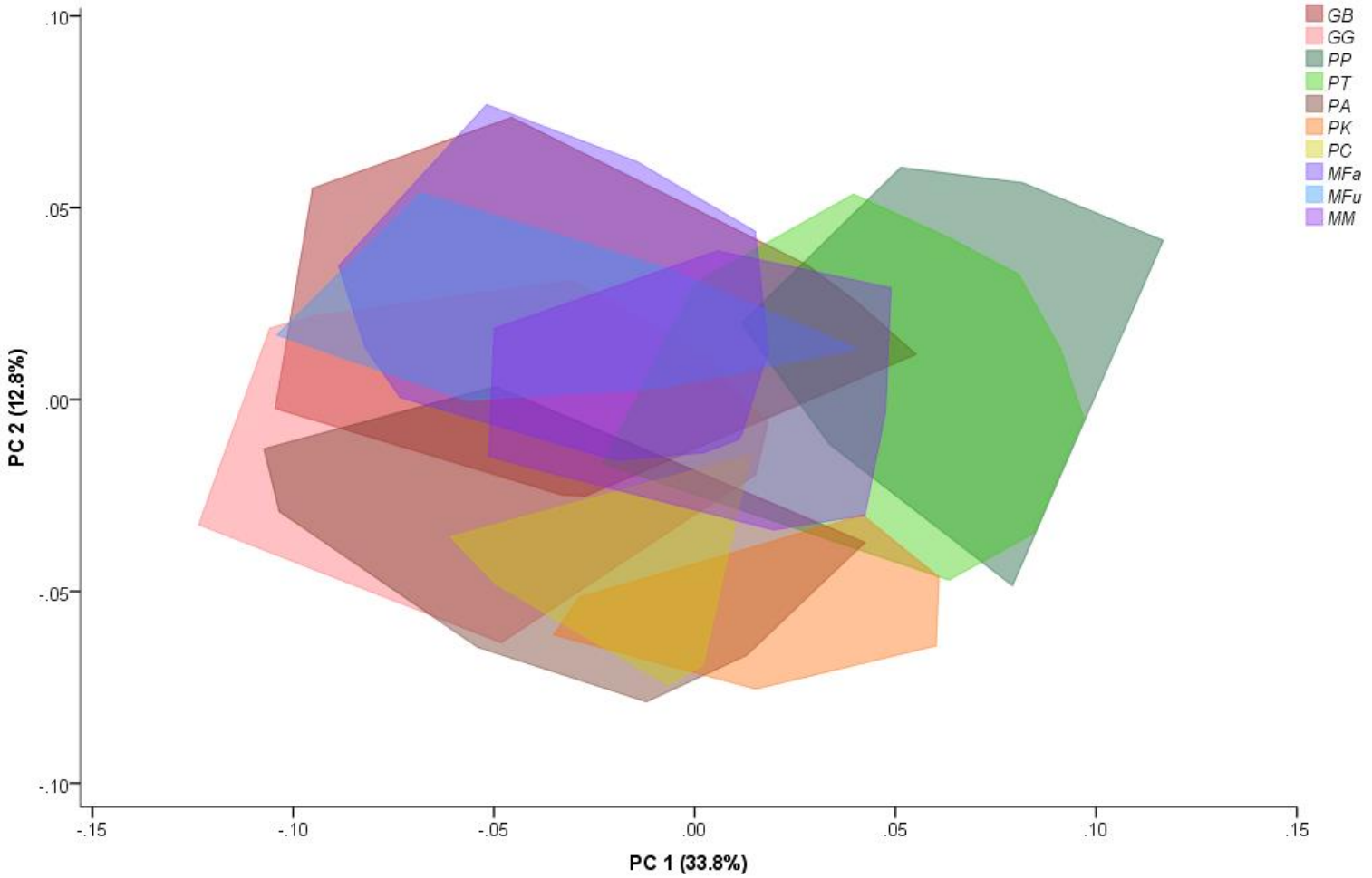

Figure S12 - Plot of PC1 (x-axis) and PC2 (y-axis), accounting for 46.4% of variation, for PCA in allometry-free shape space using dataset of 460 non-hominin primates. See table 1 for list of abbreviations. Convex hulls are shown and correspond to species; see legend for identification

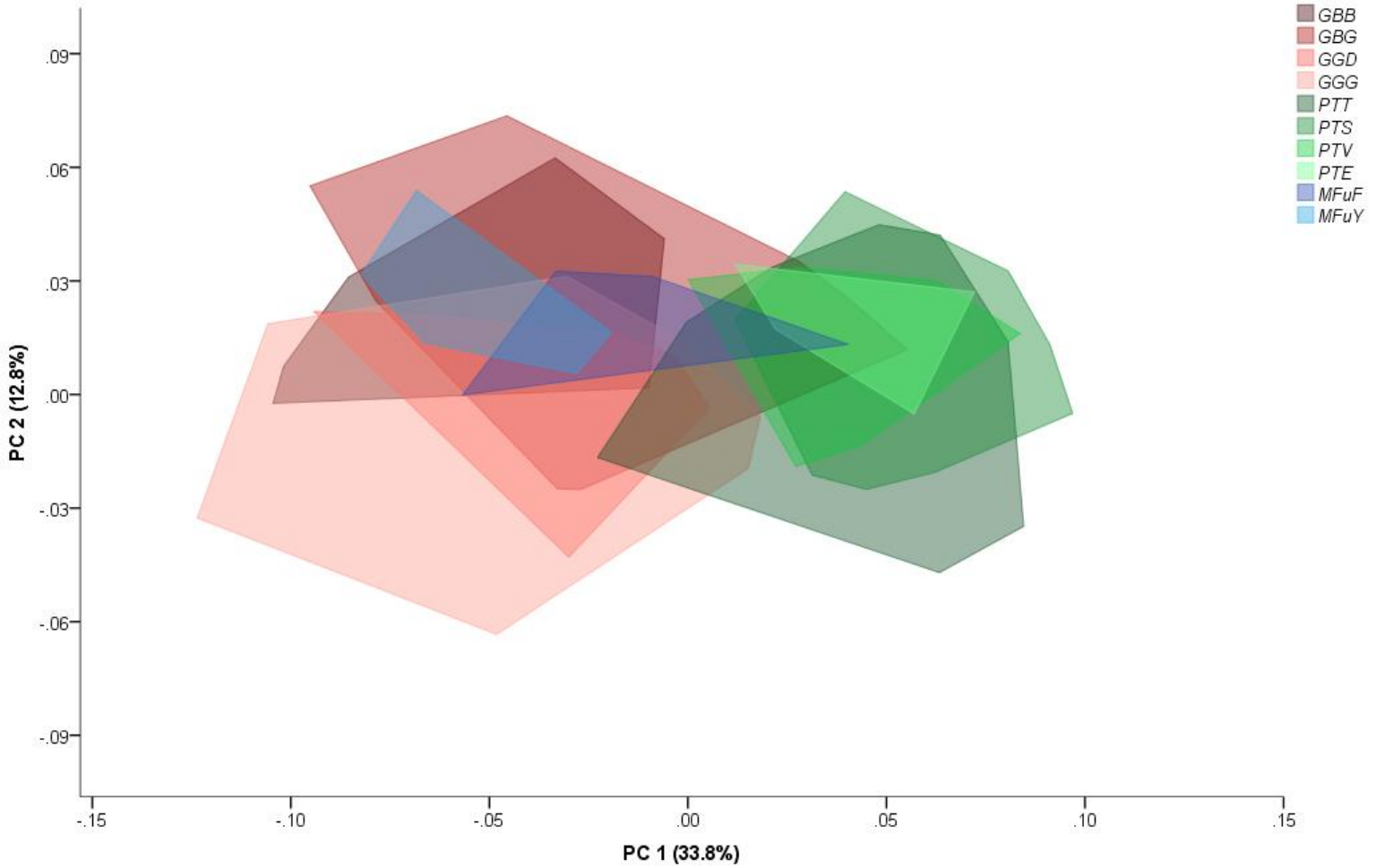

Figure S13 - Plot of PC1 (x-axis) and PC2 (y-axis), accounting for 46.4% of variation, for PCA in allometry-free shape space using dataset of 460 non-hominin primates. See table 1 for list of abbreviations. Convex hulls are shown and correspond to subspecies; see legend for identification

Discriminant Analysis: Allometry-free Shape Space

S20 - Table showing results of step-wise cross-validated discriminant analysis with subsampling (n=16) using first 39 principal components that accounted for over 95% of total sample variance from PCA in allometry-free shape space with dataset of 460 non-hominin primates. Mean percentage classification accuracy across the 1000 subsamples is shown by taxon. Specimens were classified by genus, and overall genus classification accuracy was 83.2%

	Gorilla	*Pan*	*Papio*	*Macaca*	Genus
Gorilla	69.4	2.5	7.3	20.8	69.4
Pan	0.6	94.7	0.9	3.7	94.7
Papio	2.8	0.8	95.2	1.3	95.2
Macaca	17.2	6.6	2.6	73.5	73.5

S21 - Table showing results of step-wise cross-validated discriminant analysis with subsampling (n=8) using first 39 principal components that accounted for over 95% of total sample variance from PCA in allometry-free shape space with dataset of 460 non-hominin primates. Mean percentage classification accuracy across the 1000 subsamples is shown by taxon. Specimens were classified by species, and overall species classification accuracy was 64.9%. See table 1 for list of abbreviations

	GB	*GG*	*PP*	*PT*	*PA*	*PC*	*PK*	*MFa*	*MFu*	*MM*	Species
GB	57.2	5.7	1.5	2.2	1.0	0.3	0.6	12.3	13.6	5.6	57.2
GG	5.5	52.1	0.4	1.1	6.8	4.4	1.8	10.4	9.5	7.9	52.1
PP	0.6	0.2	76.3	16.2		0.2	1.4	1.1	0.5	3.5	76.3
PT	0.7	0.6	14.9	72.2	0.3	0.8	1.5	1.9	1.2	5.9	72.2
PA	0.3	5.3		0.2	62.3	18.2	10.8	0.5	0.9	1.3	62.3
PC		1.1	0.2	1.9	16.1	56.9	19.1	0.1	0.5	4.2	56.9
PK		0.3	0.4	0.1	3.5	8.5	86.9			0.1	86.9
MFa	12.0	7.6	1.1	1.6	0.6	0.2	0.3	57.2	11.2	8.3	57.2
MFu	8.6	4.0	0.9	2.5	0.4	0.3	0.1	12.1	63.6	7.5	63.6
MM	4.2	3.7	3.5	6.9	2.3	2.8	1.3	4.7	6.7	63.9	63.9

S22 - Table showing results of step-wise cross-validated discriminant analysis with subsampling (n=4) using first 39 principal components that accounted for over 95% of total sample variance from PCA in allometry-free shape space with dataset of 460 non-hominin primates. Mean percentage classification accuracy across the 1000 subsamples is shown by taxon. Specimens were classified by subspecies, and overall subspecies classification accuracy was 39.9%. See table 1 for list of abbreviations

	GBB	*GBG*	*GGD*	*GGG*	*PP*	*PTT*	*PTS*	*PTV*	*PTE*	*PA*	*PC*	*PK*	*MFa*	*MFuF*	*MFuY*	*MM*	Subspecies
GBB	38.5	6.9	5.1	5.6	0.6	0.5	0.4	0.8	0.5	0.3	0.3	0.1	10.0	9.8	16.1	4.5	38.5
GBG	7.4	51.2	2.2	3.0	0.8	0.5	1.2	1.2	3.4	1.3	0.6	0.6	8.5	7.4	6.7	4.1	51.2
GGD	5.5	2.1	41.9	10.4	0.4	0.8	0.4	0.5	0.2	5.9	4.6	2.4	6.2	5.8	6.3	6.3	41.9
GGG	6.6	2.7	12.0	37.8	0.5	1.2	0.4	1.0	0.5	7.1	4.3	1.3	8.0	4.9	6.2	5.6	37.8
PP	0.5	0.9	0.6	0.6	50.1	10.1	10.6	11.2	8.3	0.2	0.1	1.5	1.1	1.2	0.7	2.3	
PTT	0.6	1.1	0.9	0.9	7.9	40.3	14.2	9.6	10.5	0.5	1.6	2.4	1.9	2.1	0.6	5.1	40.3
PTS	0.4	0.7	0.9	0.5	10.8	16.5	38.0	11.1	15.5	0.3	0.2	0.4	1.1	0.4	0.3	3.0	38.0
PTV	0.7	1.2	0.4	0.4	11.0	11.0	11.8	34.3	20.3	0.3	0.4	1.0	1.7	1.8	0.5	3.2	34.3
PTE	0.4	0.9	0.2	0.2	10.0	9.4	12.8	20.0	38.2	0.2	0.2	0.3	1.6	1.6	0.5	3.6	38.2
PA	0.4	0.7	3.6	4.9	0.1	0.5	0.1	0.2	0.2	54.8	19.1	11.5	1.0	0.8	0.6	1.5	
PC	0.2	0.2	2.8	1.9	0.2	2.5	0.4	0.5	0.1	16.2	51.5	17.7	0.4	2.5	0.3	2.5	
PK		0.1	0.6	0.2	0.7	0.7	0.3	0.2	0.3	4.3	10.0	81.8	0.2	0.2		0.4	
MFa	6.4	9.5	6.2	4.7	0.9	2.1	1.4	2.6	1.5	0.8	0.3	0.5	38.3	8.8	8.0	8.1	
MFuF	8.2	4.8	3.0	3.6	2.0	6.2	1.6	3.0	4.4	0.4	0.6	0.1	6.8	31.1	19.0	5.3	31.1
MFuY	11.8	4.3	3.7	2.9	0.4	0.2	0.3	0.4	0.7	0.1	0.2		6.7	17.1	47.5	3.7	47.5
MM	2.2	3.6	4.5	4.0	2.3	4.3	3.8	3.5	5.2	2.4	2.3	1.4	4.8	9.3	3.8	42.6	

SI-7: Hominins - Additional Results

Mean Pairwise Procrustes Distances

Table S23 - Mean pairwise Procrustes distances (PrD) for inter-taxon comparisons for Pleistocene hominin dataset. See table 2 for list of abbreviations. PrD shown to 3 decimal places

	Pairwise PrD
HS - HN	0.127
HS - HEsl	0.172
HN - HEsl	0.117
HNa - HS	0.201
HNa - HN	0.128
HNa - HEsl	0.118
HNa - HHa	0.129
HNa - HRu	0.119
HHa - HRu	0.100
HHa - HEsl	0.118
HRu - HEsl	0.107
HHa - AAf	0.114
HRu - AAf	0.096
AAf - ParA	0.133
ParA - ParB	0.116

Discriminant Analysis: Misclassifications

Table S24 - Percentage classifications for hominin specimens from discriminant analysis shown in table 8. See table 2 for abbreviations. n shows number of subsamples in which specimen were randomly selected

	n	*HS*	*HN*	MPH	*HEsl*	*HHa*
Chancelade	314	100.0				
Furfooz I	314	93.6	6.4			
Keilor	319	100.0				
Oberkassel I	335	99.4	0.3	0.3		
Oberkassel II	323	99.7	0.3			
Abri Pataud	326	99.7	0.3			
Brno II	322	97.5	2.5			
Cro-Magnon 1	300	100.0				
Cro-Magnon II	354	100.0				
Dolní Věstonice III	316	100.0				
Mladeč 1	314	100.0				
Mladeč 2	303	97.7	2.3			
Předmostí III	300	97.0	3.0			
Předmostí IV	323	99.7	0.3			
Zhoukoudian U.C.101	325	95.1	3.7	1.2		
Zhoukoudian U.C.102	338	96.4	3.6			
Border Cave 1	318	68.9	17.3	10.4	3.5	
Qafzeh 9	295	97.6	2.4			
Skhūl V	303	47.2	39.3	0.3	9.2	4.0
Liujiang	326	100.0				
Omo 1	314	19.7	48.7	31.2	0.3	
Jebel Irhoud 1	318	13.2	73.6	12.6	0.3	0.3
Tabun I	542		98.7	0.9	0.4	
La Quina H5	490	1.2	92.9	0.2	5.7	
Spy 1	544		99.8	0.2		
La Chapelle	516		100.0			
Guattari	534		99.6		0.4	
Gibraltar 1	502	0.2	99.6	0.2		
Le Moustier 1	537	28.3	70.6	1.1		
Amud 1	551	8.0	90.0	2.0		
Krapina C	565		99.1		0.9	
Krapina E	568		82.9	0.5	16.5	
Saint Césaire I	541	4.8	87.6	7.2	0.4	
Shanidar I	552		100.0			
Shanidar V	558		79.0	0.2	20.8	
Bodo	1000		3.0	92.8	2.9	1.3
Kabwe 1	1000		0.5	82.3	0.9	16.3
SH5	1000	0.4	35.0	24.9	38.2	1.5
Petralona	1000	0.4	24.6	69.0	5.8	0.2
Solo VI	1000	0.2	25.9	1.6	72.3	
Sangiran 17	1000		5.0	2.9	91.5	0.6
Zhoukoudian XII	1000		17.9	8.2	73.9	
KNM-ER 3773	1000		0.1	0.5	85.3	14.1
KNM-ER 3883	1000	0.1	1.7	21.5	76.7	
Dmanisi D4500	1000			0.7	78.3	21.0
Dmanisi D2282	1000		0.4	1.2	98.0	0.4
KNM-ER 1813	1000		6.0	2.7	64.1	27.2
OH 24	1000		0.5	19.8	30.7	49.0

References

Adams, D. C., Otárola-Castillo, E., & Paradis, E. (2013). Geomorph: An R package for the collection and analysis of geometric morphometric shape data. *Methods in Ecology and Evolution*, *4*(4), 393-399. doi:10.1111/2041-210x.12035

Gunz, P., & Mitteroecker, P. (2013). Semilandmarks: A method for quantifying curves and surfaces. *Hystrix, the Italian Journal of Mammalogy*, *24*(1), 103-109. doi:10.4404/hystrix-24.1-6292

Mitteroecker, P., & Gunz, P. (2009). Advances in geometric morphometrics. *Evolutionary Biology*, *36*(2), 235-247. doi:10.1007/s11692-009-9055-x

Phillips, R., O'Higgins, P., & Bookstein, F. L. (2010). EVAN (European Virtual Anthropology Network) toolbox: European Virtual Anthropology Network - EVAN (www.evan.at) and the EVAN-Society. Retrieved from www.evan.at